Appendix E: Overview of the Southern San Andreas Fault Model

By Ray J. Weldon II[1], Glenn P. Biasi[2], Chris J. Wills[3], and Timothy E. Dawson[4]

2008

[1]University of Oregon, Eugene
[2]University of Nevada, Reno
[3]California Geological Survey, Sacramento, California
[4]U.S. Geological Survey, Menlo Park, California

U.S. Department of the Interior
DIRK KEMPTHORNE, Secretary

U.S. Geological Survey
Mark D. Myers, Director

State of California
ARNOLD SCHWARZENEGGER, Governor

The Resources Agency
MIKE CHRISMAN, Secretary for Resources

Department of Conservation
Bridgett Luther, Director

California Geological Survey
John G. Parrish, Ph.D., State Geologist

U.S. Geological Survey, Reston, Virginia 2008

Contents

Introduction

This appendix summarizes the data and methodology used to generate the source model for the southern San Andreas fault. It is organized into three sections, 1) a section by section review of the geological data in the format of past Working Groups, 2) an overview of the rupture model, and 3) a manuscript by Biasi and Weldon (in review Bulletin of the Seismological Society of America) that describes the correlation methodology that was used to help develop the "geologic insight" model. The goal of the Biasi and Weldon methodology is to quantify the insight that went into developing all A faults; as such it is in concept consistent with all other A faults but applied in a more quantitative way.

The most rapidly slipping fault and the only known source of M~8 earthquakes in southern California is the San Andreas fault. As such it plays a special role in the seismic hazard of California, and has received special attention in the current Working Group. The underlying philosophy of the current Working Group is to model the recurrence behavior of large, rapidly slipping faults like the San Andreas from observed data on the size, distribution and timing of past earthquakes with as few assumptions about underlying recurrence behavior as possible. In addition, we wish to carry the uncertainties in the data and the range of reasonable extrapolations from the data to the final model. To accomplish this for the Southern San Andreas fault we have developed an objective method to combine all of the observations of size, timing, and distribution of past earthquakes into a comprehensive set of earthquake scenarios that each represent a possible history of earthquakes for the past ~1400 years. The scenarios are then ranked according to their overall consistency with the data and then the frequencies of all of the ruptures permitted by the current Working Group's segmentation model are calculated.

We also present 30-yr conditional probabilities by segment and compare to previous results. A distinctive aspect of the current model is that the probability is higher at both ends of the fault and that the ends have a much greater fraction of smaller events. There is a significant difference in the likelihood of large (M 7.7-8.0) earthquakes along the fault from north to south, with large 1857-like events common on the northern half of the southern San Andreas fault but relatively few M 7.7-8.0 expected on the southern half.

Review of Geologic Data

Parkfield Section – Following previous Working Groups (1988, 1995) we use the historical record, updated to include the recent 2004 earthquake, to calculate the average interval of 24.5 years for this section. We did not review the literature but a recent Special Issue of BSSA (eds. Harris and Arrowsmith, 2006) contains a comprehensive overview of the 2004 earthquake and issues related to recurrence at Parkfield. While this is the best constrained section on the southern San Andreas fault, there are two issues, discussed in greater detail in the Cholame and Carrizo sections, worth mentioning. First, it is unknown whether all of the early ruptures exactly filled the Parkfield section and there is some doubt as to whether all of the earthquakes were even on the section. For example, on the Cholame section Young et al. (2002) document a small displacement event that postdates 1857, suggesting the possibility that one of the early historic "Parkfield" events extended farther south onto the Cholame section or even occurred there instead of Parkfield. There is also a growing consensus that displacement associated with the northern end of 1857 was larger than originally proposed by Sieh (1978) and that multi-meter offsets extend into at least the southern end of the Parkfield section (Lienkaemper et al., 2001; 2006; Toke and Arrowsmith, 2006). Thus, the section may have a bimodal behavior with centimeters of displacement in "typical" Parkfield-like earthquakes and meters during large multi-segment ruptures like 1857. It is worth noting that multi-meter displacement at Parkfield probably requires rupture well into the Creeping section of the fault to the north. This is allowed in the current Biasi and Weldon methodology for generating scenarios, as discussed below.

The slip rate has not been changed from previous Working Groups estimate of 34+/- 3 mm/yr. This is consistent with recent geodetic estimates of ~33 mm/yr (Murray et al., 2001, 2006).

Cholame Section – The 1995 Working Group accepted the 1988 values of 4.75 +/-2 m for the characteristic slip, and an average slip rate of 34 mm/yr (although the increased the uncertainty range to +/- 5 mm/yr from 1.5). The 1995 Working Group discussed the apparent contradiction between the characteristic slip estimates of Sieh 3.5 m, 1978) and Lienkaemper and Prescott (6 m, 1989). Since they could not resolve this distinction they used the median value. In any case, the concept that has dominated thinking on the Cholame section is that the northern tailing off of slip in 1857 (and hypothetically prehistoric events) from the central Carrizo Plain requires "catch-up" events of moderate size to accommodate the high slip rate (Sieh and Jahns, 1984). Because Working Group 1995 was uncertain what range of sizes of events are necessary to fill this "slip deficit" and whether the section sometimes ruptured independently or just with Parkfield they demoted the section to B fault behavior.

Since 1995 there has been a growing consensus that the 1857 slip was at the higher end of the range considered (Arrowsmith, et al., 1997; Runnerstrom et al., 2002; Stone et al., 2002; Lienkaemper et al., 2006; Toke and Arrowsmith, 2006). In addition, new paleoseismic data from the Cholame section and from sites just south of the boundary to the Carrizo section (Young et al., 2002; Stone et al., 2002; discussed in more detail in the Carrizo section) may indicate a bimodal behavior with some ruptures having offsets in the 5-7 meter range and others centimeters to a few meters. Because of this we

continue to treat the Cholame section as a special case, but not as a B fault like Working Group 1995. We argue that approximately 1/3 of the events recorded by Young et al. (2002) on the Cholame section and multiple workers at the very northern end of the Carrizo section (discussed below) are limited to the Cholame section or a combination of Parkfield and the Cholame section (with possible minor overlap onto the northernmost part of the Carrizo section). Because of the frequency of Parkfield events and the lack of positive evidence that the Cholame section can rupture alone we arbitrarily assign most (90%) of these ruptures to a combination of Parkfield and Cholame (this results in about 5% of Parkfield ruptures including the Cholame section).

There are no paleoseismic records of sufficient length to determine an average recurrence interval. As discussed below for the Carrizo section, the Bidart paleoseismic site, on the northern Carrizo section, may represent the Cholame section as well and thus a recurrence interval of ~150 years was assigned to this section. Because the Biasi and Weldon analysis has no information about the Cholame section, rupture rates were generated by hand, as for other A faults.

Finally, we explored the possibility of moving the boundary between the Cholame and Carrizo sections. There is no structural or geometric reason to place the boundary where it is, and there appears to be no change in slip rate either. The only reason is the inferred slip distribution in 1857 that is no longer as clearly located as originally inferred by Sieh (1978). However, changing the boundary met with resistance from the geologic community, so this effort was abandoned.

Carrizo Section - The 1995 Working Group accepted the 1988 value average slip rate of 34 +/- 3 mm/yr (Sieh and Jahns, 1984), but decreased the characteristic slip from 9.5 +/-2 m to 7 +/- 4, based on evidence from geodesy, geomorphology and trenching that there are offsets ranging from more than 11 meters to less than 3 meters. The 1995 Working Group discussed the paleoseismic evidence from Phelan Creek (Sims et al., 1993) and Bidart Fan (Grant and Sieh, 1994). The former suggested an average interval of ~212 years, whereas the former suggested either a shorter interval or a cluster of three events in less than 300 years followed by a ~350 year hiatus until the 1857 event. Due to the apparent contradictions in the paleoseismic data Working Group 95 used their estimate of the characteristic event and the slip rate to calculate the average interval of ~206 years.

There is new evidence for slip rates, displacements, and timing of events, although the latter is only published in abstracts and is currently being reviewed at JGR. The slip rate data continue to be the gold standard for this section with new geodetically determined values of 36 +/- 2 (Schmalzle et al., 2006) and 30-37 mm/yr (Noriega, et al., 2006) and geologic slip rates at Van Matre Ranch of 29.3-35.6 mm/yr since 1160 AD (Noriega, et al., 2006) and ~35 mm/yr near Wallace Creek over a poorly dated ~1200 years (Liu et al., 2006). Both of the geologic slip rates are based on a few pieces of detrital charcoal so the ages may be overestimated and the slip rates underestimated (as discussed below with events), but the consistency of these rates with the geodesy and the longer term geologic rates of Sieh and Jahns (1984; since ~3700 BP and 13,250 BP) suggest a constant slip rate of ~35 mm/yr over all measured time periods.

Near Wallace Creek Liu (2003; Liu et al., 2004; 2006) has documented the offsets of what are interpreted to be the past 6 earthquakes on the Carrizo section; three,

including 1857, have slip of just less than 8 m, two just over 5 m (one of these could be larger) and one ~1.4 m. This is quite similar in average value and range to previous Working Group's interpretation. Other new data include estimates of slip in 1857 (both here and on the Cholame section) of ~11 m (Grant and Donnellan, 1994) and ~16 m (Runnerstrom et al., 2002) that appear to be larger than geomorphic or paleoseismic offsets. This may be due to problems with the geodetic observations, such as monument instability or more displacement outside the narrow fault zone than the geomorphic and paleoseismic observations focus on (Arrowsmith, pers. comm., 2006).

There is also new paleoseismic data for the timing of recent events from the Bidart fan site (Akciz, et al., 2005; 2006; in review JGR; Grant et al., 2005) that suggest an average interval of ~100 to 150 years for ground rupturing events. This work, currently only published as abstracts and a JGR manuscript, has generated considerable interest and scrutiny, and multiple "trench parties" attended by most of the California paleoseismic community has led to the impression that these results are likely to stand up to future review. It is, however, quite difficult to reconcile these observations with slip per event data, which appear to support infrequent large slip events (as discussed above). Several possibilities have been considered: 1) The well dated ruptures at Bidart Fan, for which displacement is poorly known, correlate with the poorly dated but well documented displacements from Wallace Creek. If this were the case, then the implied slip rate would be almost twice the accepted rate for the past 6 events. While such a cluster of large displacements in a short period of time has been documented at Wrightwood (Mojave South section; Weldon et al., 2002; 2004) and hypothesized for the Hog Lake site on the San Jacinto fault (Rockwell pers. comm., 2006), it is not consistent with the Van Matre Ranch slip rate over a similar period of time, or the general consistency of slip rate over many time periods for this section of the fault (discussed above). 2) The average interval at Bidart Fan spans a shorter time than the offsets at Wallace Creek, and the large offsets at Wallace Creek are made up of multiple smaller offsets. This seems unlikely because the unquestionably large offset in 1857 matches several of the prehistoric rupture displacements, and there is no geomorphic evidence for small surface offsets (Arrowsmith, pers. comm., 2006) in this area. 3) Perhaps there is a bimodal behavior, as suggested for the Cholame section above, in which some of the earthquakes have large 1857-like displacements but others have smaller displacements, associated with much smaller (and shorter rupture earthquakes. This may be supported by the one small displacement event (~1.4 m) seen by Liu et al. (2004; 2006), and the deformation seen in the trenches at Bidart Fan, which suggests that some events have much smaller displacement than others (but actual lateral displacement have not yet been determined there). 4) It must be kept in mind that all current dates are detrital charcoal, and the different sites (and even trenches at the sites) are not easily correlated, so it is possible that other interpretations will emerge as the sites are developed. Finally, all of the Carrizo sites are within ~10 km of the boundary with the Cholame section, which we have suggested has both large multi-segment ruptures and smaller local offsets; perhaps this behavior extends for some distance into the Carrizo section without actually representing the entire section.

Taken as a whole it appears that we must reduce the average interval from that used by previous Working Groups (to ~150 years, based on the JGR manuscript), but we do not feel that the evidence is strong enough to reduce it to the ~100 year value inferred

from the most recent work, since we may have sampled a temporal pulse that is not typical of the long term behavior of the section and we may be sampling excess small events that slop over from the Cholame section. Thus, the Working Group chose to use ~150 years. Because pdfs for the events were not available when the Biasi and Weldon correlation model was developed, they generated broad pdfs based on the available data (discussed in detail below). Rather than attempting to rerun their analysis, the rates of events including the northern end of the fault were modified by hand to result in an average recurrence interval of ~150 years.

Big Bend Section – In previous Working Groups (1988, 1995) this section was part of the Carrizo segment, and as such had the parameters of the Carrizo section. As discussed in the Fault Section database (Appendix A), this section was separated out due to its geometric distinction from the simple and straight sections to the north and south, and the possibility that it ruptured independently in December 21, 1812.

There are two paleoseismic sites on this section, the Frazier Mountain (Lindvall et al., 2002) and San Emigdio (Davis, 1984) sites. The first found evidence for only 2 earthquakes in the past ~500 years and the second can be interpreted to record at least 3, including compelling evidence for both the 1857 earthquake and another slightly older rupture that could be 1812. As discussed in Lindvall et al. (2002) their excavations did not span the entire fault zone so it is possible that they missed events at the site. Based on our correlation modeling (Biasi and Weldon manuscript below) we assign an average interval of ~175 years. There are no slip rate sites on this section and given the lack of significant branching structures north of the Garlock (which defines the southern end of this section) we infer that this section has the same slip rate as the Carrizo section. The most recent earthquake was in 1857, and it is possible that the December 21, 1812 earthquake ruptured this section as well (Toppozada, et al., 2002; see the Mojave North section for more detailed discussion). Recent, unpublished re-examination of the Frazier Mountain site, after this Appendix was written suggests that like the Carrizo section the recurrence interval may be shorter than modeled. However, the preliminary nature of this new work precluded it being included here.

Mojave North Section - In previous Working Groups (1988, 1995) this section was the southernmost portion of the Carrizo segment. We kept the southern boundary, inferred by previous Working Groups to be the location of a decrease in slip during 1857 from ~6 m to the north to ~4 meters to the south. The southern end of this section may be the northern end of the December 8, 1812 earthquake and the southern end of the December 21, 1812 earthquake (IF it was on the San Andreas, Toppozada et al., 2002); although, it appears more likely that the boundary between these two earthquakes was the northern boundary of the Mojave North section, where it joins the Big Bend section. Because this was the southern end of the Carrizo section it had the same slip rate, average interval, and slip per event as the rest of the Carrizo (discussed above).

While there are no new slip rate or paleoseismic data for this section, exploratory work (T. Fumal and K. Scharer, pers. comm., 2006) supports the widely held view (dating to Sieh, 1978 and Rust, 1986) that each of the last 3 earthquakes had 6-7 m of offset, and that there are several additional ~18 m offsets of landslides and other geomorphic features (first noted and one dated by Rust, 1986). These results are consistent with several ~18 m offsets, inferred to be caused by 3 earthquakes at Littlerock

in the northern part of the Mojave South section (Sickler et al., 2006; discussed in greater detail in the Mojave South section).

There is no compelling reason to preserve the Carrizo-based slip rate for the Mojave North section. If there is a slip rate change between the Carrizo and Mojave San Andreas it is most likely to be at the junction with the Garlock fault. Thus we adopt the slip rate for the Mojave South section, 28 +/- 7 mm/yr (discussed in Mojave South). Since the average interval used by previous Working Groups was calculated using the Carrizo rate we must revise it as well. Given the total absence of direct recurrence data we assign a value of ~155 years based on our correlation of earthquakes at sites to the north and south (discussed in the Biasi and Weldon manuscript).

The most recent earthquake on this section was 1857. It is also possible that either the December 8 or December 21, 1812 earthquake ruptured this section. The large displacements associated with the December 8th earthquake on the Mojave South section and anecdotal reference to tree ring evidence (Sieh, pers. comm., 1988) has led many to infer that the December 8th earthquake extended far enough north to include this section (e.g. Sieh et al., 1989); whereas the distribution of historical shaking records has led others (e.g. Fumal et al., 1993) to infer that it did not extend so far north. In addition, Toppozada et al. (2002) have proposed that the December 21, 1812 earthquake occurred on the San Andreas fault, extending the rupture of the December 8th earthquake to the north. We infer from Toppozada et al. (2002) that the most likely location of the December 21st earthquake (IF it was on the San Andreas fault at all) was the Big Bend section, so the December 8th rupture would include the Mojave North section in this scenario. Finally, it is possible, given the sparse historical data that the December 8th rupture stopped at the north end of the Mojave South section, and the December 21st earthquake extended rupture to the Mojave North. So we conclude that one of the 1812 earthquakes almost certainly included this section, it is extremely unlikely both occurred here, and that most likely this was the northern end of the December 8th earthquake.

Mojave South Section - The 1988 and 1995 Working Groups include long discussions of the paleoseismic data at Pallett Creek and Wrightwood (which was mistakenly placed on their San Bernardino Mountains segment but discussed in the context of their Mojave segment to argue that both Pallett Creek and Wrightwood fall in an overlap zone and thus cannot be used to set the average interval). Because of the uncertainty in which events "belong" on the Mojave segment, the Working Groups used slip rate and characteristic slip to calculate the average interval of 150 years (vs. paleoseismic rates for Pallett Creek of 131 and Wrightwood of 106 years). The 1995 Working Group also discussed the evidence for 6 m offsets at Pallett Creek (Salyards et al., 1992) and a higher slip rate of 32 to 38 mm/yr (Weldon, 1991; Powell and Weldon, 1992; Salyards et al., 1992; Weldon et al., 1993). However, they chose to expand the uncertainty ranges (4.5 +/- 1.5 m per event and 30 +/- 8 mm/yr slip rate) to accommodate these new data rather than change the preferred values [Note – the 1995 WG Appendix has 4.4 m, whereas their Table 1 has 4.5 m; based on the discussion, we infer they meant 4.5 m].

New evidence for the Mojave South includes additional work and analysis of the Wrightwood site (Fumal et al., 2002, Weldon et al., 2002, 2004, 2005; Biasi et al., 2002; Scharer 2005; Scharer et al., in press). Highlights include confirmation of the ~106 average interval for the past 1400 years, a similar (~109 year) average interval for

6

earthquakes between 2500 and 1000 BC, average displacement per event of ~3.7 meters and a slip rate of ~35 mm/yr.

The Littlerock site has also been completed since the 1995 Working Group report. While these data are only published in abstracts (Sickler et al., 2006; Weldon et al., 2005) the site supports a slip rate of ~36 mm/yr, three events in the past 3-400 years, and 18 +/- 2 m of slip associated with these 3 events. The average displacement in the past 3 events is greater than the ~4.5 m accepted by previous Working Groups (1988; 1995), but is consistent with observations at Pallett Creek (8.5 km to the SE; Salyards et al., 1992). Finally, the timing of what is inferred to be the third event back is consistent with the third earthquake back (Event V) at Pallett Creek (Sieh et al., 1989).

In addition, several new slip rate studies (Kenney and Weldon, 1999; Matmon, 2005) and kinematic modeling of the San Andreas system (e.g. Humphreys and Weldon, 1994) continue to support a geologic slip rate of 30-40 mm/yr.

For the purposes of this Working Group we adapt the Pallett Creek average interval of ~130 years for the Mojave South section. We agree with earlier Working Groups that Wrightwood is close enough to the section boundary (5-10 km) that it could include events from the south that do not rupture a significant portion of the Mojave South section. However, given the distance from the section boundary to Pallett Creek (almost 30 km) and the support of the Pallett Creek record emerging at Littlerock (almost 40 km from the section boundary), we believe the Pallett Creek record should be used for the average interval. Also, the separation of the old Mojave segment into Mojave North and South allows a progressive change from north to south on the San Andreas that earlier Working Groups were attempting to accommodate.

The slip rate and the average slip per event are more difficult to resolve. The ~3.7 m per event at Wrightwood appears to support the ~ 4 m value that earlier Working Groups have preferred, but if Wrightwood contains the tails of southern events that do not span the section then the Mojave South section average would be underestimated. The work at Littlerock is not formally published yet and the 6 m offsets at Pallett Creek (Salyards et al., 1992) have remained controversial. Such large offsets would appear to support the higher slip rate of ~36 mm/yr that all geologic studies (and the long term average of 160 km in 4.5 Ma) suggest, but geodetic observations are interpreted to favor a much lower rate of about 21 mm/yr (e.g. Meade et al., 2004). For this reason we continue to use a slip rate halfway between the geologic and geodetic results with an uncertainty large enough to span the preferred values of each. Similarly, we preserve the displacement per event of 4.5+/-1.5 from the 1995 Working Group because it spans the observations and its preferred value is more consistent with the adopted slip rate and average interval. The last earthquake was in 1857, as recognized by previous Working Groups, and the previous in 1812 (Dec 8th). The recognition of possible larger offset associated with 1812 makes it almost certain the 1812 earthquake spanned the entire section, and probably extended farther north than previous Working Groups inferred (as discussed above).

San Bernardino North Section – This section is the northern third of the 1988 and 1995 Working Groups' San Bernardino Mountains segment. It was meant to be "a structurally complex zone between the Mojave and Coachella Valley segments" and as such has too

complex a set of slip rates and average intervals to be described by a single section, so the current Working Group broke it into 3 sections. The current section extends from the southern end of the 1857 rupture (which is also adjacent to the northern end of the San Jacinto fault) to approximately City Creek, where secondary structures appear to transfer significant motion from the main San Andreas to faults within the San Bernardino Mountains, to the east (including the Northern strand of the San Andreas fault) and to the San Jacinto fault, to the south (including the Crafton Hills and other structures).

The 1995 Working Group report contains extensive discussion of the Wrightwood paleoseismic site, which is not on this section (in this report it is discussed with the correct Mojave South section). There is also discussion of the Pitman Canyon paleoseismic site, in particular noting that the past two events are likely to be 1812 and a prehistoric event around 1680-90 AD, as seen at Wrightwood to the north and in the Coachella Valley to the south, and ~ 4 m offset of a debris flow lobe by the 1812 rupture. By comparing the ages of events at Pallett Creek, Wrightwood, and Coachella Valley, the 1995 Working Group concluded that this section had some ruptures of its own and also shared longer ruptures from the north and south, and thus it was difficult to assign an average interval. Both the report and the more detailed appendix states that the new paleoseismic data are incorporated into the probability calculations, but Table 1 contains an average interval of 146 years, which is the characteristic slip divided by the slip rate [note - the appendix has "14 (+91, -60) yr," but presumably "14" was meant to be 146]. We agree that the broad region of slip transfer between the San Andreas and San Jacinto likely has complicated overlapping of events and all sites likely contain both the tails of distant ruptures and through-going ruptures, as discussed above for Wrightwood. The Pitman Canyon site is as close to the section boundary as the Wrightwood site is to the north of it (5-10 km), so it is as likely to be in an overlap zone between sections.

The 1995 Working Group accepted the existing slip rate of 24 mm/yr (but expanded the uncertainty to +/- 5 (from 3) mm/yr and reduced the characteristic slip to 3.5 (from the published and previously accepted 4) +/-1 m. No reason is given for the reduction ("new observations" are called upon to reduce the slip per event but the only new observation discussed is the ~4 m offset at Pitman Canyon). So by the logic of 1995 the average interval should have been 167 yr (4/0.024).

We use a value of ~175 yr based on the paleoseismic data at Pitman Canyon (supported by the tentative average rate at Lost Swamp, Weldon and Sieh, 1985, which is also on this section) and assume that 2 events there are due to overlap. Because final pdfs for the Pitman Canyon events were never formally published, we constructed composite pdfs from the slightly different preliminary values (see Biasi and Weldon manuscript for values and references) and used them in our correlation approach to determine the frequency of events for this section. We see no evidence to reduce the 4 m per slip value that was used by the 1988 Working Group. There appears to be little doubt that the last earthquake was in 1812 and it is likely that the previous was in 1680-90 AD, as documented to the north and south.

San Bernardino South Section - This section is the central third of the 1988 and 1995 Working Groups' San Bernardino Mountains segment, and as such it shared the values discussed above for the San Bernardino North section. As currently defined this section has two paleoseismic sites, Plunge Creek at the very northern end of the section (McGill

et al., 2002) and Burro Flat at the very southern end (Yule and Sieh, 2000; Yule et al., 2006, and Yule, pers. comm., 2006). These two sites can be interpreted to yield average intervals as short as ~100 (Burro Flat) to as long as 400 (Plunge Creek) years (see primary references or Biasi and Weldon manuscript for details).

An additional complication is that this section and the Banning/Garnet Hill section to the south, is surrounded by numerous active secondary faults and folds, and appears to be a region of more distributed deformation and smaller ruptures (Yule and Sieh, 2000), including events like the 1948 Desert Hot Springs on the Mission Creek strand of the San Andreas and 1986 North Palm Springs earthquakes on the Banning/Garnet Hill section. Thus, these two sections were surrounded by a C-zone (see Appendix on the Fault Section Database) to allow for additional small ruptures on and off the main San Andreas fault. This may in part explain the greater frequency of events seen at the Burro Flat site as compared to the Plunge Creek site.

We assign an average interval of 200 years, assuming that approximately half of the Burro Flat ruptures are segment filling events; this rate is also approximately consistent with the Plunge Creek site. The additional events seen at Burro Flat are assumed to span a range of sizes, as described by the recurrence distribution of C-zones. The last earthquake was almost certainly 1812. While McGill et al. (2002) found no evidence for 1812, more recent work by Yule et al. (2006), using pollen to refine C-14 dates, appears to confirm the presence of the 1812 event at Burro Flat. If rupture reached Burro Flat in 1812, either the Plunge Creek site did not record or was skipped by rupture or the evidence at Burro Flat is from a smaller local earthquake. The bulk of the available evidence, combined with the ~4 meter displacements on the northern San Bernardino section and the distribution of shaking (e.g. Fumal et al, 1992), overall supports the inference that 1812 extended to the southern boundary of this section.

Banning/Garnet Hill Section - This section is the southern third of the 1988 and 1995 Working Groups' San Bernardino Mountains segment, and as such shared the values discussed in the San Bernardino North segment in previous Working Groups. As discussed in the Fault Section database, the southern boundary (to the Coachella section) has been moved south slightly to the junction of the Banning and Mission Creek faults (the southern and northern strands of the San Andreas fault). There are no paleoseismic sites on this section, although the Burro Flat site is immediately to the northwest of it on the San Bernardino South section (discussed above) and the Thousand Palms site (Fumal et al., 2002 discussed below) is on the Mission Creek strand of the San Andreas adjacent to the southern end of the Banning/Garnet Hill section.

Due to the low slip rate on this section, it appears unlikely that the ~100 year average interval at Burro Flat can apply to this section unless many of the ruptures have small displacements (and thus short lengths). In addition, given that the slip rate on this section is less than the sections to the north and south (in most deformation models; see the Fault Section database) it is impossible to build a multi-section rupture model that includes this section and adjacent sections without this section moving less frequently than the higher slip rate adjacent sections, thus contradicting its apparently shorter average interval (IF the average interval is similar to Burro Flat's). So we conclude that this section must have additional smaller ruptures associated with the C-zone that spans this section and the San Bernardino South section. This hypothesis was initially proposed

by Yule and Sieh, 2000, may be supported the very high seismicity associated with this region and the widely distributed deformation. Based on the correlation modeling of Biasi and Weldon, we assign an average interval of ~225 years for section filling and multi-section ruptures.

Coachella Section - The northern boundary of the Coachella section was moved to the junction of the Banning-Garnet Hill fault zone and Mission Creek/North Branch of the San Andreas fault, as described in the Fault Section Database. The 1988 and 1995 Working Groups discuss the Indio paleoseismic record, which yields an average interval of ~220 years (Sieh, 1986). However, they use a slip rate of 25 mm/yr and a characteristic slip per event of 4 m (imported Cajon Creek on the northernmost portion of the San Bernardino North section – Weldon and Sieh, 1985) to calculate the average interval of 160 years. Since 1995 the Thousand Palms site on the Mission Creek strand of the fault (immediately north of the section boundary) has been published (Fumal et al., 2002) and two new sites, Coachella (Philibosian et al., 2006) and Salt Creek (Williams and Seitz, 2004; pers comm. 2006) at the northern and southern ends of the Coachella section, respectively, are currently being developed. While the Thousand Palms site provides a well characterized average interval of ~212 years and the timing of the dated events essentially match those at Indio (Sieh, 1986), there has been some reluctance to accept this value because the site is on only one strand of the fault.

More recent work near Coachella (Philibosian et al., 2006) confirms the dates of the 5 earthquakes at Thousand Palms (Fumal et al., 2002) and Indio (Sieh, 1986), but also finds evidence for an additional earthquake during the past 1200 years that might have been missed at the other sites. This possible extra event may be supported by the number of events recognized at the Salt Creek site during the past 1200 yrs (Williams and Seitz, 2004; pers. comm. 2006). Given the excellent match in ages of the 5 events at Indio, Coachella and Thousand Palms, and the fact that the Indio, Coachella, and Salt Creek sites are only published in abstracts, we adopt the Thousand Palms average interval of ~212 years.

Rupture rates

Rupture rates of all possible section combinations were developed from the geologic data developed above, the rules for developing Geologic Insight, Maximum and Minimum rate models for all A faults, and an automated correlation process developed by Biasi and Weldon (BSSA manuscript included below). It is important to recognize that the Biasi and Weldon correlation approach was simply used as a tool to develop the rupture model presented here. All Geologic Insight models for A fault were developed by expert opinion, which includes intuition informed by experience and interpretation of the available data. An "expert" will consider whether the ages of paleo-events overlap enough across section boundaries to be the same earthquake or not, or whether their displacements are similar enough to be a single rupture, or whether the cumulative number of events or slip in a period of time makes it likely that sections share events. To aid this process, and to cover the wide range of possible correlations allowed by the large dataset for the Southern San Andreas fault, Biasi and Weldon developed an automated correlation process, and then ranked the possible correlations in order of consistency with the data. A subset of the highest ranked scenarios produced by this automated process was considered and a Geologic Insight model for the southern San Andreas fault was developed from it and the general A fault geologic insight rules.

Tables 1 and 2 present the current Working Groups estimates of all possible segment filling ruptures for the southern San Andreas fault. The Maximum and Minimum rate models in Table 1 were constructed by the same process used for all A faults, described elsewhere in this report. Table 2 shows the same geologic insight recurrence model in a more intuitive format; entries are a) the number of ruptures of a particular magnitude that a section participates in during a 10,000 year period, and b) the recurrence interval of earthquake that the section participates in. In all cases the net average interval for earthquakes in each section is made to be consistent with that discussed in the geologic data section.

Table 1a. Southern San Andreas rupture rates. Sections are Parkfield (PK), Cholame (CH), Carrizo Plain (CC), Big Bend (BB), North Mojave (NM), South Mojave (SM), North San Bernardino (NSB), South San Bernardino (SSB), Banning/Garnet Hill (BG), and Coachella (CO).

Rupture Rates (per year)	Geologic Insight	Minimum Rate	Maximum Rate
PK	0.03460	0.03431	0.04072
CH	0.00005	0.00000	0.00635
CC	0.00030	0.00000	0.00635
BB	0.00030	0.00000	0.00561
NM	0.00020	0.00000	0.00625
SM	0.00050	0.00110	0.00751
NSB	0.00070	0.00000	0.00561
SSB	0.00005	0.00000	0.00500
BG	0.00050	0.00000	0.00444
CO	0.00250	0.00000	0.00472

Rupture Rates (per year)	Geologic Insight	Minimum Rate	Maximum Rate
PK+CH	0.00160	0.00080	0.00000
CH+CC	0.00030	0.00000	0.00000
CC+BB	0.00001	0.00000	0.00000
BB+NM	0.00001	0.00000	0.00000
NM+SM	0.00070	0.00000	0.00000
SM+NSB	0.00060	0.00000	0.00000
NSB+SSB	0.00080	0.00000	0.00000
SSB+BG	0.00090	0.00000	0.00000
BG+CO	0.00070	0.00000	0.00000
PK+CH+CC	0.00070	0.00000	0.00000
CH+CC+BB	0.00001	0.00000	0.00000
CC+BB+NM	0.00001	0.00000	0.00000
BB+NM+SM	0.00025	0.00000	0.00000
NM+SM+NSB	0.00010	0.00000	0.00000
SM+NSB+SSB	0.00040	0.00000	0.00000
NSB+SSB+BG	0.00040	0.00000	0.00000
SSB+BG+CO	0.00040	0.00000	0.00000
PK+CH+CC+BB	0.00040	0.00000	0.00000
CH+CC+BB+NM	0.00001	0.00000	0.00000
CC+BB+NM+SM	0.00040	0.00000	0.00000
BB+NM+SM+NSB	0.00001	0.00000	0.00000
NM+SM+NSB+SSB	0.00020	0.00080	0.00010
SM+NSB+SSB+BG	0.00030	0.00000	0.00000
NSB+SSB+BG+CO	0.00040	0.00000	0.00000
PK+CH+CC+BB+NM	0.00070	0.00000	0.00000
CH+CC+BB+NM+SM	0.00050	0.00000	0.00000
CC+BB+NM+SM+NSB	0.00010	0.00000	0.00000
BB+NM+SM+NSB+SSB	0.00005	0.00000	0.00000
NM+SM+NSB+SSB+BG	0.00010	0.00000	0.00000
SM+NSB+SSB+BG+CO	0.00040	0.00000	0.00000
PK+CH+CC+BB+NM+SM	0.00200	0.00070	0.00010
CH+CC+BB+NM+SM+NSB	0.00001	0.00000	0.00000
CC+BB+NM+SM+NSB+SSB	0.00010	0.00000	0.00000
BB+NM+SM+NSB+SSB+BG	0.00001	0.00000	0.00000
NM+SM+NSB+SSB+BG+CO	0.00010	0.00000	0.00000
PK+CH+CC+BB+NM+SM+NSB	0.00050	0.00000	0.00000
CH+CC+BB+NM+SM+NSB+SSB	0.00005	0.00000	0.00000
CC+BB+NM+SM+NSB+SSB+BG	0.00005	0.00000	0.00000
BB+NM+SM+NSB+SSB+BG+CO	0.00005	0.00000	0.00000
PK+CH+CC+BB+NM+SM+NSB+SSB	0.00010	0.00000	0.00000
CH+CC+BB+NM+SM+NSB+SSB+BG	0.00001	0.00000	0.00000
CC+BB+NM+SM+NSB+SSB+BG+CO	0.00001	0.00000	0.00000
PK+CH+CC+BB+NM+SM+NSB+SSB+BG	0.00005	0.00000	0.00000
CH+CC+BB+NM+SM+NSB+SSB+BG+CO	0.00001	0.00000	0.00000
PK+CH+CC+BB+NM+SM+NSB+SSB+BG+CO	0.00010	0.00500	0.00000
TOTAL	0.05421	0.04271	0.09203

Note 1: *If less frequent than 0.00001, set = 0.00001. In subsequent analysis (see Appendix G), all of these were set as "unlikely" for consistency with other A faults.*

Table 1b. Recurrence intervals of ruptures in the S. San Andreas.

Rupture Recurrence Intervals	Geologic Insight	Minimum Rate	Maximum Rate
PK	29	29	25
CH	20000	na	157
CC	3333	na	157
BB	3333	na	178
NM	5000	na	160
SM	2000	910	133
NSB	1429	na	178
SSB	20000	na	200
BG	2000	na	225
CO	400	na	212
PK+CH	625	1250	na
CH+CC	3333	na	na
CC+BB	100000	na	na
BB+NM	100000	na	na
NM+SM	1429	na	na
SM+NSB	1667	na	na
NSB+SSB	1250	na	na
SSB+BG	1111	na	na
BG+CO	1429	na	na
PK+CH+CC	1429	na	na
CH+CC+BB	100000	na	na
CC+BB+NM	100000	na	na
BB+NM+SM	4000	na	na
NM+SM+NSB	10000	na	na
SM+NSB+SSB	2500	na	na
NSB+SSB+BG	2500	na	na
SSB+BG+CO	2500	na	na
PK+CH+CC+BB	2500	na	na
CH+CC+BB+NM	100000	na	na
CC+BB+NM+SM	2500	na	na
BB+NM+SM+NSB	100000	na	na
NM+SM+NSB+SSB	5000	1251	10010
SM+NSB+SSB+BG	3333	na	na
NSB+SSB+BG+CO	2500	na	na
PK+CH+CC+BB+NM	1429	na	na
CH+CC+BB+NM+SM	2000	na	na
CC+BB+NM+SM+NSB	10000	na	na
BB+NM+SM+NSB+SSB	20000	na	na
NM+SM+NSB+SSB+BG	10000	na	na
SM+NSB+SSB+BG+CO	2500	na	na
PK+CH+CC+BB+NM+SM	500	1430	10010
CH+CC+BB+NM+SM+NSB	100000	na	na
CC+BB+NM+SM+NSB+SSB	10000	na	na
BB+NM+SM+NSB+SSB+BG	100000	na	na
NM+SM+NSB+SSB+BG+CO	10000	na	na
PK+CH+CC+BB+NM+SM+NSB	2000	na	na
CH+CC+BB+NM+SM+NSB+SSB	20000	na	na

Rupture Recurrence Intervals	Geologic Insight	Minimum Rate	Maximum Rate
CC+BB+NM+SM+NSB+SSB+BG	20000	na	na
BB+NM+SM+NSB+SSB+BG+CO	20000	na	na
PK+CH+CC+BB+NM+SM+NSB+SSB	10000	na	na
CH+CC+BB+NM+SM+NSB+SSB+BG	100000	na	na
CC+BB+NM+SM+NSB+SSB+BG+CO	100000	na	na
PK+CH+CC+BB+NM+SM+NSB+SSB+BG	20000	na	na
CH+CC+BB+NM+SM+NSB+SSB+BG+CO	100000	na	na
PK+CH+CC+BB+NM+SM+NSB+SSB+BG+CO	10000	200	na
TOTAL	18	23	11

Note 2: *The "total" is dominated by Parkfield (and Parkfield events that are inferred to include Cholame). Excluding these the RI would be about 70 years. While 70 years might seem unlikely given the current open interval of 150 yrs, the ~70 yr interval ending in 1857 contained at least 3 earthquakes (~1690, 1812, and 1857) and possibly 4 (if there are two 1812 events on the SSAF).*

While the Maximum and Minimum rate models presented in Table 1 are considered very unlikely, based on the logic developed to generate absolutely limiting rate models, they are possible. The Minimum Rate model that essentially forces as many ruptures as possible to span the entire fault zone builds on "wall-to-wall" scenarios published by Sieh et al. (1989), Grant and Sieh (1994), and Weldon et al. (2004; 2005). All of these papers note the similarity in timing of events at many paleoseismic sites along the fault. While such earthquakes that span the entire southern San Andreas are much longer than the two historic ruptures and require average displacements larger than most observed, they are not completely ruled out by the sparse data for prehistoric events. Similarly, the Maximum Rate model that requires essentially all ruptures occur on single sections may be supported by the similarity of timing of paleoseismic events along the fault, as well. If the southern San Andreas fault can rupture in a progressive series like the North Anatolian and Xianshuihe faults have this century, the currently available C-14 dating would not be able to distinguish such a series from a single long rupture, thus yielding the generally overlapping paleoseismic dates. While the historic record and the available displacement data do not appear to support this model, the number and quality of coseismic displacements are low enough to permit it, and the historic record of 1812 and 1857 AD could be unusually long and at the end of a hypothetical temporal cluster.

Table 2a. Number of quakes in a 10,000 year period that each section participates in; for the "Geologic Insight" Model.

Section	≤7.1	7.1-7.4	7.4-7.7	7.7-8.0	≥8.0
PK	366.0	1.5	9.0	29.0	2.0
CH	17.0	7.9	9.6	34.3	2.3
CC	2.0	9.6	14.7	35.1	2.7
BB	5.0	1.0	4.1	44.9	2.9
NM	2.0	3.6	12.1	44.4	2.9
SM	1.0	11.5	16.5	46.4	2.9
NSB	11.0	9.0	16.5	17.4	2.9
SSB	4.5	15.0	16.5	11.3	2.9
BG	5.0	14.5	15.0	8.1	2.2
CO	25.0	3.5	11.5	5.3	1.4

Table 2b. Recurrence intervals for earthquakes that each section participates in; for the "Geologic Insight" Model.

Section	≤7.1	7.1-7.4	7.4-7.7	7.7-8.0	≥8.0
PK	27	6667	1111	345	5000
CH	588	1266	1042	292	4348
CC	5000	1042	680	285	3704
BB	2000	10000	2469	223	3448
NM	5000	2778	826	225	3448
SM	10000	870	606	216	3448
NSB	909	1111	606	575	3448
SSB	2222	667	606	885	3448
BG	2000	690	667	1235	4545
CO	400	2857	870	1905	7143

With the exception of Parkfield (that is based on the historical record), the dominant mode of rupture for the northern part of the fault is large 1857-like event that occur every 2-300 years. There is a much greater diversity in rupture sizes and types for the southern part of the southern San Andreas fault, which is strongly driven by the relatively low and variable slip rates between the sections. For example, only about half of the events on the Coachella section extend north because the slip rate drops by about ½ to the north due to the transfer of strain to the Central CA shear zone (see Appendix A for deformation models); age control alone (e.g. Fumal et al. 2002b) would suggest a larger number of events correlating between the Coachella Valley and sections to the north. Similarly, the progressive decrease in slip rate from the Southern Mojave to the North and South San Bernardino sections to the Banning/Garnet section (due to slip transfer to the San Jacinto fault) produces smaller and more variable ruptures to accommodate the rapidly changing slip rates. If the deformation model that was used to assign slip rates were incorrect, then the results would change considerably.
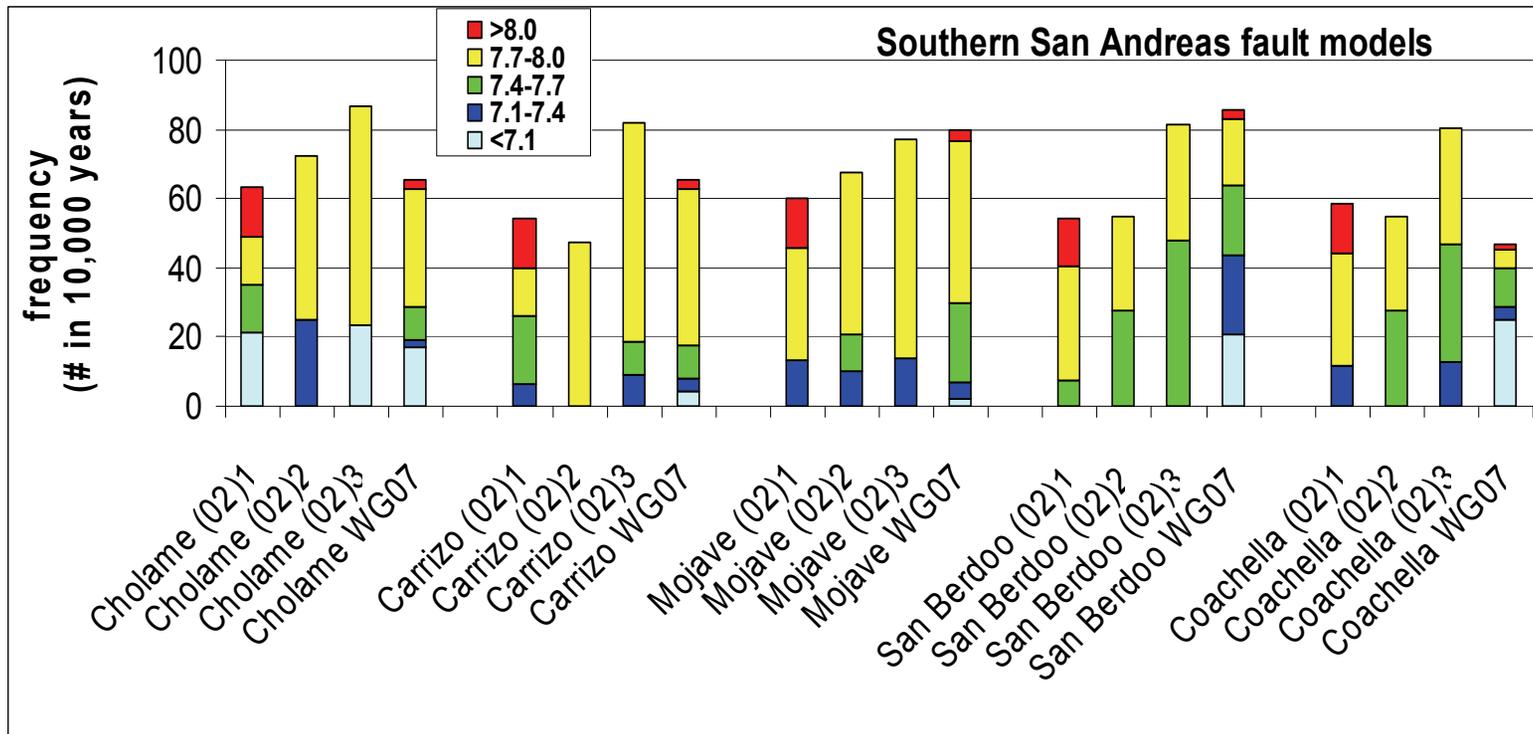
Figure 1. Comparison of the current "Geologic Insight model" with the three models adopted by the National Seismic Hazard Map 2002. Because there are more fault segments in the current model than 2002, we plot both results in the segmentation scheme of 2002 by combining the earthquakes on the current shorter segments. In general the results compare well but the current model has a greater diversity of earthquake sizes and rupture distributions than 2002, fewer very large earthquakes, more earthquakes in the central part of the southern San Andreas and fewer on the ends.
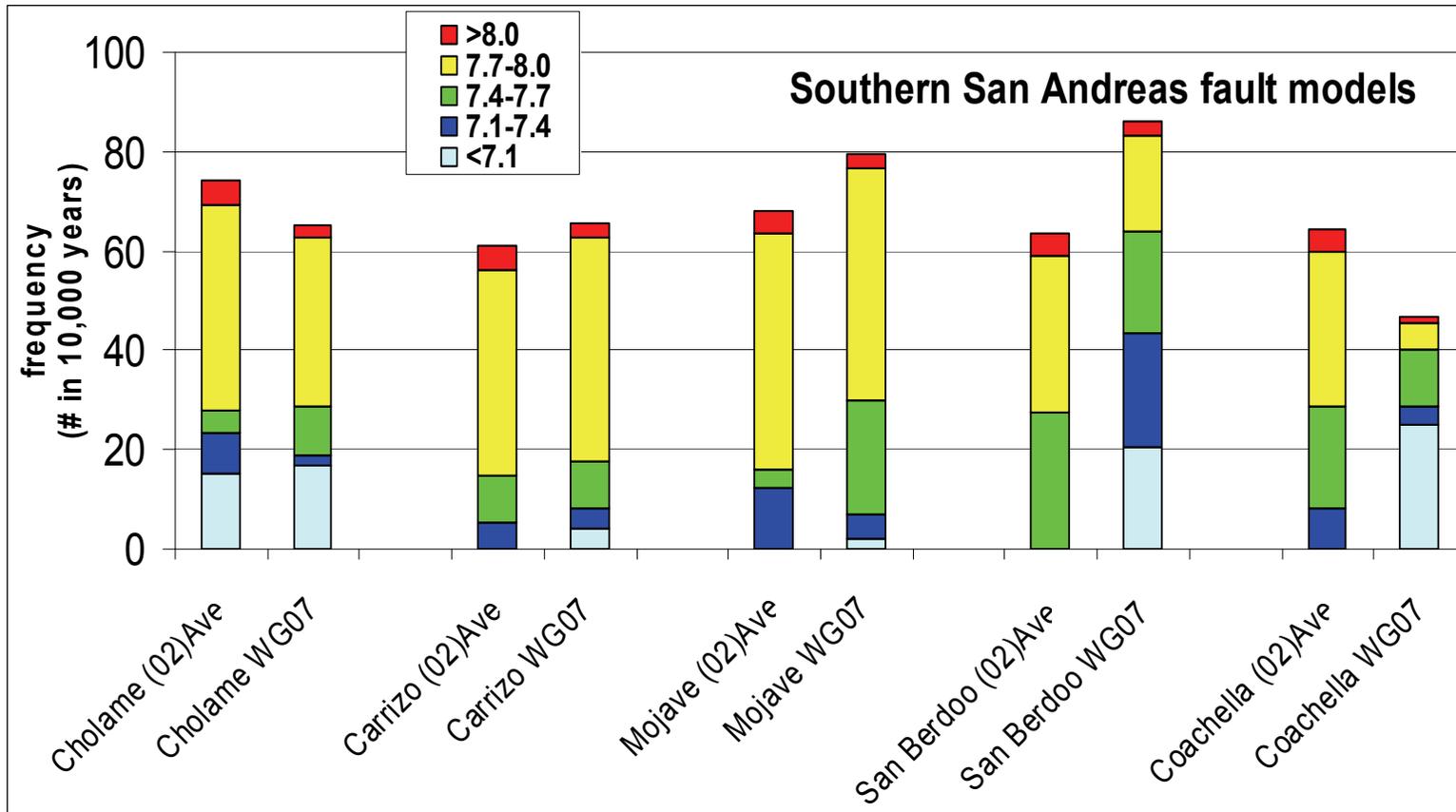
Figure 2. Comparison of the current "Geologic Insight model" with the average of the three models adopted by the National Seismic Hazard Map 2002. Because there are more fault segments in the current model than 2002, we plot both results in the segmentation scheme of 2002 by combining the earthquakes on the current shorter segments. The greatest differences are an increase of earthquakes in the Mojave and San Bernardino region and generally smaller and more diverse ruptures on the southern half of the southern San Andreas. **Note: This figure is not directly comparable to Figure 34 in the Main Report because here we plot the probability of an earthquake including any portion of the 2002 segments, so that we can compare our results to the NSHM. Figure 34 in the Main Report shows the probability of a rupture at any point along the fault. For the old San Bernardino segment (includes current North San Bernardino, South San Bernardino, and Banning/Garnet Hill sections) there is a lesser probability of an event occurring at any point along the fault, but because we have a much greater diversity of smaller earthquakes in the current model, there is a slightly greater probability that some portion of the old San Bernardino segment will rupture.**

The results are similar to previous characterizations of the southern San Andreas fault, but also include significant differences, as seen in Figures 1 and 2, comparing our model to the three models adopted by the National Seismic Hazard Map in 2002. Overall, the number of events is similar, with the Cholame and Coachella sections lower in our model and the Mojave and San Bernardino higher. The sections with lower rates are lower because of decreased slip rate on the fault; in part because the slip rate on the Coachella section has been reduced to add slip rate to the San Jacinto fault (see section on deformation models), and because all slip rates are reduced by 10% to allow for aftershocks, postseismic slip and other non-main shock processes (Appendix D). The Mojave section increases despite this reduction in rate because the short average intervals observed at the Pallett Creek and Wrightwood paleoseismic sites was not fully honored in previous models. Finally, the San Bernardino section increases because we have divided the section into multiple sections with different slip rates. This was done to accommodate transfer of slip from the San Andreas to the San Jacinto fault and to reduce the slip rate on the San Andreas through the San Gorgonio Pass region (see deformation models). The lower slip rates and additional sections with different slip rates induce an increase in the number and diversity of smaller earthquake; thus increasing the number of earthquakes in this region, even though the net moment release is much smaller. Finally, there are fewer very large earthquakes in our model than past models. Again, this is due to the very low slip rate through the southern San Bernardino and San Gorgonio Pass region, which effective stops most northern earthquakes (like 1857 and 1812). While the timing of many paleoearthquakes north and south of the San Bernardino and San Gorgonio Pass regions are similar (Fumal et al., 2002b) the low slip rate precludes frequent through-going ruptures. Thus, if the low slip rate currently adopted by the Working Group were to be found to be in error, more ruptures would correlate through this area, decreasing the overall number of events on the San Andreas fault south of the Mojave but increasing their size.

30-Year Conditional Probabilities

Figure 3 shows the 30-yr conditional probability of rupture of M > 6.7 on each section of the southern San Andreas fault. Colors indicate the different size ruptures that are expected to occur. Since most ruptures span multiple sections of the fault, the total probability of a rupture M ≥ 6.7 is ~0.59, only about twice the average section value. A distinctive aspect of the current model is that the probability is higher at both ends of the fault and that the ends have a much greater fraction of smaller events. This makes physical sense in that both ends of the fault are transitions into creeping regions (the Creeping section to the north and the Brawley Seismic zone to the south) that produce small earthquakes. The central section, Mojave South, has a slightly higher conditional probability than its neighbors due to overlap of many large earthquakes in this region. With the exception of the smaller earthquakes on the ends, probabilities are dominated by large 1857-type events (M ~ 7.9).

There is a significant difference in the likelihood of large (M 7.7-8.0) earthquakes along the fault from north to south, with relatively few M 7.7-8.0 expected at the southern end. This is a function of several reinforcing properties of the current model, including 1) the decrease in slip rate on the fault, reaching a minimum in the San Gorgonio Pass region (Banning/Garnet section), 2) The general lack of agreement in timing of prehistoric earthquakes north and south of the southern termination of the 1857 rupture (at Mojave South), 3) The lack of paleoseismic records from the central part of the 1857 rupture, so modeled events tend to span the entire region from Parkfield to Mojave South, and 4) The presence of the 1812 rupture on the relatively slowly slipping San Bernardino sections. The big jump in conditional probability from San Gorgonio Pass to the Coachella is due to the large jump in slip rate (due to merging of the Eastern California shear zone with the southernmost San Andreas) and the long time (≥300 years) since the last earthquake. This discontinuity also requires that the most likely Coachella rupture is ~ M 7 because it is unlikely to extend through the low slip rate and fairly recently ruptured San Bernardino and Banning/Garnet sections.

Due to the increase in the number of sections on the southern San Andreas fault and differences in methodology, it is difficult to exactly compare our current model exactly to pre-existing models. To approximately compare we have lumped our ruptures into the sections of UCERF 1.0, which is basically the time dependent portion of the 2002 National Seismic Hazard Map model (labeled "02" on Figure 4). The most significant difference (which is only partially evident in Figure 4) is the much greater diversity of ruptures in the current model. There are 55 discrete single or multi-section ruptures and additional unsegmented "floating" ruptures (that add 4% of the conditional probability). UCERF 1.0 contained 10 distinct rupture types (split into 3 models), but is dominated by single section and 1857-type ruptures. In general, UCERF 1.0 has slight higher conditional probabilities per section, particularly for the Cholame section that had many smaller events to "fill in" the tail in displacement seen in the 1857 rupture. Higher probabilities on the Carrizo, Mojave and San Bernardino sections were due to more single section ruptures in UCERF 1.0. Also, note that in the current model the Parkfield

19

section participates with other sections in larger events, as it did in the 1857 earthquake, whereas it does not in UCERF 1.0.

There are also significant differences in M < 6.7 earthquakes, shown in Figure 5. Most significantly, because Parkfield recently ruptured, the conditional probability has decreased from UCERF 1.0. In addition, there are finite (although small; note the scale change on Figure 5) probabilities of earthquakes less than M 6.7. This is due to smaller sections, especially in the San Bernardino region, the high probability of a Coachella event coupled with its small size, the C-zone in San Gorgonio Pass to capture distributed deformation along the San Andreas, and to a lesser extent the widely distributed presence of the unsegmented floating earthquake.
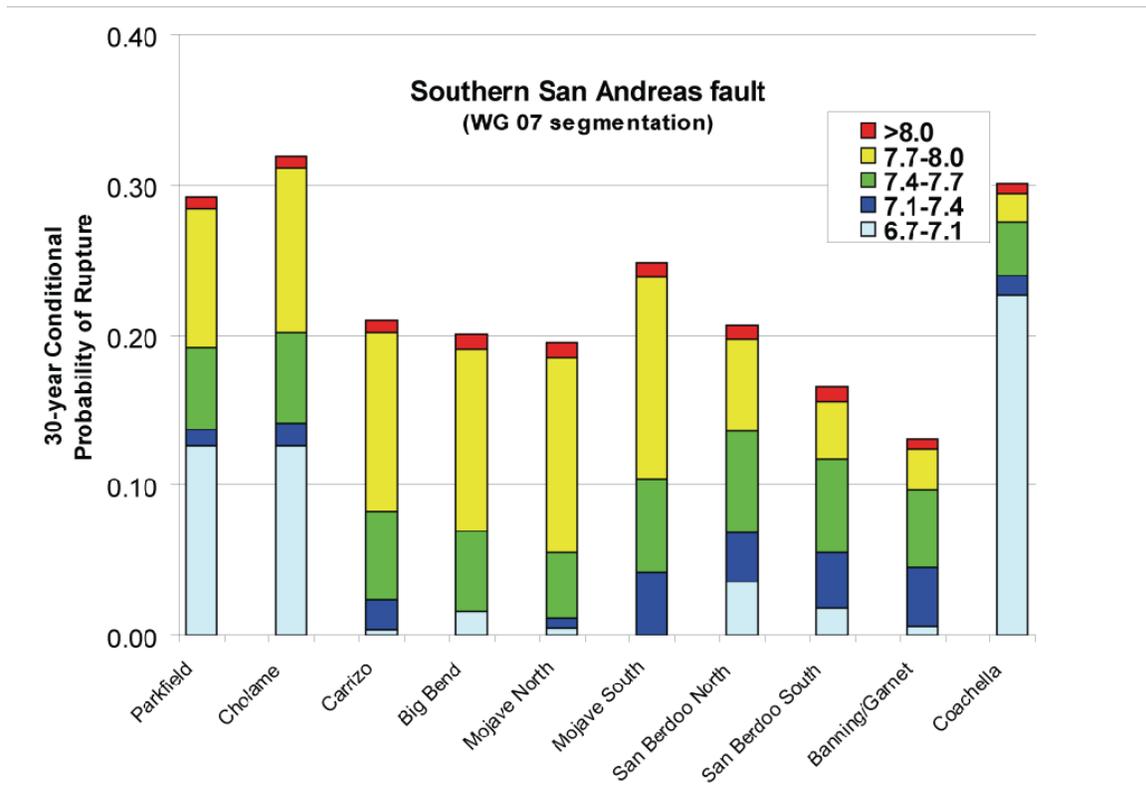
Figure 3. 30 yr conditional probability of an earthquake greater than M 6.7 rupturing the section. Colors indicate the relative probability of the size of the earthquake.
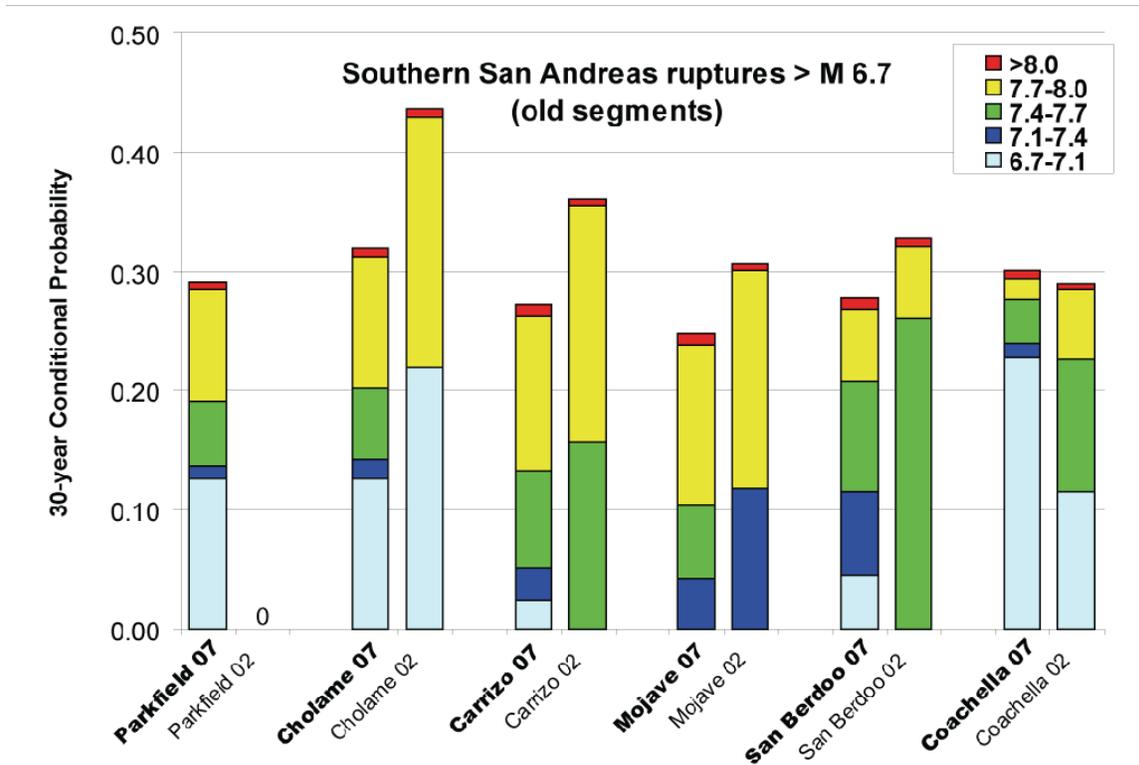
Figure 4. Comparison of 30 yr conditional probability of an earthquake greater than M 6.7 including the section. Colors indicate the relative probability of the size of the earthquake. Note that the combination of the three San Bernardino sections into the old San Bernardino segment, significantly raises the conditional probability over the individual values shown in Figure 3. **Note: This figure is not directly comparable to Figure 34 in the Main Report because here we plot the probability of an earthquake including any portion of the 2002 segments, so that we can compare our results to the NSHM. Figure 34 in the Main Report shows the probability of a rupture at any point along the fault. For the old San Bernardino segment (includes current North San Bernardino, South San Bernardino, and Banning/Garnet Hill sections) there is a lesser probability of an event occurring at any point along the fault, but because we have a much greater diversity of smaller earthquakes in the current model, there is a slightly greater probability that some portion of the old San Bernardino segment will rupture.**

**Figure 5.** Comparison of 30 yr conditional probability of an earthquake less than M 6.7 including the section. Note the scale change from Parkfield to other sections. Zeros indicate columns with 0 conditional probability in previous model. The decrease in Parkfield is due to the 2004 event, and the increase in the San Bernardino and Coachella sections is due to the smaller section lengths.

Modifications of the Biasi and Weldon Method for the Working Group

The Biasi and Weldon methodology discussed below is an automated correlation process for paleoseismic data. Because we wanted the southern San Andreas fault to have a model consistent with those generated for all the other A faults, we have adjusted the results based on information and inferences pertinent to the Working Group are not included in the B&W analysis.

First, we applied the multiple deformation models adopted by the Working Group to generate multiple models that satisfy the slip rate along strike.

Second, we segmented the unsegmented scenarios generated by the Biasi and Weldon approach. Segmenting the inherently unsegmented scenarios cause several problems that are subsequently adjusted by hand. For example, the Wrightwood site has experienced more earthquakes in the past 1400 years than the sites to the north or south; in the Biasi and Weldon methodology these extra earthquakes occur as small earthquakes on the boundary between the Mojave south and San Bernardino North sections and cannot be assigned to either the Mojave South or San Bernardino North sections in the Working Group's segmented model. Because the current Working Group methodology requires one recurrence interval per section, and past Working Groups have inferred that because Wrightwood is very close to the segment boundary, extra events may actually be slightly overlapping ruptures from the nearby San Bernardino North section, or perhaps "background" events that do not fill a section, and thus are already in the segmented model. So we remove some of these extra events from the Working Group's segmented model, keeping the average earthquake interval equal to the value at Pallett Creek, which is on the same section as Wrightwood. Further discussion of which paleoseismic sites are inferred to represent the section behavior in the Working Group's segmented model are discussed in the section entitled "Review of Geologic data".

Third, we modify the results to apply several additional rules developed for all A faults that are not part of the Biasi and Weldon methodology. These include a) allowing all single and multiple segment rupture possibilities (some were not found in the Biasi and Weldon scenarios), b) all models must include historical events (so the historic 1812 and 1857 we added to each scenario), and c) all models must have reasonable weight for all published scenarios. For example, "wall-to-wall" earthquakes that rupture the entire southern San Andreas fault are quite rare due to the low slip rate through the San Gorgonio Pass and San Bernardino sections, and do not occur at all for the deformation model with the lowest slip rate, but because they are part of the published literature they are included in all deformation models.

Fourth, the scenarios generated by the Biasi and Weldon methodology are constructed from a limited time interval of approximately 1400 years (the period of time covered by history and reasonably complete paleoseismic data). It is unlikely that such a short time period is completely representative of the range of possible fault behavior, so we smoothed the results to allow ruptures similar to those observed to be represented at a similar rate to those actually observed. For example, 1857 events occur quite frequently in the scenarios so by smoothing we infer that similar events (adding or subtracting one

or two sections on each end) occur at reasonably similar frequencies. This also helps reduce the impact of irregularly spaced paleoseismic sites that do not well sample all the sections, and thus prevent distinguishing between similar ruptures in a segmented model. It also helps remove biases due to segmentation of the unsegmented Biasi and Weldon model (see Appendix to Biasi and Weldon MS).

Fifth, we attempted to span a range of possibilities for several parameters and scaling relationships that are uncertain or were not finalized at the time the scenarios were made. For example, we generated scenarios with two rupture length to average displacement relationships (Wells and Coppersmith, 1994 and Hanks and Bakun, 2002), and considered a variety of rupture displacement shapes including boxcars (the average displacement occurs along the entire length of the rupture) and the square root of sine shape developed from an empirical dataset (as described in the Biasi and Weldon manuscript).

Sixth, information for several sections, Parkfield, Cholame, Big Bend, and the overlapping C-zone on the San Gorgonio/Garnet Hill section is not explicitly built into the Biasi and Weldon scenario-making methodology because the behavior of these sections include inferences that are not paleoseismic. So the results from the Biasi and Weldon methodology need to be adjusted to reflect additional information or assumptions specific to individual sections. These explicit assumptions and inferences are discussed in the "Review of Geology data" section.

Finally, the Biasi and Weldon scenario-making methodology permits ranking possible scenarios by several different criteria, and one of the criteria, cumulative displacement, depends upon the specific deformation model (because slip rate along the fault is used to determine what the best cumulative displacement would be for a series of events). If all of the various ranking possibilities and deformation models are explored the number of scenarios to consider becomes overwhelming and include many scenarios that are extremely unlikely to be real. For example, if one ranks scenarios by how well they fit the age control of the paleo-earthquakes (and ignore all other criteria) one would find that the top ranked scenarios would be those that are constructed from single segment ruptures because the C-14 ages of paleo-earthquakes are not exactly the same from segment to segment; so the best age match has a different earthquake for each paleo-earthquake at each site. Clearly, scenarios made largely from single segment ruptures are unlikely to match other criteria, like cumulative displacement or consistency with the (long) open interval because their displacements will be too small and there will be too many events, respectively. In addition, this particular extreme possibility is already considered in our hand-built Maximum Rate model, which allows every segment to rupture independently. Alternatively, if one chose scenarios that have the fewest events (i.e. best fit the long open interval) one would have many ruptures that would span the entire fault and have too much displacement and poor matches to the variable age control (and this particular extreme model is already covered by our hand-built Minimum Rate model).

Thus, we established thresholds for all criteria (as described in the Biasi and Weldon, in review) so we can limit our consideration to scenarios with reasonable values for all ranking criteria. The thresholds we applied include no more than 26 earthquakes in the past 1350 years (an average interval of about 50 years, which has about a 5% chance

24

of being consistent with the open interval), a cumulative displacement (measured in 10 km increments along the fault) within 7 meters (approximately the maximum displacement seen in a single event) of what would be predicted by the deformation model, and age overlap of at least 5% of the individual C-14 pdfs with the assigned age for the event (see Biasi and Weldon manuscript for details).

Once minimum thresholds were established the range of possible scenarios was narrowed considerably. For example, consider Table 3, which shows the probability of rupture extent for all ruptures in the top 25 scenarios for each deformation model ranked by the criteria discussed above. The age range in this model is from approximately 600 AD to the present.

Table 3 is read as the number of ruptures with its northern end on the section listed vertically that has its southern end at the section listed horizontally. So for deformation model 2.1 about 14 ruptures that extend as far north as Parkfield extended as far south as the Mojave section. While the values differ somewhat by model, all models suggest that the most likely rupture that extends as far north as Parkfield ends at the southern Mojave. This is exactly what 1857 did, suggesting that 1857-like ruptures are well represented in the paleoseismic dataset. [Note that when we segment our ruptures into the Working Group segmentation scheme we give every single or multiple segment rupture a minimum value of 10% of the lowest observed, as we did for all other A faults.]

From the limited suite of scenarios consistent with our threshold criteria we generated sets of highly ranked scenarios and summary tables like shown in Table 3. Scenarios were ranked by 1) consistency with cumulative displacement (essentially consistency with slip rate along the fault), 2) consistency with age control (best match to the C-14 data, adjusted for multi-site bias as described in the Biasi and Weldon manuscript), and 3) fewest events to satisfy the data (i.e. most consistent with the long open interval). We also explored using consistency with displacement data for individual events, minimizing the range of individual displacements at a site (i.e. require characteristic slip), and limiting the largest or smallest displacement seen at a site. We concluded that the available data are currently inadequate to significantly distinguish (rank) scenarios by these additional criteria. For each of these criteria we generated a set for each of the three deformation models. Using the "geologic insight" provided by the ~500 most highly ranked scenarios and 9 summary tables, and the additional rules for A faults (discussed above), we constructed the "geologic insight" model presented in Tables 1 and 2.

Table 3. Probability of rupture extent in a selected set of scenarios.
(Modified from Biasi and Weldon, in review BSSA)

10000*annual prob of rupture, 1400 years per scene, 100 scenes 140000 total years

Model 2.1f	Pkfl	Chol	Carr	BBnd	MojN	MojS	NSBr	SSBr	SGor	Coac	Total
Pkfl	0.29	0.29	0.29	3.19	8.28	14.05	0.68	0.95	0.29	0.29	28.57
Chol	0.00	0.02	2.17	0.02	0.02	0.02	0.02	0.02	0.02	0.02	2.36
Carr	0.00	0.00	1.87	0.06	0.06	1.59	1.32	0.90	0.35	0.06	6.21
BBnd	0.00	0.00	0.00	0.02	0.02	2.28	0.02	0.02	0.02	0.02	2.43
MojN	0.00	0.00	0.00	0.00	0.03	1.05	0.91	0.28	0.56	0.03	2.86
MojS	0.00	0.00	0.00	0.00	0.00	3.36	6.86	3.71	5.14	0.86	19.93
NSBr	0.00	0.00	0.00	0.00	0.00	0.00	15.00	21.14	4.64	4.57	45.36
SSBr	0.00	0.00	0.00	0.00	0.00	0.00	0.00	0.29	9.57	4.71	14.57
SGor	0.00	0.00	0.00	0.00	0.00	0.00	0.00	0.00	5.21	3.43	8.64
Coac	0.00	0.00	0.00	0.00	0.00	0.00	0.00	0.00	0.00	17.07	17.07

Number of segment(s) rupture per century: 1.48 RI: ~70 years

10000*annual prob of rupture, 1400 years per scene, 100 scenes 140000 total years

Model 2.2f	Pkfl	Chol	Carr	BBnd	MojN	MojS	NSBr	SSBr	SGor	Coac	Total
Pkfl	0.29	0.29	0.29	2.65	8.41	14.05	0.81	1.22	0.29	0.29	28.57
Chol	0.00	0.02	1.91	0.02	0.02	0.02	0.02	0.02	0.02	0.02	2.07
Carr	0.00	0.00	1.87	0.06	0.06	1.94	0.69	1.04	0.55	0.06	6.29
BBnd	0.00	0.00	0.00	0.02	0.02	2.15	0.02	0.02	0.02	0.02	2.29
MojN	0.00	0.00	0.00	0.00	0.02	0.91	0.42	0.21	0.28	0.02	1.86
MojS	0.00	0.00	0.00	0.00	0.00	3.64	7.36	3.93	5.14	0.93	21.00
NSBr	0.00	0.00	0.00	0.00	0.00	0.00	15.50	21.00	4.21	4.50	45.21
SSBr	0.00	0.00	0.00	0.00	0.00	0.00	0.00	0.50	9.57	4.21	14.29
SGor	0.00	0.00	0.00	0.00	0.00	0.00	0.00	0.00	7.71	0.36	8.07
Coac	0.00	0.00	0.00	0.00	0.00	0.00	0.00	0.00	0.00	18.57	18.57

Number of segment(s) rupture per century: 1.48 RI: ~70 years

10000*annual prob of rupture, 1400 years per scene, 100 scenes 140000 total years

Model 2.3f	Pkfl	Chol	Carr	BBnd	MojN	MojS	NSBr	SSBr	SGor	Coac	Total
Pkfl	0.29	0.29	0.29	3.15	8.78	14.13	0.82	0.41	0.14	0.29	28.57
Chol	0.00	0.02	1.84	0.02	0.02	0.02	0.02	0.02	0.02	0.02	2.00
Carr	0.00	0.00	2.36	0.07	0.07	1.59	1.32	0.69	0.62	0.07	6.79
BBnd	0.00	0.00	0.00	0.03	0.03	2.35	0.03	0.03	0.03	0.03	2.50
MojN	0.00	0.00	0.00	0.00	0.03	1.12	0.77	0.21	0.35	0.03	2.50
MojS	0.00	0.00	0.00	0.00	0.00	3.14	6.29	2.93	6.50	1.57	20.43
NSBr	0.00	0.00	0.00	0.00	0.00	0.00	14.86	18.50	7.07	4.50	44.93
SSBr	0.00	0.00	0.00	0.00	0.00	0.00	0.00	0.29	9.79	5.00	15.07
SGor	0.00	0.00	0.00	0.00	0.00	0.00	0.00	0.00	4.86	9.07	13.93
Coac	0.00	0.00	0.00	0.00	0.00	0.00	0.00	0.00	0.00	10.29	10.29

Number of segment(s) rupture per century: 1.47 RI: ~70 years

Additional References

(References not included in accompanying Biasi and Weldon manuscript.)

Akciz, S.O., Grant, L.B., and Arrowsmith, J.R. (*in revision*). An average recurrence interval of 144 years for repeated rupture of the San Andreas Fault in the Carrizo Plain, California, since A.D. 1280, *J. Geophys. Res.*

Akciz, S.O., Grant, L.B., Arrowsmith, J.R., Zielke, O., Toke, N.A., Noriega, G., Cornoyer, J., Starke, E., Rousseau, N., and Campbell, (2006). Does the new paleoseismological evidence from the Carrizo Plain section of the San Andreas Fault indicate abnormally high late Holocene slip rates? *AGU* Abstract.

Akciz, S., Grant, L.G., and Arrowsmith, J.R., (2006). New and Extended Paleoseismological Evidence for Large Earthquakes on the San Andreas Fault at the Bidart Fan Site, California, Presented at the 100th Anniversary Earthquake Conference (*SSA*), San Francisco, CA, April 18-21, 2006.

Akciz, S., Grant, L.B., Arrowsmith, J.R., Zielke, O., Toke, N.A., Noriega, G., Stark, E., and Cornoyer, J. (2005). Constraints on ruptures along the San Andreas fault in the Carrizo Plain: Initial results from 2005: Bidart Fan site excavations. SCEC Annual Meeting, Proceedings and Abstracts.

Arrowsmith, J.R., McNally, K., and Davis, J. (1997). Potential for earthquake rupture and M7 earthquakes along the Parkfield, Cholame, and Carrizo segments of the San Andreas fault, *Seism. Res. Lett.* 68, no. 6, 902916.

Biasi, G.P. and Weldon, R.J. (2005). A Bayesian approach to correlation of paleoearthquake on a fault, Eos Trans., AGU, 86(52), Fall Meeting Supplement, Abstract U42A-05, 2005.

Biasi, G.P., and Weldon, R.J.II (2000). Paleoseismic date refinement and implications for seismic hazard estimation, Quaternary Geochronology Methods and Applications, *American Geophysical Union Reference* Shelf 4, Noller, J. S., *et al., eds.,* p. 517-520.

Biasi, G.P., Weldon R.J.II, Fumal, T.E., and Seitz, G.G. (2002). Paleoseismic event dating and the conditional probability of large earthquakes on the southern San Andreas fault, California, *Bull. Seism. Soc. Am.* 92, no. 7, 2761-2781.

Bennett, R.A., Friedrich, A.M., and Furlong, K.P. (2004). Codependent histories of the San Andreas and San Jacinto fault zones from inversion of fault displacement rates. *Geology*, 32, 961-964.

Davis, T.L. (1983). Late Cenozoic structure and tectonic history of the western "Big Bend" of the San Andreas Fault and adjacent San Emigidio Mountains, *Ph.D. Dissertation,* University of California, Santa Barbara, 123 pp.

Fay, N.P., and Humphreys, E.D. (2005), Fault slip rates, effects of elastic heterogeneity on geodetic data, and the strength of the lower crust in the Salton Trough region, southern California, *J. Geophys. Res.* 110, B09401, doi:10.1029/2004JB003548.

Fialko, Y. (2006). Interseismic strain accumulation and the earthquake potential on the southern San Andreas fault system. *Nature*, 441: 968-971.

Fumal, T.E., Weldon, R.J.II, Biasi, G.P., Dawson, T.E., Seitz, G.G., Frost, W.T., and Schwartz, D.P. (2002a). Evidence for large earthquakes on the San Andreas fault at the Wrightwood, California, paleoseismic site: A.D. 500 to Present, *Bull. Seismo. Soc. Am.* 92, no. 7, 2726-2760.

Fumal, T. E., Rymer, M.J., and Seitz, G.G. (2002b). Timing of large earthquakes since A.D. 800 on the Mission Creek strand of the San Andreas fault zone at Thousand Palms Oasis, near Palm Springs, California, Bull. *Bull. Seismo. Soc. Am.* 92, no. 7, 2841-2860.

Fumal, T.E., Pezzopane, S.K., Weldon R.J.II, and Schwartz. D.P. (1993). A 100-year average recurrence interval for the San Andreas fault at Wrightwood, California, *Science*, 259, 199-203.

Grant, L.B., Arrowsmith, J.R., Akciz, S. (2005). A Composite Chronology of Earthquakes From the Bidart fan Paleoseismic Site, San Andreas Fault, California. *Eos Trans. AGU,* 86(52), Fall Meet. Suppl., Abstract U42A-07.

Grant, L.B., and Donnellan, A. (1994). 1855 and 1991 Surveys of the San Andreas fault: implications for fault mechanics, *Bull. Seismo. Soc. Am.* 84, 241246.

Grant, L.B. and Sieh. K. (1994). Paleoseismic evidence of clustered earthquakes on the San Andreas fault in the Carrizo Plain, California, *J. Geophys. Res,* 99, 6819-6841.

Hanks, T.C. and Bakun, W.H. (2002). A bilinear source-scaling model for M-log A observations of continental earthquakes, *Bull. Seismo. Soc. Am.* 92, 1841-1846.

Harris, R.A., and Archuleta, R.J. (1988). Slip budget and potential for a M7 earthquake in Central California, *Geophys.. Res. Lett.* 15, 1215 1218.

Harris, H.A. and Arrowsmith, J.R. (2006). Introduction to the Special Issue on the 2004 Parkfield Earthquake and the Parkfield Earthquake Prediction Experiment *Bull. Seismo. Soc. Am.*; September 2006; v. 96; no. 4B; p. S1-S10; doi:10.1785/0120050831

Humphreys, E.D., and Weldon, R.J., 1994, Deformation across the western United States: A local determination of Pacific-North American transform deformation: *J. Geophys. Res.* 99, p. 19975–20010. doi:10.1029/94JB00899.

Jing, L.-Z., Klinger, Y., Sieh, K., Rubin, C., and Seitz, G. (2006). Serial ruptures of the San Andreas fault, Carrizo Plain, California, revealed by three-dimensional excavations. *J. Geophys. Res.* 111(B2): B02306, doi:10.1029/2004JB003601.

Johnson, H.O., Agnew, D. C. and Wyatt, F.K. (1994). Present-day crustal deformation in southern California. *J. Geophys. Res.* 99, 2395123974.

Lienkaemper, J.J. (2001). 1857 slip on the San Andreas fault southeast of Cholame, California, *Bull. Seismo. Soc. Am.* 91, no. 6, 16591672.

Lienkaemper, J.J. and Prescott, W.H. (1989). Historic surface slip along the San Andreas Fault near Parkfield, California, *J. Geophys. Res.* 94, 17,647-17,670, 1989.

Lienkaemper, J.J. and Sturm, T.A. (1989). Reconstruction of a channel offset in 1857(?) by the San Andreas Fault near Cholame, California, *Bull. Seismo. Soc. Am. 79*, 901-909.

Lienkaemper, J.J., Baker, B., and McFarland, F.S. (2006). Surface Slip Associated with the 2004 Parkfield, California, Earthquake Measured on Alignment Arrays *Bull. Seismo. Soc. Am.* 96: S239 - S249.

Lindvall, S.C., Rockwell, T.K., Dawson, T.E., Helms, J.G., and Bowman, K.W. (2002).Evidence for two surface ruptures in the past 500 years on the San Andreas fault at Frazier Mountain, California, *Bull. Seismo. Soc. Am.* 92, 2689-2703.

Liu, J., Klinger, Y., Sieh, K., and Rubin, C. (2004). Six similar sequential ruptures of the San Andreas fault, Carrizo Plain, California, *Geology,* 32, 649-652.

Liu, Jing, Part I. Slip Behavior of the San Andreas Fault Through Several Earthquake Cycles Part II. A Structural Interpretation of the Aftershock "Cloud" of the 1992

Mw 7.3 Landers Earthquake, PhD. Thesis, *California Institute of Technology* Pasadena, California 2003.

See also Jing, L.-Z., [same person]

Matmon, A., Schwartz, D. P., Finkel, R., Clemmens, S., and Hanks, T. (2005). Dating offset fans along the Mojave section of the San Andreas fault using cosmogenic Al-26 and Be-10, Geol. Soc. Amer. Bull., 117, 795-807, doi:10.1130/B25590.1.

McGill, S. F., Dergham, S. A., Barton, K., Berney-Ficklin, T., Grant, D., Hartling, C., Hobart, K., Minnich, R., Rodriguez, M., Runnerstrom, E., Russell, J., Schmoker, K., Stumfall, M., Townsend, J., and Williams, J. (2002). Paleoseismology of the San Andreas fault at Plunge Creek near San Bernardino, southern California, *Bull. Seismo. Soc. Am.*, 92, 2803-2840.

Meade, B.J., and Hagar, B.H. (2005). Block models of crustal motion in southern California constrained by GPS measurements: *J. Geophys. Res.* 110, no. B03403.

Murray, J.R., Segall, P., Cervelli, W. Prescott, W., and Svarc, J. (2001), Inversion of GPS data for spatially variable slip-rate on the San Andreas fault near Parkfield, CA, *Geophys. Res. Lett.* 28, 359-362.

Murray J., and Langbein, J., (2006). Slip on the San Andreas Fault at Parkfield, California, over Two Earthquake Cycles, and the Implications for Seismic Hazard, *Bull. Seismo. Soc. Am.*, 96: S283 - S303.

Noriega, G. R., Arrowsmith, J R., Grant, L. B., and Young, J. J., (2006). Stream Channel Offset and Late Holocene Slip Rate of the San Andreas Fault at the Van Matre Ranch Site, Carrizo Plain, California, *Bull. Seismo. Soc. Am.*, 96, 33-47.

Philibosian, B, Fumal, T., Kendrick, K., and R Weldon, R. (2006). Paleoseismic Investigation of the San Andreas Fault at Coachella, California, 2006 *AGU*

Powell, R.E., and Weldon, R.J**.**, 1992, Evolution of the San Andreas Fault, *Annual Review of Earth and Planetary Sciences*, v. 20, p. 431-468.

Runnerstrom, E. E., Grant, L.B., Arrowsmith, J.R., Rhodes, D.D., and Stone, E.M. (2002) Displacement across the Cholame Segment of the San Andreas Fault between 1855 and 1893 from Cadastral Surveys *Bull. Seismo. Soc. Am.*, v. 92, No. 7, pp. 2659–2669.

Rust, D. J., (1986). Neotectonic behavior of the San Andreas zone in the Big Bend: Geological Society of America Abstracts with Programs, v. 18, p. 177.

Rust, D. J., (1982). Radiocarbon dates for the most recent large prehistoric earthquakes and late Holocene slip rates: San Andreas fault in part of the Transverse Ranges north of Los Angeles: Geological Society of America Abstracts with Programs, v. 14, p. 229.

Salyards, S.L., Sieh, K.E., and Kirschvink, J.L. (1992). Paleomagnetic measurement of nonbrittle coseismic deformation across the San Andreas fault at Pallett Creek, *J. Geophys. Res.* 97, 12457-12470.

Scharer, K.M., Weldon, R.J.II, Fumal, T.E., and Biasi, G.P., (2007) Paleoearthquakes on the Southern San Andreas Fault, Wrightwood, California, 3000 to 1500 B.C.: A New Method for Evaluating Paleoseismic Evidence and Earthquake Horizons, *Bull. Seismo. Soc. Am.* Vol. 97, No. 4, pp. 1054–1093, August 2007, doi:10.1785/0120060137.

Schmalzle, G., Dixon, T., Malservisi, R., and Govers, R. (2006), Strain accumulation across the Carrizo segment of the San Andreas Fault, California: Impact of laterally varying crustal properties, *J. Geophys. Res.* 111, B05403, doi:10.1029/2005JB003843.

Schwartz, D., and Weldon, R. (1986). Late Holocene slip rate of the Mojave segment of the San Andreas fault zone, Littlerock, California: Preliminary results: Eos (Transactions, *American Geophysical Union*), v. 67, p. 906

Seitz, G., and Weldon, R. (1994). The Paleoseismology of the southern San Andreas Fault at Pitman Canyon, San Bernardino, California, *Geological Society of America*, Cordilleran Section Guidebook, Trip 8, Geological Investigations of an Active Margin, *eds.*, McGill, S.F., and T.M. Ross, p. 152-156.

Seitz, G., Biasi, G., and Weldon, R. (1996). An improved paleoseismic record of the San Andreas Fault at Pitman Canyon, *Geological Society of America*, Special volume; Quaternary Geochronology: applications in Quaternary geology and paleoseismolgy, (Noller, Sowers, and Lettis, *eds.*).

Seitz, G., Biasi, G., and Weldon, R. (1996). The Pitman Canyon paleoseismic record suggests a re-evaluation of San Andreas Fault segmentation, Proceedings of the Symposium on Paleoseismology, International Union for Quaternary Research XIV International Congress, *Terra Nostra* 2/95, *eds.*, Michetti, A.M., and P.L. Hancock, Journal of Geodynamics.

Seitz, G., Biasi, G., and Weldon, R.J., (2000). An improved paleoseismic record of the San Andreas fault at Pitman Canyon: in Noller, J.S., et al., eds., Quaternary Geochronology Methods and Applications: *American Geophysical Union* Reference Shelf #4, p. 563–566.

Sickler, R., Weldon, R.; Fumal, T.; Schwartz, D.; Mezger, L.; Alexander, J.; Biasi, G.; Burgette, R.; Goldman, M.; Saldana, S. (2006) Slip rate of the San Andreas Fault near Littlerock, California. *Seismological Research Letters* 77(2): 250-251.

Sieh, K.E. (1978). Slip along the San Andreas fault associated with the great 1857 earthquake, *Bull. Seismo. Soc. Am.*68, 17311749.

Sieh, K.E. (1986) Slip rate across the San Andreas fault and prehistoric earthquakes at Indio, California, EOS Transactions, 67, 1200.

Sieh, K.E., and R. H. Jahns (1984). Holocene activity of the San Andreas fault at Wallace Creek, California, Geol. Soc. Am. Bull. 95, 883-896.

Sieh, K., Stuiver, M., and Brillinger, D. (1989). A more precise chronology of earthquakes produced by the San Andreas fault in southern California, *J. Geophys. Res.* 94, 603-623.

Sims, J.D. (1994). Stream channel offset and abandonment and a 200-year average recurrence interval of earthquakes on the San Andreas fault at Phelan Creeks, Carrizo Plain, California, in *Proceedings of the workshop on paleoseismology, US Geological Survey Open-File Report 94-568*, (edited by C. S. Prentice, D. P. Schwartz and R. S. Yeats), 170-172.

Sims, J.D., Ito, T., Hamilton, J., Foss, A.J., Garvin, C.D., and Meier, D.B. (1994) A 200-year average recurrence interval of earthquakes on the San Andreas fault at Phelan Creeks, Carrizo Plain, California: reconstruction from paired offset paleochannels, *unpublished manuscript*.

Sims, J.D., Ito, T., Hamilton, J.C., and Meier, D.B (1989). Late Holocene record of earthquakes and slip along the San Andreas fault in excavations on the Carrizo Plain, Central California, *EOS, Transactions of the American Geophysical Union, 70*, 1349, 1989.

Stone, E.M., 2002. Recent rupture history of the San Andreas Fault southeast of Cholame in the northern Carrizo Plain, California. *Bull. Seismo. Soc. Am.* 92(3), 983-997.

Toke, N.A. and Arrowsmith, J.R. (2006). Reassessment of a Slip Budget along the Parkfield Segment of the San Andreas Fault *Bull. Seismo. Soc. Am.*96, No. 4, pp. S339-S348; doi:10.1785/0120050829.

Toppozada, T.R., Branum, D.M., Reichle, M.S., and Hallstrom, C.L. (2002). San Andreas fault zone, California: M>5.5 earthquake history: *Bull. Seismo. Soc. Am* 92, no. 7, p. 2555-2601.

van der Woerd, J., Klinger Y., Sieh, K., Tapponnier P., Ryerson, F.J., and Meriaux A.S. (2006). Long-term slip rate of the southern San Andreas Fault from 10 Be- 26 Al surface exposure dating of an offset alluvial fan: Journal of Geophysical Research, V. 111, n. 1, B04407, doi:10.1029/2004JB003559.

Weldon, R.J.II, Fumal, T.E., Powers, T.J., Pezzopane, S.K., Scharer, K.M., and Hamilton, J.C. (2002). Structure and earthquake offsets on the San Andreas fault at the Wrightwood, California paleoseismic site, *Bull. Seismo. Soc. Am.* 92, no. 7, 2704-2725

Weldon, R., Scharer, K., Fumal, T., and Biasi, G. (2004). Wrightwood and the earthquake cycle: what a long recurrence record tells us about how faults work, *GSA Today,* 14, No. 9, 4-10.

Weldon, R.J., Fumal, T.E., Biasi, G.P., and Scharer, K.M. (2005). Past and future earthquakes on the San Andreas fault, *Science,* v.308, p. 966-967.

Weldon, R.J. (1991) Active tectonic studies in the United States, 1987-1990, *Reviews of Geophysics*, Supplement (US National Report to the International Union of Geodesy & Geophysics), p. 890-906.

Weldon, R. J., Meisling, K. E., and Alexander, J. (1993). A Speculative history of the San Andreas fault in the central Transverse Ranges, *in*, Powell, R. E., Weldon, R. J., and Matti, J. *eds.*, The San Andreas fault system; displacement, palinspastic reconstruction, and geologic evolution, *Geological Society of America*, Memoir 178, p. 161-178.

Weldon, R.J., and Sieh, K.E. (1985). Holocene rate of slip and tentative recurrence interval for large earthquakes on the San Andreas fault, Cajon Pass, southern California: Geological Society of America Bulletin, v. 96, no. 6, p. 793-812.

Williams P.L. and Seitz, G.G. (2004). San Andreas fault in the Coachella Valley at Salt Creek: Development of Long-Term earthquake chronology and event offsets, Abstract for SCEC Annual Meeting.

WGCEP (Working Group on California Earthquake Probabilities) (1988). Probabilities of Large Earthquakes Occurring in California on the San Andreas Fault System: U.S. Geological Surv. Open-File Report 88-398, 62 pp.

WGCEP (Working Group on California Earthquake Probabilities) (1990). Probabilities of large earthquakes in the San Francisco Bay Region, California: U.S. Geological Survey Circular 1053, 51 p.

WGCEP (Working Group on California Earthquake Probabilities) (1995). Seismic hazards in southern California: Probable earthquakes, 1994 to 2024: Bulletin of the Seismological Society of America, v. 85, no. 2, p. 379- 439.

WGCEP (Working Group on California Earthquake Probabilities) (1999). Earthquake Probabilities in the San Francisco Bay Region: 2000 to 2030 - A Summary of Findings: U.S. Geological Survey Open-File Report 99- 517, Online Version 1.0, 36 p.

WGCEP (Working Group on California Earthquake Probabilities) (2003). Earthquake probabilities in the San Francisco Bay region: 2002-2031: U.S. Geological Survey Open-File Report 03-214.

Young, J.J., Arrowsmith, J.R., Colini, L., and Grant L.B. (2002). 3D excavation and measurement of recent rupture history along the Cholame segment of the San Andreas fault, Bull. Seism. Soc. Am. 92, 26702688.

Yule, D., and Sieh, K. (2001). The paleoseismic record at Burro Flats: Evidence for a 300-year average recurrence for large earthquakes on the San Andreas fault in San Gorgonio Pass, Southern California: Geological Society of America Abstracts with Programs, v. 33, no. 3, p. A31

Yule, D., and Sieh, K. (2003). Complexities of the San Andreas fault near San Gorgonio Pass: Implications for large earthquakes: Journal of Geophysical Research, V. 108, no. B11, 20 p.

Yule, D. and Howland, C. (2001). A revised chronology of earthquakes produced by the San Andreas fault at Burro Flats, near Banning, California, in SCEC Annual Meeting, Proceedings and Abstracts, Southern California Earthquake Center, Los Angeles, 121.

San Andreas Fault Rupture Scenarios From Multiple Paleoseismic Records: "Stringing Pearls"

Glenn P. Biasi and Ray J. Weldon II

Abstract We present a new method to objectively combine paleoseismic event data from multiple sites into multiple-site rupture scenarios. By construction the method develops all possible combinations between sites allowed by available event age probability distribution functions (pdfs). The possibility of missing events in individual paleoseismic records is also accommodated. Scenario rupture histories for the southern San Andreas fault (SSAF) are constructed from this pool of possible ruptures. For each scenario we draw from the pool in such a way that each paleoearthquake is included exactly once. Scenarios so constructed are possible histories of rupture on the fault with respect to including all reported events and dating evidence. A pool of 10,000 scenarios was constructed in this manner. We score each scenario by the average quality of its agreement with the event-dating evidence, by the cumulative displacement over all ruptures compared to a prediction from the fault slip rate and elapsed time, and by the minimum number of events required to satisfy the data. Scenarios with fewer events are considered more likely because of the increasing statistical improbability of the current long open interval of the SSAF with increasing numbers of events in the scenario. We considered matching slip-per-event data, but few sites have per-event estimates and cumulative displacement was judged to be more robust.

Comparing total displacement to predictions from fault slip rate and elapsed time proved to be the strongest discriminator among scenarios. Three slip rate models from the 2007 Working Group on California Earthquake Probabilities (WGCEP) were considered. For models with slow slip rates through the San Bernardino and San Gorgonio sections of the SSAF, best fitting scenarios tend not to allow full fault length ruptures. Long ruptures have large displacements in the middle and thus leave little displacement for the remaining ruptures on interior segments. The choice of best-fitting scenarios depends on the length-average surface displacement regression model used. The Hanks-Bakun (2002) model we used yields a significantly larger number of acceptable scenarios than that of Wells and Coppersmith (1994), and a model that limits displacement with increasing rupture length would extend ruptures further.

In the northern half of the SSAF, favorable scenarios tend to include 1857-like ruptures for three of the most recent five ruptures extending from Carrizo to approximately Wrightwood. Scenarios with good displacement fits tend to include one to two ruptures that involve the southern half of the SSAF, from the Coachella to San Bernardino section, but most earthquakes in that portion appear to be shorter and exhibit less consistency from event to event. This may be due to more variable recurrence intervals and slip rates between sites that cannot be modeled by a few through-going events. By combining paleoseismic data into large sets of scenarios and selecting viable scenarios using external constraints, our method provides rupture histories useful for seismic hazard assessment without having to first settle which event at a site correlates with that at adjoining sites. This should allow paleoseismic data to be used with greater power to understand the seismic hazard posed by faults like the southern San Andreas.

Introduction

A major challenge for the paleoseismic study of large crustal faults is to integrate results from a number of individual site-based investigations into a rupture history for the fault. Even on the southern San Andreas fault, one of the best studied in the world, linking results from site to site has proven difficult because of the uncertainty in paleoearthquake dates and because of the distance between sites. Hand-constructed rupture scenarios among individual site records (e.g., Sieh 1984; Grant and Sieh, 1994; Weldon et al., 2004) have proven useful, but this approach leaves open the question of how likely these scenarios are compared to alternatives.

In an effort to explore possible rupture histories more completely, we use event chronologies from multiple paleoseismic sites in a way that finds all possible correlations of the event data. This approach allows the possibilities to be examined systematically and quantitatively, and to be ranked or ordered by desired criteria. The method is developed and presented using multiple-event paleoseismic records of the southern San Andreas fault in southern California (Figure 1).

We model the fault as a line segment along which ruptures occur. This fault model is a considerable simplification since it neglects changes in fault alignment, partitioning of strike-slip and thrust activity and, locally, the presence of multiple strands of the fault. This simplification also removes the geometry and any *a priori* segmentation of the fault into ruptures. As such, the results can be used to test segmentation models or segmentation can be added as a separate constraint or ranking criterion. The complete process from event data to ranked scenarios is outlined in Figure 2.

Slip rate models used our modeling are adopted without modification from the WGCEP. Multiple "deformation models" were generated by expert opinion from an exhaustive review of the available slip rate data. The most significant difference between them is a trading off of slip between the southern San Andreas and San Jacinto faults. The preferred model of the WGCEP has the two faults as co-equal in slip rate south of the Transverse Ranges, and the two alternatives have each fault about 30% higher and lower, respectively. Because all models have substantial slip across the Eastern California Shear Zone that is fed from the SSAF to the south, and the San Jacinto joins with the SSAF north of San Gorgonio pass, all models have a relatively low slip rate in the San Gorgonio pass region. Finally, line integrals and geologic moment tensors derived from the deformation models (WGCEP Report Appendix P) demonstrate that the slip rate models are kinematically consistent with each other and the plate motion, so it is difficult to change a single portion of the model (such as the rate in the San Gorgonio pass) without changing many other faults as well. Details are discussed in WGCEP Report Appendix A.

Paleoseismic Event Data

The basic data for this study are coseismic disruptions of the ground surface identified and dated at paleoseismic sites on the San Andreas fault. Site names and references for the paleoseismic event data used in this work are listed in Table 1.

Fifty-six paleoseismic site observations of earthquakes are included in this study (Figure 1, Table 2). In general, site records are included if multiple ground-rupturing events are documented, if the record is likely to be complete, and if individual event dates are available. Event probability density functions (pdfs) were available for the Pallett Creek, Wrightwood, and Thousand Palms Oasis sites (Biasi et al., 2002; Fumal et al., 2002b). Dating evidence from Plunge Creek (McGill et al., 2002) was used to develop event pdfs for the two events reported there. For sites at which event pdfs were not available (Indio, Sieh, 1986; Burro Flat, Yule and Howland, 2001), Gaussian shapes were assigned using published mean dates and uncertainties . Some synthesis of separate studies was applied to the Carrizo and Pitman sites. Three studies in the Carrizo Plain area (Bidart Fan, Grant and Sieh, 1994; Wallace Creek, Liu et al, 2004; Phelan Creek, Sims 1994) were considered. In the Carrizo Plain the synthesis included event displacements and dates. The sites are close enough to one another, and individual event displacements large enough, that we considered it likely that displacements at each of the sites would extend to the others. We used the interpretation of Liu et al. (2004) that the events identified in that study corresponded with those at Bidart Fan although we recognize that this is becoming increasingly controversial (see discussion of the Carrizo section in WGCEP Report Appendix E). Because our objective was not to redate the events, but rather to summarize what was published about them, we combined the original dating evidences, of the three studies and made event date pdfs of them. The resulting date ranges overlapped strongly, so we used the information of their order of occurrence to further constrain their pdfs (Biasi et al., 2002). Because the method of constructing multiple-event ruptures depends largely on overlap with other sites, the broad pdfs we use allow a wide range of correlations, and more informative pdfs can be integrated as they become available. A similar synthesis was applied to the multiple published records from Pitman Canyon site (Seitz et al, 1997; Seitz, 1999). All event pdfs were represented on a common set of bins 10 years in width. The choice of ten year bin widths allows most events be represented by a few to 20 bins. Sensitivity studies suggest that the results do not depend much on the choice of bin width. The available data for each section is discussed in Appendix E and event date distributions themselves are given in Appendix B of the WGCEP report.

Late in the final review cycle of the WGCEP report new event date pdfs of the most recent four pre-1857 ground ruptures at Bidart Fan were made available (Akciz, pers. comm., 2007). The new event dates derive from supplemental ^{14}C dating of samples obtained from the Grant and Sieh (1994) investigation. These data imply that the recurrence interval at Bidart Fan is shorter than previously thought and are incorporated by hand in the final WGCEP model. If the dates are associated with the displacements of Liu et al. (2004), the implied slip rate over the most recent ~900 years or less appears inconsistent with geodetic and geologic estimates. We were not able, with the available time and information, to develop an alternative treatment that incorporates all the data in an entirely satisfactory manner. To give an idea of the impact of separating the event dates from the Carrizo displacements, an Addendum is provided that assumes an average displacement model for Carrizo events. The model and method are discussed in later sections of this report.

Forming Ruptures

The first step toward fault rupture scenarios is to combine individual site evidence of ground rupture into a pool of all possible ruptures. To begin, each event at each site is included in the rupture pool as a one-site rupture. To build longer ruptures, each of these is used as a "master event", and its date pdf is compared with date pdfs at the next neighboring site. If an overlapping date pdf is found, a second rupture is defined that involves both sites (Figure 3). If more than one event pdfs overlap at the neighboring site, each is paired with the master event and both are included in the pool of possible ruptures. If no neighboring event pdf overlaps, either the rupture did not reach the next site or evidence for it was not discovered. Because site investigations do not always record evidence for every event we maintain the possibility that the rupture did pass by the site, but that it somehow avoided detection. Allowing the master event to correlate despite a lack of evidence also prevents a poor site from "blocking" a rupture that otherwise would be favored by adjoining sites. Ruptures constructed by assuming site evidence is missing are considered less likely than direct overlaps and penalized in a later stage in the process. Ruptures with two sites are extended by matching the master event to the third site's event pdfs, then the fourth, etc. The process may be likened to stringing pearls. After extending through neighbors to the southeast, each rupture is also extended successively through neighboring sites to the northwest.

All sites are limited in the time span of their record. The limit varies by paleoseismic site from 700 years at Plunge Creek to 1450 years at Wrightwood. We assigned maximum ages of constraint based the original investigators' reporting (Table 1). If the mean date of the "master event" of the rupture being constructed is older than the age in Table 1, then that site is skipped when building ruptures and no penalty is assigned. Thus the number of contributing paleoseismic sites decreases with increasing age. This could create the appearance of a greater frequency of single-site ruptures for the oldest events of long records (e.g., Wrightwood) and also longer ruptures where there are large gaps between sites. However, most of the available paleoseismic records for the SAF extend back 1100 years or more. Second, when evaluating scenarios of ruptures, we score them only on the basis of ruptures after a date after which most sites contribute.

The number of ruptures that result from combining the available paleoseismic event data depends on the degree of overlap of date pdfs required to pair up. One parameterization of the overlap of pairs of event pdfs i and j is the area of overlap of pdfs:

$$Overlap\ area(i,j) = \sum min(pyr_i(\tau),\ pyr_j(\tau)) \tag{1}$$

where the sum is over τ=bins of the discrete date pdfs; area is measured in time-probability space, and *pyr* is probability that the earthquake was in that 10-year bin. Figure 4 illustrates four identical model date distributions overlapping by different numbers of bins. For this example an overlap area minimum of 0.3 corresponds to a 50 year window within each pdf in which the event might have occurred (Figure 4). The total number of possible ruptures in the pool depends on the overlap criteria (Figure 5). The overlap criteria might be justified heuristically by noting that to match two pdfs that overlap by a fraction x requires that the true event date be in the oldest tail of one and the youngest tail of the other. For matched uniform distributions the probability of this would

be x^2, or for an overlap criteria of 0.3, a probability of 0.09. For non-uniform distributions the product is not so easily computed, but the idea approximately holds. Perhaps unexpectedly, the overlap area can be small if a sharply defined date overlaps with a broad one, because it measures the smaller height of the broad date and the narrower range of the sharp one, so the magnitude of overlap area is not a consistent means of assessing overlap quality. We set the minimum overlap criteria with the master event to the relatively low value of 0.02 to ensure that virtually all possibilities are retained. This allows date ranges to match that only overlap in extreme tails of their distributions. Visual inspection of scenarios generated by different cut offs found that many ruptures formed under this liberal pairing standard will subsequently be removed as additional screening standards are applied; thus the exact choice of this cut off has little effect on which scenarios are ultimately accepted as "best". Allowing liberal pairing does decrease the computational efficiency of finding successful scenarios.

A form of joint probability is also tabulated for all event pairs:

$$Product\ overlap(i,j) = log10(\sum pyr_i(\tau) * pyr_j(\tau)) \tag{2}$$

The product overlap is the sum of probabilities a bin at a time that events i and j occurred in the same time bin. The product overlap of pdfs (or of a pdf with itself) is a measure of compactness (Figure 6); narrow, well-defined dates have relatively high values, and wide date pdfs have low product overlaps.

The product and overlap area measures of dating congruence are well defined for ruptures spanning two paleoseismic sites. For ruptures involving more sites, some extension of these measures must be devised. The overlap area measure for ruptures is computed as the mean overlap area among contributing individual dates in the rupture. For the overlap area to be uniquely determined, events were first ordered by mean date, and pairs (i,j) were formed successively; e.g., (1,2), (2,3), etc. "Missed" events contribute to the number of sites but not the overlap area, thus lowering the mean for the rupture as a whole. The product overlap for ruptures is summed in the same pair-wise order, but not normalized by the number of events in the rupture. This causes product overlap scores for ruptures to decrease with increasing length (Figure 7). Pairs with a "missing" event are given a product score of -2, which was selected to be about a factor of two lower than the product overlap of a poorly determined event with itself (Figure 6). Trends in product and mean overlap measures with rupture length are shown in Figures 7a and b, respectively.

Rupture Dating

Because most rupture date pdfs in our analysis are formed from more than one event pdf, a procedure is needed to combine the contributing pdfs. Event pdfs are combined directly, including their uncertainties, and, each associated event pdf is given equal weight. This amounts to accepting reported dates without choosing preferred dates among them And could be modified if evidence were available to assign a greater or lesser weight to a site.

To apply these rules, all event pdfs are represented on a common set of bins 10 years wide with bin values. To form rupture date pdfs we sum probabilities of each contributing event pdf, bin by bin. The result is divided by the number of contributors, giving the combined pdf a unit area. The rupture mean date estimate is computed using

$$mean\ date\ estimate = \sum(bin\ year * pyr) \qquad (3)$$

This date estimate is the center of gravity of the combined pdf on the time axis. The mean estimate of the rupture is used for plotting and for comparing event ordering in rupture histories to investigator-reported order.

Weighting each contributing event date equally can lead to unexpected results. For example, two pdfs that overlap little could have a mean between them where neither contributing pdf prefers it. Measures are discussed below to address such cases.

The width measure of the date estimate is found by:

$$width = sqrt(var(rupture\ date)) = sqrt(\sum(pyr*(bin\ date\text{-}mean\ date)^2)) \qquad (4)$$

The mean and width measures in Eqns 3 and 4 are used to identify ruptures that strongly contradict the dating evidence. First we test ruptures for a significant difference between the mean and median dates of the contributing pdfs (Figure 8a), which means that the dating evidence for the proposed rupture is so divided that it is unlikely to have come from a single underlying earthquake. Ruptures with medians more than 40 years from their means are discarded. Second, ruptures are removed if they have too great a width, as measured by Equation 4 (Figure 8b). We discard cases with a width measure greater than 90 years. Ruptures removed by these two criteria are typically strongly bimodal, and the modes are separated by more than the width of a typical paleoseismic event date. Third, we discard ruptures with an average overlap over all contributing event pdfs of less than 0.1 (Eqn 1). Fourth, ruptures are required to have an average log product overlap greater than -1.5. Parameters governing the selection of ruptures are summarized in Table 3.

Example ruptures developed by the above procedure are shown on Figure 9. The master rupture for this example (Figure 9a) has a mean date in the mid-1500s. Figures 9b, c, and d, add successive events and lengthen the rupture to include four sites. The net rupture pdf is shown with a dotted overlay. Ideally the event dates will include a common mode in their individual contributors. The event added in Figure 9d is an exception, and overlaps with the 1500s only in its older tail. In Figure 9e an alternative third rupture is inserted. It includes a mode in the mid-1500s consistent with the other dates, but includes another mode in the late-1300s. This causes the rupture date pdf to include a minor mode there, under the egalitarian principle. A third alternative rupture is shown in Figure 9f. This event overlaps by a few percent with the master pdf, but has a center closer to 1700. The ruptures in Figures 9e and f both have widths near 80 years and a mean overlap near 0.55, so they are not removed by the automatic screening described previously.

Assigning Lengths to Ruptures

Each rupture includes some number of paleoseismic sites linked on the basis of dating evidence. To model how much farther each rupture extends beyond the linked sites (i.e., the rupture "tails"), we use co-seismic displacement estimates at the end sites and a relationship between displacement and rupture length. Figure 2 gives a visual summary of the process. Before describing the process in detail we note that the rupture cannot, by construction, extend to the next unlinked paleoseismic site. For most ruptures this bounds the length of the tails and limits their importance for scenario evaluation.

Where available, a probability distribution around a direct estimate of co-seismic displacement is used (Table 4a; Wrightwood, Weldon, et al., 2002 and 2005; Wallace Creek, Liu et al., 2004). Displacement measurements have also been made at Pallett Creek (Sieh, 1984; Salyards et al., 1993). Discrete offsets measured by Sieh(1984) suggested a slip rate of ~9 mm/yr. Salyards et al. (1993) modeled paleomagnetic rotations of soft sediments and added it to brittle displacements to estimate total offsets for two of the three most recent events. We used displacements they re-measured, and scaled the other displacements of Sieh (1984) by the factor suggested by Salyards et al. (1993). This approach is a compromise, but at least preserves the relative displacements suggested by the measurements Sieh (1984).

If per-event displacement estimates are not available, we construct a distribution of displacement around the average displacement based on the site recurrence interval (Table 4b) and the local fault slip rate from geodetic or geologic estimates (Table 5). The distribution of displacement was taken to be log-normally distributed and limited to approximately ½ to 2x of the average. This range of variation was adopted after evaluation of its interaction with the displacement-rupture length regressions (discussed below). We considered two methods to assign rupture tails given a displacement value at an end site. The first was to use half the surface rupture length (SRL)estimated from a modified version of the Wells and Coppersmith (1994) regression for length given average surface displacement (AD):

$$log10(SRL) = 1.68 + 1.00 \, log10(AD). \tag{5}$$

In this equation the intercept of Wells and Coppersmith was adopted, but the slope was increased to improve the fit of length estimates for AD in the 3-8 meter range where the majority of the SSAF observations occur. For single-site ruptures this method was adopted for lack of better information. However, we found the tail lengths added by this method to be unrealistically long for multiple-site ruptures. For example, at Carrizo, a 7 meter displacement would extend over 160 km NW of Carrizo by this method, beyond the creeping section of the fault.

The second method implements an average displacement-gradient constraint on surface rupture. Biasi and Weldon (2006) summarized 13 surface ruptures into an average rupture shape that tapers on either end. Using the analytical approximation of that shape (discussed below), one finds that from the last observation of the average displacement to the end of the rupture is a distance of 19800*AD (i.e., about 20% of the rupture length). We adopted half this value for the rupture tail length so the total rupture lengths would be determined primarily by the sites in the rupture and only secondarily by

the more speculative extrapolation from the displacement sample. Thus tails of multiple-site ruptures are assigned by drawing from end site measured or sampled displacement distributions (Table 4), and multiplying by 9900.

Rupture lengths are limited by the fact that, by construction, they do not reach any next adjoining sites along the fault. If the rupture extension based on displacement would be greater than this distance, we constrain the rupture to stop a small distance (5 km) short of the next site.

The ends of the southern San Andreas fault at the northwest in the creeping zone (~milepost 0) and southeast at Brawly Seismic zone (~milepost 550) could likewise be treated as bounds for the rupture length, but doing so creates artificially abrupt model rupture ends. In addition, real ruptures are known to extend beyond both ends. On the northwest end, some workers infer that the 1857 rupture had 3-5 m of slip as it entered the Parkfield section (see WGCEP Report Appendix E). Compared to slip in recent earthquakes at Parkfield, the 1857 slip was apparently atypical and could have extended into the creeping section of the fault. To the southeast, at Salt Creek, Seitz and Williams (pers. comm.) report ~2.5 m average displacements within a few kilometers of the Brawly Seismic zone, suggesting that ruptures continue past the end of our modeled fault. Thus ruptures are allowed to extend northwest beyond Carrizo and southeast beyond Indio based on displacements at the respective sites. Specifically, if Carrizo displacement choices are 4 meters or greater, we assume that the event correlates with one of the frequent Parkfield events and construct a rupture tail beyond Parkfield by drawing from a log-normal distribution with an 1857-like 4 m average displacement and the nominal 9900 extension multiplier. Correlation of Indio events with Salt Creek are assumed if sampled displacements at Indio are greater than 1.9 meters and a tail is scaled using a pick from a 2.5 m average displacement distribution. Rupture tail extensions involving Parkfield and Salt Creek lead to what we believe are more realistic displacement histories from Carrizo to Indio, but they have limited effects on conclusions about the fault rupture history.

Each time a rupture is used in a scenario history its length is determined by the above procedure. In general any given rupture will be selected many times when a large number of scenarios are constructed, and each time it appears, it will have a different tail length. Figure 10 shows a histogram of rupture lengths for a suite of 10,000 scenarios. The sample is large enough that the histogram of rupture lengths is stable and presumably representative of the population (Figure 10).

Displacement Within a Rupture

To assign surface rupture displacements within ruptures we used an analytical approximation to the average shape found from a set of mapped surface ruptures (Figure 11). The input data consist of 13 mapped displacement profiles. To combine them Biasi and Weldon (2006) normalized each by its length and average displacement. The averaged shape is well approximated by the function $(sin(\pi x/L))^n$ with $n = \frac{1}{2}$. We recognize that this shape is unlikely to have matched any individual southern San Andreas fault rupture. Before adopting this shape we considered rescaling actual rupture

displacement profiles and using them instead of the analytical shape. Were a large enough suite of scenarios considered, the individual displacements would average to our analytic shape. We considered triangular rupture profiles, but these have the basic choice of which side of the middle to put the peak. If this choice is randomized, the result would not be far from the shape in Figure 11. Using the mean displacement profile (Figure 11) amounts to using the best estimate based on the shape of the contributing ruptures. If a more rectangular shape is desired, a smaller value of exponent n may be used. For example with $n = 1/5$, the resulting shape is nearly boxcar-like, and the maximum displacement would be only 20% greater than the average displacement.

The analytical shape is scaled to the rupture length, sampled on one km points, and adjusted in height (displacement) to match the average displacement from a length-average displacement regression. Two regressions were considered. The preferred relation comes from the Hanks and Bakun (2002) regression of moment magnitude versus rupture area. Area is estimated as the product of the rupture length and an average thickness of brittle crust of 12.7 km. Average displacement is then found as 0.02*rupture length. We also implemented the average displacement versus length regression from Wells and Coppersmith (1994; Equation 5). This regression is well known, but was developed by a linear regression heavily weighted toward shorter ruptures. As a result, the average and peak displacements for ruptures of 300 to 500 km length are larger than predicted by the Hanks-Bakun regression, which itself exceeds geologic observations. Thus it should perform adequately in an average sense, but cannot be expected to fit any particular rupture exactly. The underlying issue is whether AD scales without limit with rupture length. This topic has been energetically debated and is beyond the scope of this paper.

Rupture Scenarios

Scenarios here refer to possible histories of ground-rupturing earthquakes on the southern San Andreas fault. Scenarios are constructed by drawing at random from the pool of all constructed ruptures until every event at every paleoseismic site is accounted for and none are repeated (Figure 2). The historical 1857 and 1812 ruptures are common to all scenarios and included with their estimated displacement profiles and lengths. By constructing many such scenarios, an ensemble is built that can be investigated for patterns of rupture occurrence and the degree to which they satisfy outside constraints such as dating congruence and fault slip rate, total slip at any point on the fault, and segmentation.

Drawing at random from the pool of constructed ruptures has a bias toward short ruptures. It arises because combinations from the pool are correlated. As an example, suppose events A and B with compatible ages are reported at two adjoining paleoseismic sites. Possible earthquakes are A+B together as one rupture or A and B as separate events. These outcomes require three ruptures, A, B, and A+B. However, drawing A first from the rupture pool requires B be selected to account for all site events, and vice-versa. Only if the longer rupture A+B is chosen first will one rupture engage both sites. Thus two-thirds of "random" choices from the rupture pool result in individual site ruptures. However, there are only two scenarios in this case - separate events or one event that

ruptured at both sites. In order to make scenarios equally likely, we adjusted the rupture pool. Note that this adjustment does not change scenarios one might eventually find, but only the efficiency with which scenarios with fewer total ruptures are found by random sampling. No inferences are drawn from how often a rupture is chosen; we simply want to efficiently choose as many different scenarios as possible for subsequent ranking.

We found as a matter of expediency that it was also worthwhile to limit the number of rupture scenarios. The probabilistic motivation for some sort of limit comes from the length of the open interval for the SSAF since 1857. Figure 12 shows that the larger the number of individual ruptures, the less likely it is that the current >150 year open interval for a ground-rupturing earthquake on the SSAF would be observed. The smallest number of ruptures found in each of two independent ensembles of 10,000 scenarios each was 19. Weldon et al. (2005) explored this question with scenarios constructed by hand. They found the present paleoseismic record of the past 1350 years difficult to explain with fewer than about 16 earthquakes, even with qualitative standards of time congruence (i.e., the method in Figure 4). We retained only scenarios with 26 or fewer ruptures. This limit is somewhat ad hoc, but as shown in Figure 12, these scenarios are only half as likely as those with 20 ruptures. The consequences of the cutoff for scenario evaluation are developed further in the next section.

A final screening is applied to each scenario before it is accepted as a possible history of the SSAF. The pearl-stringing rules allow an event at one site, especially if it is relatively broad, to be linked to more than one at another site (e.g., Figure 9). Occasionally ruptures selected for a scenario will include some pair of events at an individual site that the rupture dates imply occurred out of order. We test therefore for original field ordering for each paleoseismic site, and drop scenarios with events out of order.

Evaluation of Rupture Scenarios

Having developed a large pool of rupture scenarios, there remains the question of how to evaluate them and how to select those most representative of fault behavior. Five evaluation criteria are considered (Figure 13).

Displacement scoring: The displacement score uses the fact that at any point on the fault displacements among ruptures affecting that point can be summed and compared with an independent prediction from geologic and/or geodetic measurements of slip and a long-enough time to average over several earthquake cycles. We find that it is the strongest single discriminator among scenarios. Displacements are totaled for ruptures in the grading period (here, >900 A.D.) at 20 km points along the fault and the mean difference is used as the displacement score. Slip rate Model 2.1 (Table 5) is used throughout Figures 13 (a, b, c, d). Scenarios are graded only from mileposts 70 to 490; outside these bounds there is less constraining information and model end effects could influence results.

Number of earthquakes: The number of earthquakes in a scenario is shown in Figure 13 by symbol color, and for the relatively rare scenarios with 20 or fewer earthquakes, by special symbols (Figure 13 d, e). Over 95% of the scenarios in this

ensemble account for the paleoseismic data with 23 or more ruptures (Figure 13a). Figure 12 gives the relative probabilities of the present open interval since 1857 as a function of the number of ruptures in the scenario.

Time overlap score: One qualitative measure of the degree of dating agreement in ruptures of a scenario is the average overlap score of its constituent ruptures (Figure 13b, reference Figure 7b). We have called this the time overlap, or "Venn" score. The Venn score is anti-correlated with the number of ruptures in a scenario because in most cases, the more sites there are per rupture, the more likely it is that those ruptures would include contributing dates with poor overlap (e.g., Figure 9).

Product time scoring: The product time score (Figure 13c) is a somewhat more quantitative estimate of the average quality of agreement of dating evidence in the scenario's constituent ruptures. This time score measure has not been normalized by the number of events per rupture, so scenarios with fewer ruptures and thus more events per rupture have more negative (lower average rupture probability) scores (Figure 7a). The product time score times the number of ruptures is an upper estimate of the log probability of the scenario based on dating evidence alone. For example, the probability of a scenario with a product time score of -2 and 24 ruptures would be of the order of 10^{-48}. Numerically the dating evidence probability of these scenarios is vanishingly small, but the relative scores provide some basis for selection.

Adjusted product time scoring: The adjusted product time score (Figure 13e) corrects the product time score for the differences in the average number of events per contributing rupture. Scenarios with 19 ruptures (our lowest number) have lower product scores than those with 26 ruptures (our chosen upper limit) by a factor of 26/19. The adjusted time score takes out this effect. This results in a more readily interpreted measure of time congruence among events in the selected ruptures.

Figure 14 is a detailed view of the best fitting scenarios from Figure 13 based on minimum adjusted time score and displacement fit. The subset here requires an average total displacement misfit less than 7.0 meters, and an adjusted product time score better than -1.9. The precise choices for both criteria are somewhat subjective. The 7 m limit is proposed as a conservative upper bound on the average deficit or excess in slip along the central 420 km of the San Andreas fault. The adjusted time score corresponds to a low average overlap among event dates. Referring to Figures 13d,e, these cut-off criteria remove all scenarios with 19 and 20 ruptures, and leave only a few scenarios with 21 ruptures. Most of the eliminated scenarios fit badly in a total-displacement sense (Figure 13d) because they include long ruptures that, in our modeling, scale to large displacements.

Scenarios can be summarized graphically by plotting ruptures in space and time (Figure 15a, b). Ruptures are plotted at their mean dates showing rupture extent and a scaled rupture profile based on the shape of Figure 9 and Hanks-Bakun L-AD scaling. Displacements for ruptures in the ~1100 year period since 900 A.D. are totaled and plotted in the lower half of each figure. Displacement totals are compared, in this case, to totals using WGCEP Model 2.1 (Table 5). Figure 15a shows a scenario with the fewest total ruptures among the 10,000 scenario pool. It includes 19 ruptures total, and only 14 in the post-900 A.D. interval. To account for all the paleoseismic site evidence, the

average number of sites per rupture and the rupture lengths are greater than scenarios with more ruptures. This scenario includes two full-length events, one in the earliest 1500's and another around A.D. 1050. Long ruptures scale in our model to large average displacements. Maximum displacements are also large - for this scenario approaching 14 meters (Figure 15a, lower, "+" symbols). The total displacement for the scenario in Figure 15a exceeds that predicted from the Model 2.1 fault rate by an average of 14.7 meters. This scenario plainly does not fit well in the southern half of the fault.

Figure 15b shows a better fitting scenario. This scenario has a mean misfit of 1.46 meters and fits well through the central portion of the fault, including the rapid decrease in slip rate in and south of the San Bernardino segments (mileposts 334-410). The overall fit to the total displacement predicted by Model 2.1 (Table 5) is achieved by the use of a few 1857-like earthquakes in the northern 300 km of the fault and a mixture of short to intermediate length ruptures in the southern half of the model. A significant misfit is observed only at the southernmost point (milepost 490), where the elevated slip rate on the Coachella segment is under-predicted. The fit in Figure 15b is improved by the fact that this scenario uses the maximum number of allowed ruptures to achieve the fit (26 ruptures; see Figure 14c, upper-right corner). This particular scenario might be criticized for the large maximum displacement (12 m, "+" symbols) predicted by the >440 km long rupture in the mid-1500's. Overall, however, he pattern of large and small ruptures exhibited in Figure 15b is typical of good-fitting scenarios.

Figure 16 shows six rupture scenarios for each of the three slip-rate models in Table 5, and the Hanks and Bakun (2002)L-AD relation. In each model, the top two scenarios are the best-fitting among the 10,000 scenarios in an average displacement misfit sense. For all three slip rate models good mean displacement misfits are found, although Model 2.3 is best among them because the model has a higher slip rate through San Bernardino and San Gorgonio Pass and a lower discontinuity in slip rate with the southern Mojave segment. In the Carrizo to Northern Mojave segments, successful scenarios usually include three earlier ruptures similar in location and extent to the 1857 rupture. The middle two scenarios for each slip-rate model are the best using the adjusted time fitting criteria. The selection of ruptures in these scenarios are generally similar to those best fitting the displacement total, with some compromise in the quality of the displacement fit. In the bottom two plots, scenarios are shown which account for the paleoseismic site events in the fewest number of ruptures while still passing the subset criteria described above. Displacement misfits are larger on average by 4 to 5 meters compared to the best fitting scenarios. The average displacement misfit is achieved by a reasonable fit northwest of milepost 300 and a substantial over-prediction of slip through the San Bernardino and the San Gorgonio segments. Subject to that qualification, a reasonable fit to the paleoseismic data since A.D. 900 can be achieved with as few as 15 southern San Andreas fault ruptures. If rupture displacement scales with rupture length, a large displacement misfit seems required for end-to-end ruptures to be included in scenarios.

Figure 17 parallels Figure 16, but uses the Wells and Coppersmith (1994) relationship as modified in Equation 5 for average displacement. This relationship predicts larger average displacements for a given rupture length, so scenarios fitting model displacement totals have shorter ruptures on average than those using the Hanks and Bakun (2002) L-AD regression. Overall, however, the best displacement misfits are

consistently inferior to those using the Hanks and Bakun (2002) regression. The general patterns of rupture are similar to those in Figure 16 The L-AD relation in Equation 5 scales to displacements so large that end-to-end ruptures exceed the 7 meter mean misfit cutoff we have adopted. Thus, if end-to-end ruptures have occurred in the most recent 1100 years on the southern San Andreas fault, average displacements similar or smaller than those of Hanks and Bakun seem required.

The relative compatibility of the three WGCEP slip rate models (Table 5) with the paleoseismic site evidence may be estimated using the pool of scenarios. This is done by counting the number of scenarios that passing a standard time and mean displacement misfit criteria for a given slip rate model. The number of scenarios passing a mean displacement misfit less than 7 meters and an adjusted time score of -1.9 (Figure 13) is shown in Table 6 for the three slip rate models and the two length-displacement regressions considered. The number of scenarios passing this cutoff is proportional to the slip rate through the Southern San Bernardino and San Gorgonio segments (Table 5). Between the two regression models, the Hanks and Bakun (2002) regression allows more scenarios to succeed for each of the slip-rate models than does the Wells and Coppersmith regression as expressed in Equation 5. The poorer performance of Wells and Coppersmith relationship traces to the larger AD from Equation 5 for a given length. The larger AD leads to taller rupture profile maxima and a greater tendency for long ruptures to exceed the total slip.

Ensembles of fault rupture scenarios passing some misfit criteria can be used to evaluate segmentation models and quantify the frequency of single- and multi-segment ruptures. However, segmentation per se, and the Working Group's use of it are beyond the goals of this paper, and application of scenarios to segmentation is reserved to Appendix B.

Discussion

In presenting the particular data and circumstances of the southern San Andreas fault rupture history we have often only touched on details and alternatives that could be important in using our method on other faults. In the first portion of the discussion we develop some of the less obvious properties of our analysis, including assumptions, limitations, and generalizations. In the second portion we discuss the robust qualities of southern San Andreas fault behavior that appear in our modeling of the paleoseismic rupture evidence. Figure 2 may be useful for visualizing elements of the discussion.

Rupture Correlation and Scenario Evaluation

At its most basic level, our analysis can be summarized as being a way to avoid the need to prove correlations between paleoseismic events by forming rupture scenarios from a pool of all possible ruptures, then selecting successful scenarios on the basis of external constraints. Dating precision alone is unlikely to ever be adequate to demonstrate correlations, especially among events relatively close in time. The method of linking events, or stringing pearls, provides a formalism to find all the ruptures that the paleoseismic event data suggest might have occurred. Presumably, the ruptures that

actually happened on the fault are among the possibilities. At root our analysis can succeed when the event data itself and the outside constraints combine to usefully limit the ensemble of scenarios to a fraction with diagnostic properties.

The length and scaled average displacement of ruptures are fundamental qualities. The spacing of paleoseismic sites gives each rupture a core length. Adding to that core length are the rupture "tails" extrapolated from a measured or sampled rupture displacement at the end sites. Neither the distribution of rupture displacements nor the rule to extrapolate from displacement to length is well known. We adopted an average tapering rate to zero displacement (rupture end) of 9900*D (meters), but realize that both faster and slower rates have been observed. In assigning rupture tail lengths, the uncertainty in the extrapolation rule (9900*D, or something else) is approximately replaced by sampling from variability in the model for D and a fixed rule given D. Ruptures in the rupture pool will appear in multiple scenarios and be assigned different tails each time, so we expect ruptures to sample much of their uncertainty in length.

Translating rupture length to average displacement is another significant source of uncertainty. We explored this with two relationships, that of Wells and Coppersmith, 1994, adapted to lower displacements for long ruptures (Equation 5), and that of Hanks and Bakun (2002). To a point the length-average displacement relationship trades off with rupture tail length in scenario selection. The Wells and Coppersmith (1994) relationship predicts larger displacements for a given rupture than Hanks and Bakun (2002), but it can work with the total displacement criterion because some other scenario will include the same rupture with shorter tails. For the longest ruptures, however, the differences in regressions become pronounced, and, ultimately, fewer scenarios pass a total displacement misfit cutoff (Table 6) using Wells and Coppersmith (1994). Other length-average displacement relationships could be investigated, including one in which average displacement does not scale indefinitely with increasing length. The smaller AD is relative to rupture length, the greater the number of long ruptures will be in accepted scenarios. We find in terms of final interpretations, however, that the two scalings of length to average displacement, lead to fundamentally similar interpretations.

In terms of the paleoseismic data itself, one of the most determinative properties is the number of ruptures at a site since some certain time. The number of events in a complete record constrains scenarios through the total rupture displacement prediction using the date of the oldest event and the fault slip rate. For example, accepting the WGCEP Model 2.1 rate of ~29 mm/yr slip rate at Pallett Creek and the record of 10 ground rupturing events since A.D. 650, the average slip per event at Pallett Creek would be nearly 4 m. This one observation means that successful scenarios will include many large (M>~7.5) ground rupturing events. There may be some smaller displacement events, but on average, each rupture with less than 4 meters displacement must be compensated by another with slip greater than 4 meters. It might be argued that the paleoseismic record is incomplete at some displacement level, and that moderate earthquakes actually account for much of the total displacement. However, displacements smaller even than 1 meter are reported and included in the paleoseismic records (e.g., Weldon et al., 2005; Sieh, 1984). One would have to argue for systematic omission of half of the ground-rupturing earthquakes at Pallett Creek to get the average slip per event to ~2 m and an average earthquake in the low M 7 range. This would be very inconsistent

with the historical record of only two SSAF earthquakes in the historical period. The simpler alternative is that the southern San Andreas fault commonly ruptures in relatively large events.

If displacement-per-event data was generally available, the displacement predictions of model ruptures might be compared with them. If paleoseismic evidence at a site in the middle of a long rupture indicates a small co-seismic displacement, the long rupture can be considered less likely than a shorter rupture involving the same event evidence. In general the comparison of model rupture displacements to measured displacements will be only approximate because of the variability along strike of real ruptures (Hemphill-Haley and Weldon, 1999).

We have not included the uncertainty in WGCEP slip rates in our analysis for two reasons. First, the three models in Table 5 already express the range of rate uncertainties as judged by the working group. Second, when judging ensemble properties of the pool of scenarios, including the slip rate uncertainty does not change which among them fit best. The scenario total displacements already sample the space around the slip-rate prediction, and uncertainties in the rate do not add anything. Uncertainty in the slip rate might have a use in evaluating individual scenarios or in comparing at a more detailed level than our total fit criterion considers.

The selection of scenarios on the basis of the total displacement criteria is limited to some degree by what one considers an acceptable mean distance from the predicted total. That is, if 32 meters of displacement is predicted in 1100 years, the issue remains of how much variability from 32 meters is acceptable. Weldon et al. (2004) suggest that the fault could be locally out of equilibrium by a few meters and rarely up to 7 m. Whether such a deficit or surplus could be sustained for the whole fault is unknown.

We have not attempted to define a present slip deficit from the most recent events in 1857, 1812, and ~1690. If the deficit is real, scenarios that over-predict total slip from the paleoseismic data would be less likely than those that under-predict it. We note that a symmetric slip deficit uncertainty exists at whatever time we start counting events – i.e., a flurry shortly after AD 900 would start the displacement totals above their long-term rates. Still, it is tempting to interpret the under-prediction of slip on the Coachella segment (e.g., Figures 15-17) as, in some measure, a reflection of a rupture history behind the actual strain accumulation.

Results for the San Andreas Fault

Some likely qualities of pre-historic rupture on the southern San Andreas fault have emerged from our study:

- First, it appears unlikely that the fault experienced a Parkfield-to-Indio rupture in the most recent 1100 years if the rupture profile and displacement scaling we adopted is approximately correct. The quality of the southern San Andreas paleoseismic data is such that it seems unlikely to simply be an accident of the particular record we have. End-to-end events occur rarely in acceptable scenarios, and only with large relative displacement surpluses. However, if the slip rate is found in future studies to be

higher through the San Gorgonio Pass region, end-to-end events become more likely due to similarities in timing of events north and south of this region.

- Second, the total displacement criterion favors scenarios with three previous events similar to the 1857 rupture. This correlation is more due to the treatment of the Carrizo record as complete than because of the large displacement measurements at Wallace Creek (Liu et al., 2004) per se. Long ruptures often linking to Pallett Creek are strongly suggested to account for the displacement totals from the slip rate and elapsed time.

- Third, the number of single-site ruptures at Wrightwood indicates that something unusual is occurring there. Perhaps the fault itself is unusual near Wrightwood so as to involve many small or overlapping ruptures. Scharer et al. (2007) find that the recurrence rate in the most recent 14 events is similar to a similar long sequence deeper in the section, so the short recurrence interval of the upper section is probably not exceptional.

- Fourth, paleoseismic data in successful scenarios are more consistent with the derived Hanks-Bakun length to average surface displacement regression than with the Wells and Coppersmith (1994) regression modified to predict smaller average displacements (Eqn 5). It appears that for at least the southern San Andreas fault, ruptures may have displacements more or less typical of other regions from which global regressions are derived.

- Finally, an Addenda is provided discussing the consequences of new evidence for a shorter recurrence interval at Bidart Fan. It shows that the principal conclusions about rupture patterns in scenarios are not strongly changed by the new dating results, primarily because a few relatively large earthquakes are required to account for the total fault displacement between Carrizo and the southern Mojave section.

Summary

We present a new method for analyzing event data from multiple paleoseismic sites on a single continuous fault. The method differs from previous approaches to multi-site correlation in that rather than developing a few possible correlations by hand, all correlations allowed by event dating are entertained. A pool of ruptures constructed in this manner is sampled at random to construct rupture scenarios for the fault. Scenarios account for all the paleoseismic site evidence, and thus are, at some level, possible histories of the fault. Scenarios are can be evaluated by several criteria, including average dating congruence and the total displacement among ruptures. We find that for the southern San Andreas fault scenarios exist that are reasonably consistent in total displacement and dating congruence standards considering the most recent 1100 years of data. These scenarios tend to have common features including three ruptures generally similar in location and extent to the historical 1857 rupture. The lower fault slip rate through San Bernardino and San Gorgonio Pass checks the tendency of ruptures to form continuous ruptures from the Mojave to the Coachella sections. Ruptures in the southern half of the fault appear more variable in length and somewhat less regular in time than in the northern half of the fault.

Acknowledgments

References

Biasi, G.P., R. J. Weldon II, T. E. Fumal, and G. G. Seitz (2002). Paleoseismic event dating and the conditional probability of large earthquakes on the southern San Andreas fault, California, *Bull. Seism. Soc. Am.* **92,** no. 7, 2761-2781.

Biasi, G. P. and Weldon, R. J. (2005). A Bayesian approach to correlation of paleoearthquake on a fault, *Eos Trans., AGU, 86(52)*, Fall Meeting Supplement, Abstract U42A-05.

Biasi, G. P. and Weldon, R. J. (2006). Estimating surface rupture length and magnitude of paleoearthquakes from point measurements of rupture displacement, *Bull. Seism. Soc. Am.,* **96**, 1612-1623.

Fumal, T. E., Weldon, R. J., G. P. Biasi, T. E. Dawson, G. G. Seitz, W. T. Frost, and D. P. Schwartz (2002a). Evidence for large earthquakes on the San Andreas fault at the Wrightwood, California, paleoseismic site: A.D. 500 to Present, *Bull. Seism. Soc. Am.* **92,** no. 7, 2726-2760.

Fumal, T. E., M. J. Rymer, and G. G. Seitz (2002b). Timing of large earthquakes since A.D. 800 on the Mission Creek strand of the San Andreas fault zone at Thousand Palms Oasis, near Palm Springs, California, *Bull. Seism. Soc. Am.* **92,** no. 7, 2841-2860.

Fumal, T.E., S. K. Pezzopane, R. J. Weldon II, and D. P. Schwartz (1993). A 100-year average recurrence interval for the San Andreas fault at Wrightwood, California, *Science,* **259**, 199-203.

Grant, L. B. and K. Sieh (1994). Paleoseismic evidence of clustered earthquakes on the San Andreas fault in the Carrizo Plain, California, *J. Geophys. Res,* **99,** 6819-6841.

Hanks, T. C. and W. H. Bakun (2002). A bilinear source-scaling model for M-log *A* observations of continental earthquakes, *Bull. Seism. Soc. Am.* **92**, 1841-1846.

Hemphill-Haley, M. A. and R. J. Weldon II (1999). Estimating prehistoric earthquake magnitude from point measurements of surface rupture, Bull. Seism. Soc. Am. 89, 1264-1279.Lindvall, S. C., T. K. Rockwell, T. E. Dawson, J. G. Helms, and K. W. Bowman, (2002). Evidence for two surface ruptures in the past 500 years on the San Andreas fault at Frazier Mountain, California, Bull. Seism. Soc. Am. 92, 2689-2703.

Liu, J., Y. Klinger, K. Sieh, and C. Rubin (2004). Six similar sequential ruptures of the San Andreas fault, Carrizo Plain, California, *Geology,* **32,** 649-652.

McGill, S. F., Dergham, S. A., Barton, K., Berney-Ficklin, T., Grant, D., Hartling, C., Hobart, K., Minnich, R., Rodriguez, M., Runnerstrom, E., Russell, J., Schmoker, K., Stumfall, M., Townsend, J., and Williams, J. (2002). Paleoseismology of the San Andreas fault at Plunge Creek near San Bernardino, southern California, *Bull. Seism. Soc. Am.*, **92**, 2803-2840.

Salyards, S. L., K. E. Sieh, and J. L. Kirschvink (1992). Paleomagnetic measurement of non-brittle coseismic deformation across the San Andreas fault at Pallett Creek, *J. Geophys. Res.* **97**, 12457-12470.

Seitz, G. G., R. J. Weldon II, and Biasi, G. P. (1997). The Pitman Canyon paleoseismic record: a re-evaluation of southern San Andreas fault segmentation, *J. Geodynam.* **24,** 129-138.

Sieh, K. E. (1984). Lateral offsets and revised dates of large earthquakes at Pallett Creek, California, *J. Geophys. Res.* **89**, 7641-7670.

Sieh, K. E. (1986) Slip rate across the San Andreas fault and prehistoric earthquakes at Indio, California, *EOS Transactions*, **67,** 1200.

Sieh, K., M. Stuiver, and D. Brillinger (1989). A more precise chronology of earthquakes produced by the San Andreas fault in southern California, *J. Geophys. Res.,* **94**, 603-623.

Sims, J. D. (1994). Stream channel offset and abandonment and a 200-year average recurrence interval of earthquakes on the San Andreas fault at Phelan Creeks, Carrizo Plain, California, *Proceedings of the Workshop on Paleoseismology: U.S. Geological Survey Open-File Report 94-568*, 170-172.

Weldon, R., K. Scharer, T. Fumal, and G. Biasi (2004). Wrightwood and the earthquake cycle: what a long recurrence record tells us about how faults work, *GSA Today*, **14,** No. 9, 4-10.

Weldon, R. J. II, T. E. Fumal, T. J. Powers, S. K. Pezzopane, K. M. Scharer, and J. C. Hamilton (2002). Structure and earthquake offsets on the San Andreas fault at the Wrightwood, California paleoseismic site, *Bull. Seism. Soc. Am.* **92,** no. 7, 2704-2725

Wells, D. L., and K. J. Coppersmith (1994). New empirical relationships among magnitude, rupture length, rupture width, rupture area, and surface displacement, Bull. Seism. Soc. Am. 84, 974-1002.

Yule, D. and C. Howland (2001). A revised chronology of earthquakes produced by the San Andreas fault at Burro Flats, near Banning, California, in *SCEC Annual Meeting, Proceedings and Abstracts*, Southern California Earthquake Center, Los Angeles, 121.

University of Nevada Reno
Seismological Laboratory MS-174
Reno, NV 89557
glenn@seismo.unr.edu
(GB)

University of Oregon
Department of Geological Sciences
Eugene, OR 97403
ray@uoregon.edu
(RW)

Table 1. Paleoseismic sites

Site Number	Site Name	Date of Oldest Constraint (A.D.)	Number of Events	Milepost SE of Creeping Section
106	[1]Carrizo	560	6	93
110	[2]Pallett Creek	550	10	299
111	[3]Wrightwood	550	14	321
113	[4]Pitman Canyon	900	7	347
114	[5]Plunge Creek	1300	3	378
116	[6]Burro Flat	600	7	407
117	[7]Thousand Palms	750	5	465
118	[8]Indio	900	4	481

1. Liu et al. (2004), Wallace Creek; Grant and Sieh (1994), Bidart Fan; Sims (undated), Wallace Creek. If the displacements reported by Liu et al. (2004) are single ruptures, they probably would have spanned all sites. In light of our objective to study event correlation at a larger scale, site investigations at Bidart and Wallace Creek were summarized into a single paleoseismic record. We consulted reported radiocarbon evidence and constructed earthquake date distributions using the OxCal program (Ramsey et al, 2002).
2. Biasi et al. (2002); Salyards et al. (1993); Sieh et al. (1989); Sieh (1984).
3. Weldon et al. (2004); Fumal et al. (2002a); Weldon et al. (2002); Biasi et al. (2002).
4. Seitz et al. (1997); Seitz (1999).
5. McGill et al. (2002).
6. Yule and Sieh (1999).
7. Fumal et al. (2002b).
8. Sieh (1984).

Table 2. Event dates from eight paleoseismic sources

Notes for all paleoseismic sites:
1. Mean = sum(yr*pyr) where yr is a date bin and pyr is the probability of the event being in that bin
2. Sqrt(var) = sqrt(sum(pyr*(yr-mean)^2)); actual PDF weights are used
3. Median: date where 50% of the PDF weight is on either side
4. Differences between mean and median reflect asymmetry in the underlying PDF

Source	Mean	sqrt(var)	Median	Event Name
	1857			Historical
	1571	116	1596	Carr2shv
Combined	1384	77	1373	Carr3shv
Carrizo Plain	1277	103	1318	Carr4shv
	1078	82	1050	Carr5shv
	599	85	608	Carr6shv

- Combined record from Grant, Liu, and Sims investigations
- Ordering constraints were applied
- Newer results are recognized but not available in time to include

Source	Mean	sqrt(var)	Median	Event Name
	1857			Historical
	1812			Historical
	1547	31	1546	V
	1360	7	1361	T
	1084	16	1087	R
Pallett Creek	1067	16	1065	N
	956	19	952	I
	842	17	846	F
	764	7	758	D
	645	12	646	C

- PDFs are from Biasi et al, 2002

Source	Mean	sqrt(var)	Median	Event Name
	1857			Historical
	1812			Historical
	1685	18	1681	W3
	1536	13	1531	W4
	1487	18	1478	W5
	1360	7	1361	W5T
	1264	29	1257	W6
Wrightwood	1116	37	1111	W7
	1016	27	1007	W8
	850	20	852	W9
	781	18	782	W10
	722	11	722	W11
	697	16	688	W12
	634	31	628	W13
	533	69	527	W14

- PDFs are from Biasi et al, 2002
- Event W5T PDF repeats Pallett Creek T; see Weldon et al. 2004
- Events W13 and W14 are too old for useful matching elsewhere, and not used in scenarios

Source	Mean	sqrt(var)	Median	Event Name
Pitman Canyon	1812			Historical
	1704	50	1706	Pit2
	1559	78	1567	Pit3
	1437	70	1419	Pit4
	1313	52	1305	Pit5
	1173	81	1180	Pit6
	931	91	942	Pit7

- PDFs synthesized from Seitz et al. 1997 and Seitz 1999

Source	Mean	sqrt(var)	Median	Event Name
Plunge Creek	1812			Historical (1)
	1619	48	1619	Plunge1
	1499	114	1499	Plunge2

- PDFs synthesized from data in McGill et al. 2002
- (1) Yule (2006)

Source	Mean	sqrt(var)	Median	Event Name
Burro Flat	1812			Historical (1)
	1684	37	1673	Burro2
	1500	23	1495	Burro3
	1475	78	1478	Burro4
	1347	21	1347	Burro5
	1107	37	1098	Burro6
	774	48	774	Burro7

- PDFs shaped as Gaussians on date ranges provided by Yule
- (1) Yule (2006) includes 1812 as a historical event

Source	Mean	sqrt(var)	Median	Event Name
Thousand Palms Oasis	1683	34	1674	TP1
	1503	25	1494	TP2
	1230	29	1223	TP3
	982	79	978	TP4
	824	29	830	TP5

- PDFs shaped from OxCal; Fumal et al. 2002

Source	Mean	sqrt(var)	Median	Event Name
Indio	1680	23	1675	Indio1
	1480	58	1475	Indio2
	1300	45	1295	Indio3
	1020	10	1015	Indio4

- PDFs shaped as Gaussians on date ranges in Sieh 1986

Table 3. Summary of parameters and values used for making and retaining ruptures

Parameter name	Value	Description
minoverlap	0.02	Minimum required product overlap to match events into a rupture.
ppenalty	0.01	Probability weight for a "missed" event
cutoff	1.5	-log10(product probability average) Pair-wise probability product must average greater than this for rupture to be retained.
minvennscore	0.10	Real event overlap area must average >*minvennscore*
max_mean_median	40 yrs	Rupture mean date must be closer than *max_mean_median* from the median. Detects poor event date overlaps.
rmax_stdev	90 yrs	Accept ruptures with date distributions < *rmax_stdev* width parameter

Table 4a. Events with displacement measurements/estimates
Mean, D low, and D high in meters.

Site	Event	Mean Displ	Min Displ	Max Displ
Wrightwood	W3	3.5	1	7
Wrightwood	W4	7	3	9
Wrightwood	W5	0.7	0.1	2.8
Wrightwood	W5T	0.7	0.1	2.8
Wrightwood	W6	3.7	1.9	5.6
Wrightwood	W7	1.8	1.1	3.4
Wrightwood	W8	1.5	0.7	3.1
Wrightwood	W9	6.6	3	9.9
Wrightwood	W10	5.2	2.5	7.5
Wrightwood	W11	3	1.2	6.3
Wrightwood	W12	4.1	1.4	8.2
Wrightwood	W13	1.8	1	5.1
Wrightwood	W14	1.9	1	3.8
Pallett Creek	C	6.7	3.3	10
Pallett Creek	D	6.7	3.3	10
Pallett Creek	F	6.7	3.3	10
Pallett Creek	I	0.5	0.25	1
Pallett Creek	N	0.33	0.16	0.66
Pallett Creek	R	2.67	1.33	5.33
Pallett Creek	T	4.3	2.1	6.4
Pallett Creek	V	5.5	2.5	8.5
Carrizo	Carr1	7.9	7.7	8.1
Carrizo	Carr2	7.6	6.8	8.4
Carrizo	Carr3	5.2	4	6.4
Carrizo	Carr4	1.4	0.4	2.4
Carrizo	Carr5	8	7	9
Carrizo	Carr6	5.4	4.2	6.6

Table 4b. Basis for average displacement estimates
Oldest = calendar A.D.; Timespan in years; RI in years

Site	N events	Oldest	Timespan	RI
Pitman	7	931	1075	154
Plunge	2	1499	507	254
Burro	7	774	1232	176
TPalms	5	824	1182	236
Indio	4	1020	986	247

Table 5. Segment bounds and slip rates. Mpst = milepost (km) of WGCEP segment boundaries

	Pkfl	**Chol**	**Carr**	**BBnd**	**MojN**	**MojS**	**NSbr**	**SSBr**	**SGor**	**Coac**
Mpst:	-8 -27	27 -89	89- 149	149- 198	198- 236	236- 334	334- 370	370- 410	410- 473	473- 546
Model 2.1	34	34	34	34	29	28	22	16	10	20
Model 2.2	34	34	34	34	29	28	18	12	6	16
Model 2.3	34	34	34	34	34	34	25	20	14	24

Table 6. Number of scenarios passing time and displacement subsets

Model number	**2.1**	**2.2**	**2.3**
H-B, # passing	1997	1710	2308
W-C, # passing	389	259	515
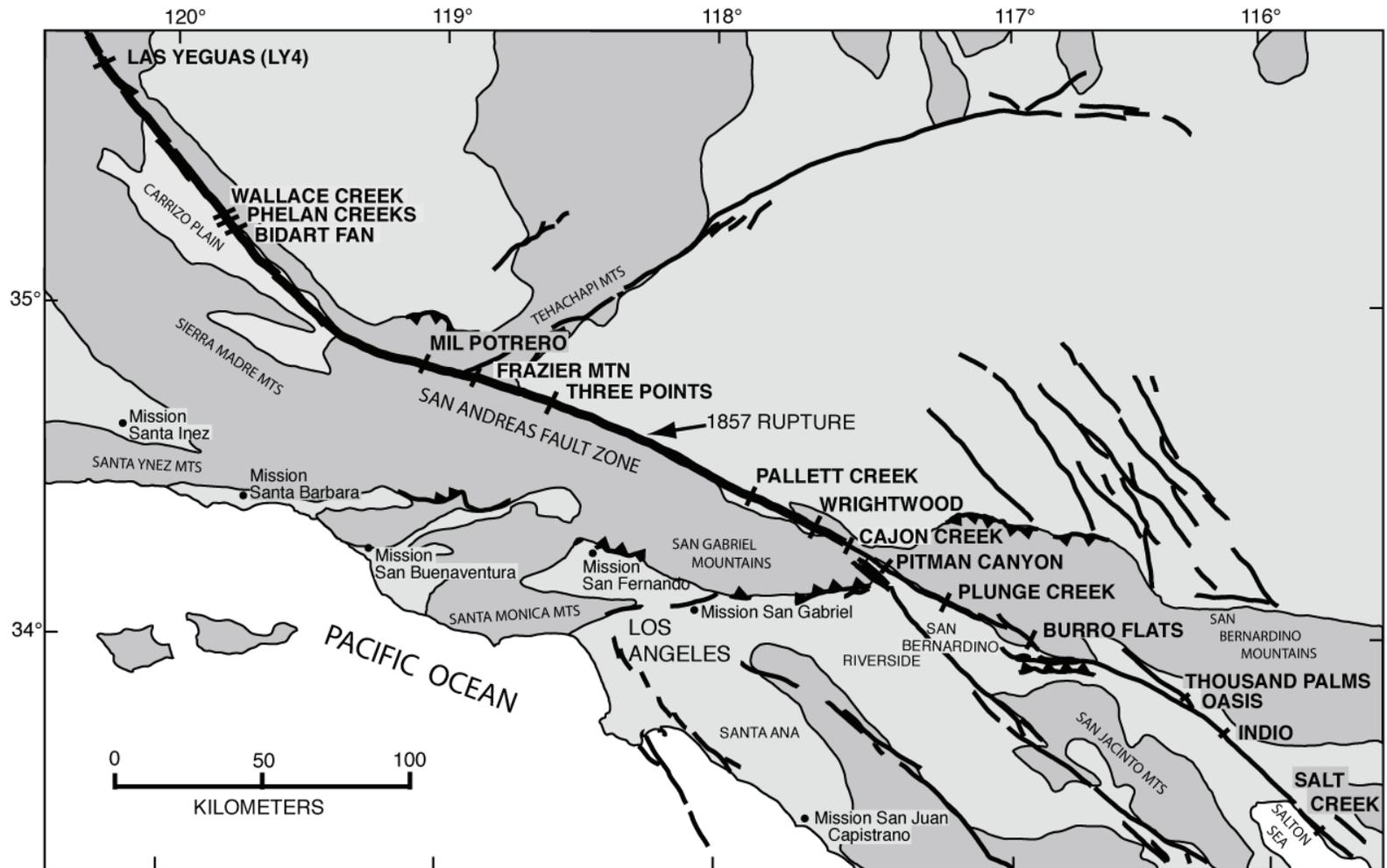
Figure 1. Paleoseismic sites on the southern San Andreas fault. Darker areas are elevated. Of the paleoseismic sites on the San Andreas fault, eight are used in this analysis (Table 1).
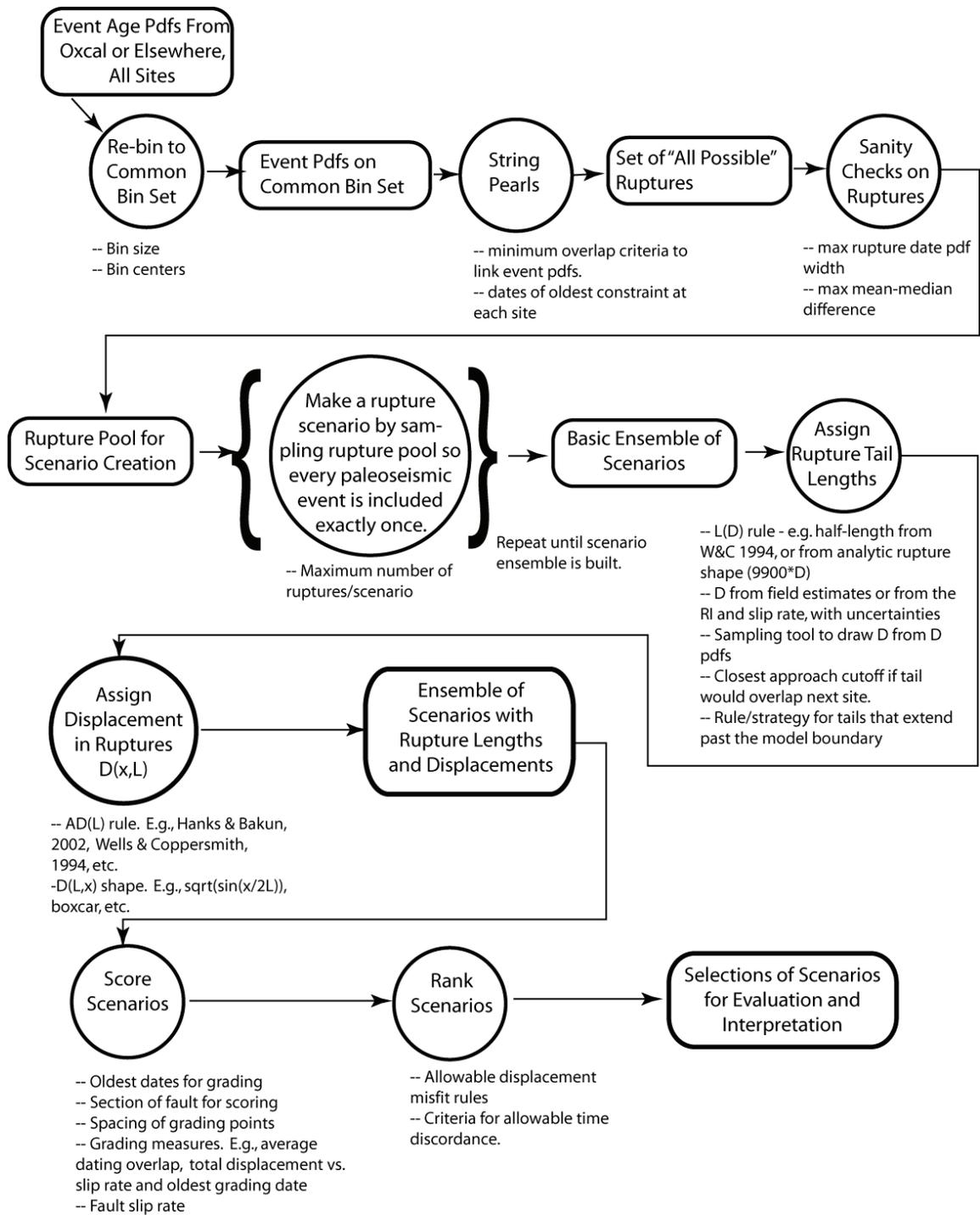
Figure 2. Flow chart for rupture and scenario development. Rectangles are discrete products or files. Circles denote processes. Text under circles indicates input parameters and/or relationships to the process in the circle.
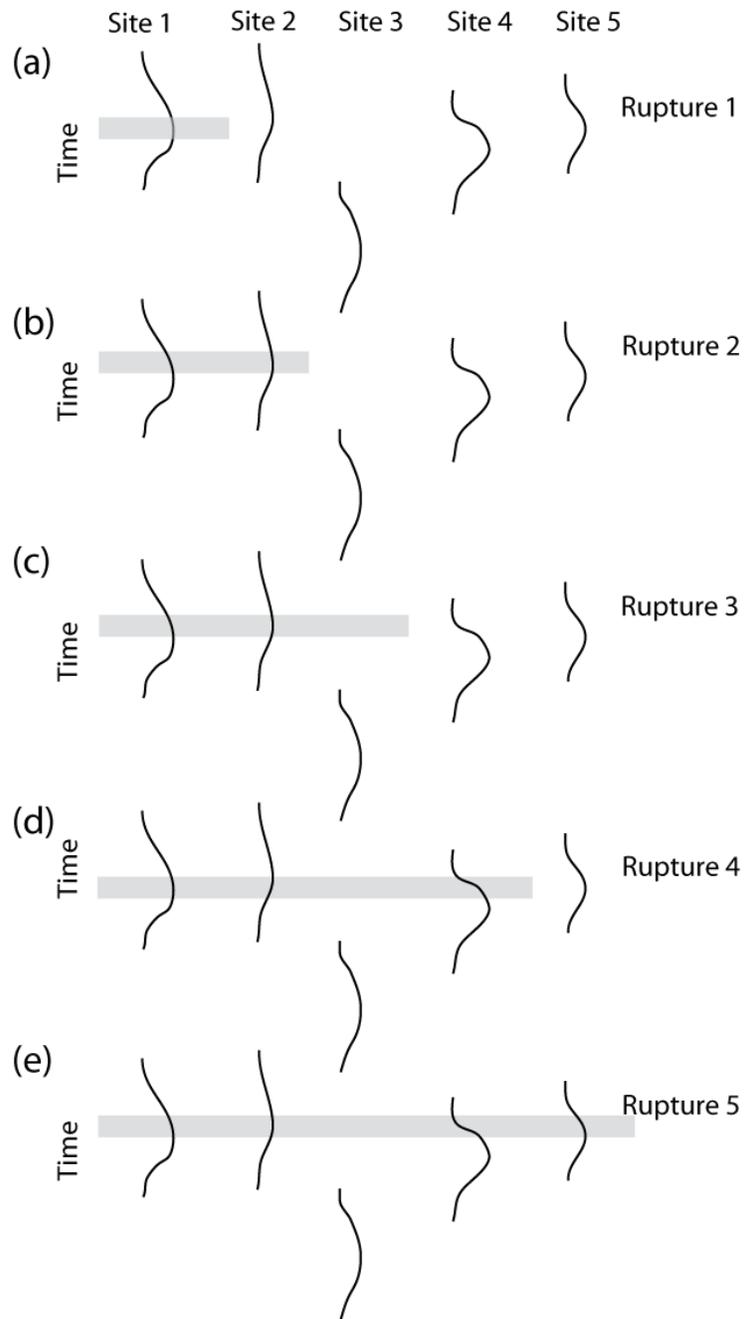
Figure 3. "Stringing pearls" to make multiple-site ruptures with paleoevent data from physically separated sites. Schematic event pdfs are shown for five sites. (a) Each individual event will become a rupture, shown as a gray bar. (b) A second rupture will include both sites 1 and 2. (c) Site 3 illustrates the case where there is no overlap with the "master" event at site 1. In this case rupture 3 is still constructed, but a "miss" is noted for the rupture at site 3. This keeps the record at site 3 from trumping that at the adjoining sites. A penalty is ascribed to rupture 3 since it missing events are presumed to be unlikely. (d) and (e) show extensions of rupture 3 to sites 4 and 5 respectively. The complete rupture set for this set of events will include cases beginning at site 2, then site 3, etc., with formal duplicates removed.
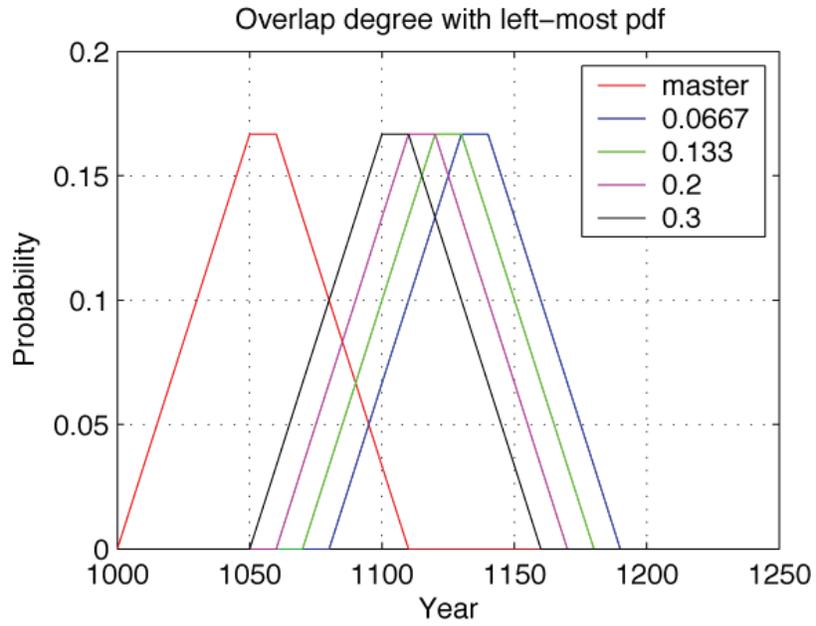
Figure 4. Overlap for four identical model date distributions overlapping by different amounts.
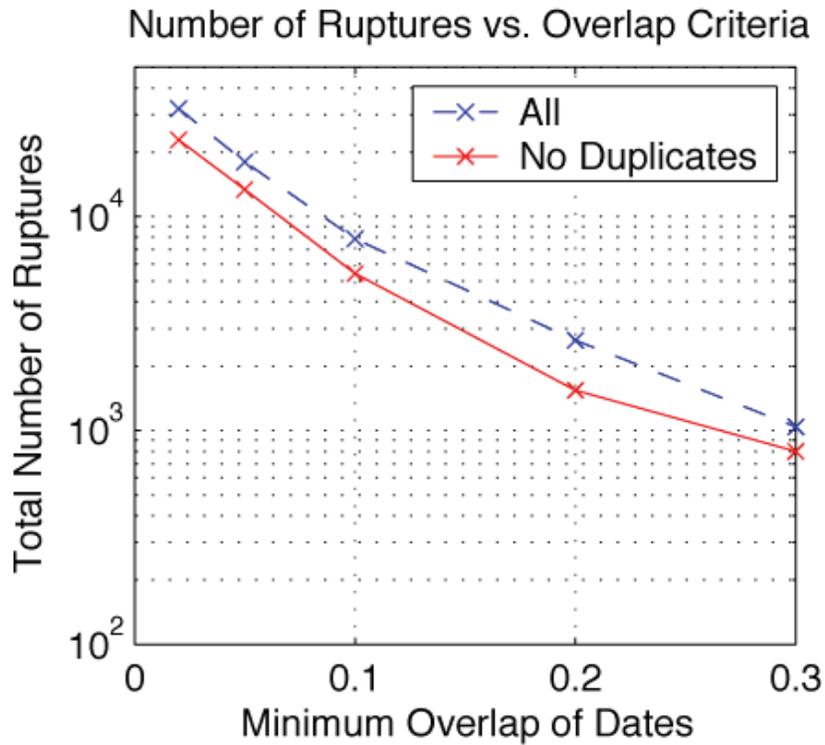
Figure 5. Number of ruptures in rupture pool versus overlap required in event dates. Overlap is measured from the first (master) event from which the rupture is constructed.
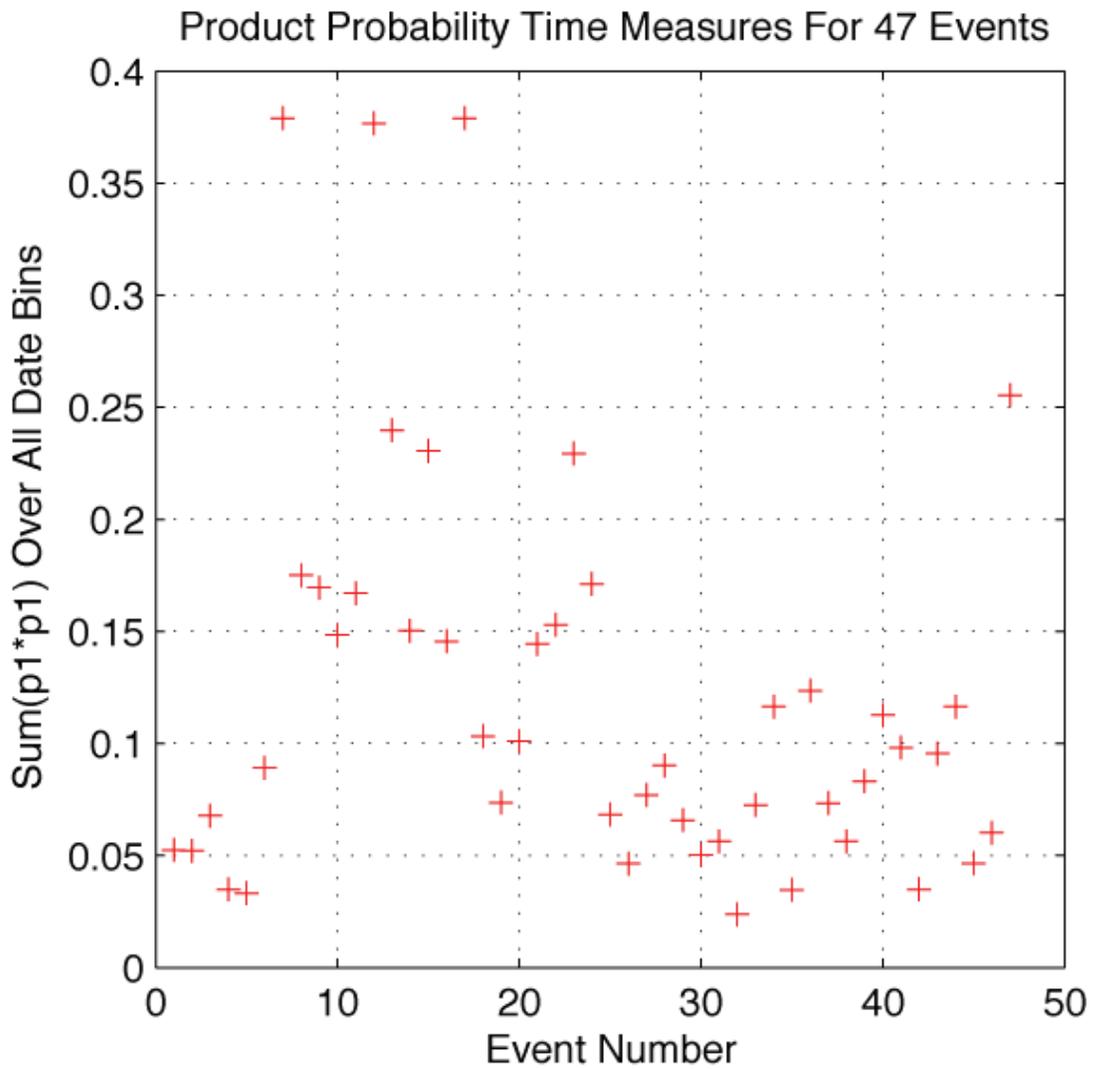
Figure 6. Product overlaps of event pdfs with themselves range from 0.02 to 0.38. Events 6 to 24 are the relatively precise event dates from Pallett Creek and Wrightwood sites (Biasi et al., 2002).
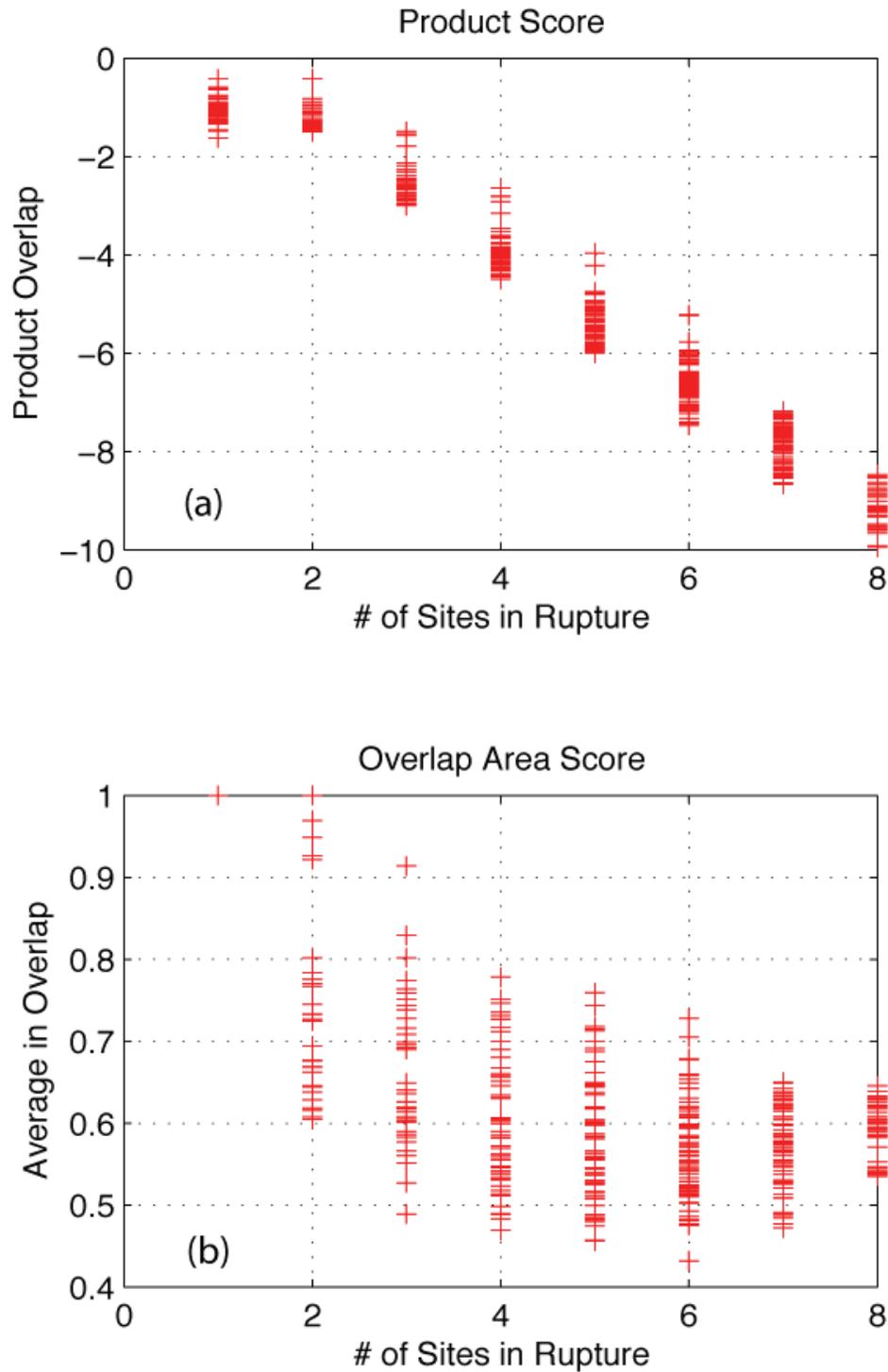
Figure 7. (upper) The cumulative product overlap decreases predictably with increasing numbers of events in the rupture. The mean product overlap cutoff causes the sharp lower bound on the distributions at each rupture length ordinate. (lower) The mean overlap score also decreases with increasing rupture length. The apparent improvement in overlap for 7- and 8-site ruptures is an artifact of the mean overlap cutoff.
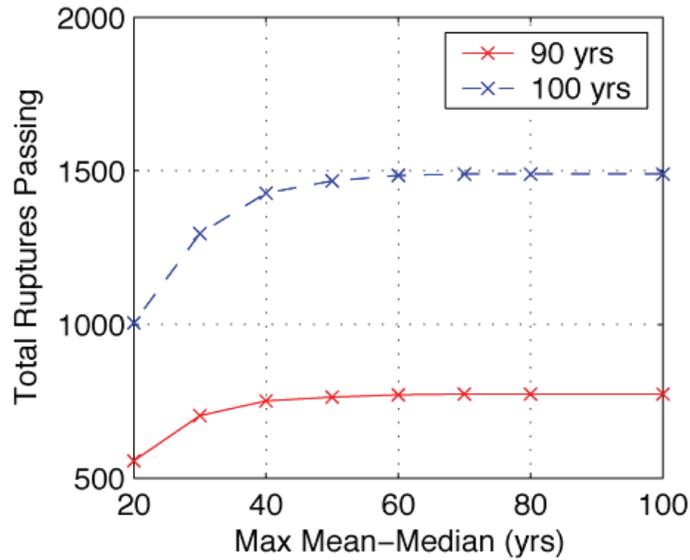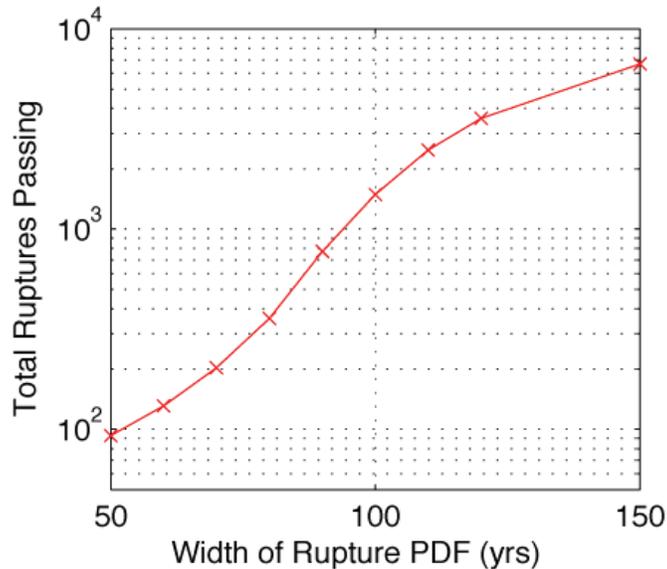
Figure 8. (a) The number of ruptures retained is plotted vs. the difference between mean and median for two rupture pdf width cutoffs. Ruptures with a mean-median difference greater than 40 years were removed. With an allowed width of 100 years vs. 90, a factor of two increase in the number of ruptures results. Note, however, that all the ruptures retained this way would have widths two to four times the width of a typical event date pdf. (b) The width of the rupture date (square-root of the variance) is plotted versus the number of ruptures retained. A value of 90 years was selected as a cutoff for retaining ruptures.
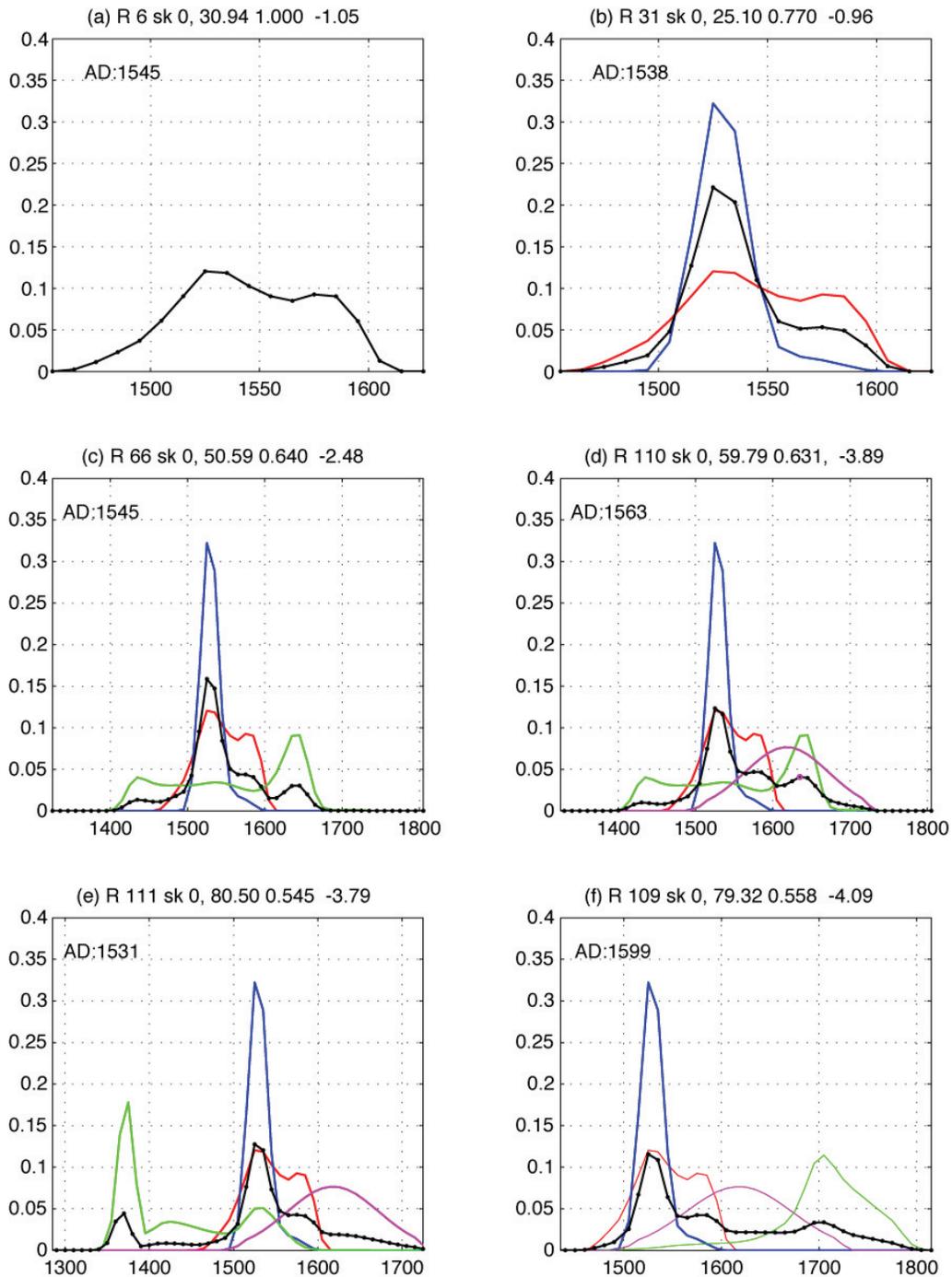
Figure 9. Six example ruptures built following the approach in Figure 3. The resulting rupture date pdfs are plotted with dots to distinguish them from the contributing event dates. (a) The date distribution for event V at Pallett Creek using the reassessment of Biasi et al., 2002. In this case the rupture date pdf and contributing event date are the same. (b) After adding a well-defined event from Wrightwood, the rupture date narrows. (c) A broad Pitman Canyon event (Pit-3) introduces a small mode in the mid-1600's. (d) Same as (c), but with a Plunge Creek event. (e) and (f): Same as (d), but with two alternative Pitman Canyon events in (Pit-2 and Pit-4), respectively.
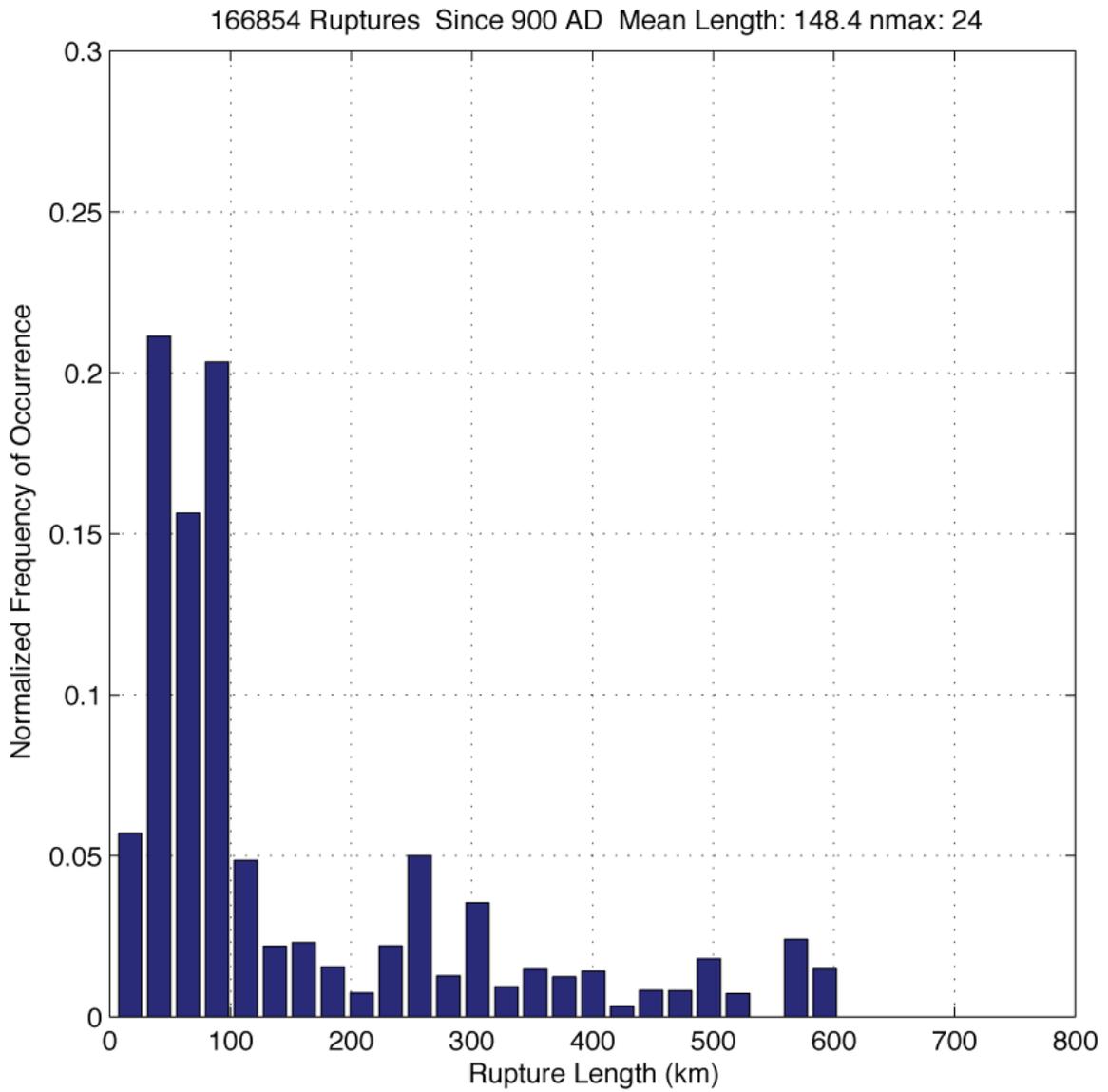
Figure 10. Histogram of rupture lengths for rupture scenarios with 22 or fewer ruptures. The upper number of ruptures was restricted because the scenario pool is dominated by scenarios with more shorter ruptures.
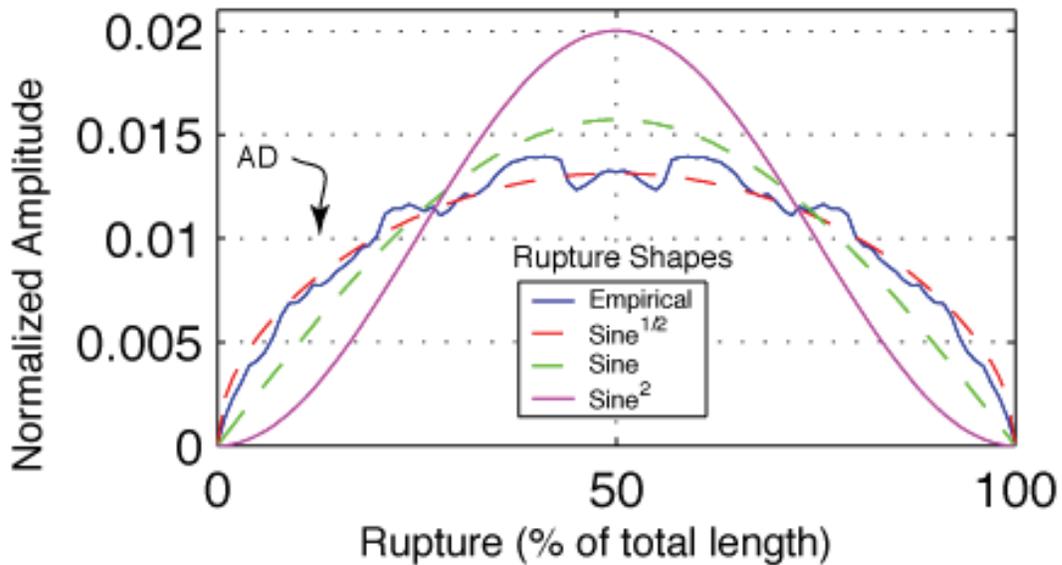
Figure 11. Solid line: Mean rupture profile based on 13 mapped ruptures after normalizing to unit length and summing with the rupture profile reflected right-to-left. If profiles are not reflected, the shape of the empirical profile would depend on how the contributing profiles are aligned. AD label at the 0.01 level indicates the average displacement for all profiles. The *sqrt(sin(πx/L))* shape is much less peaked than typical mapped rupture shapes. For details see Hemphill-Haley and Weldon (1999) and Biasi and Weldon (2006).
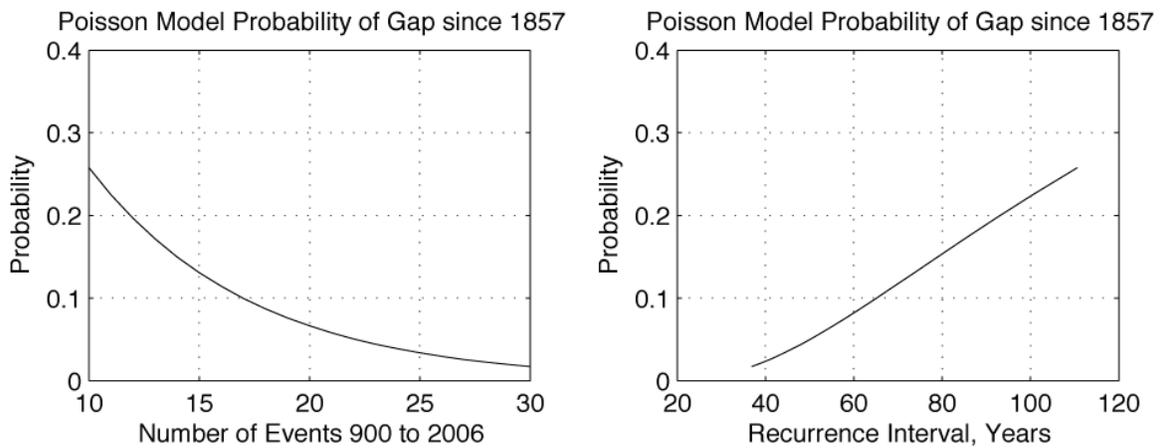

Figure 12. Poisson probabilities of the open interval since 1857 for various numbers of ruptures since A.D. 900. For any realistic number of ruptures, the present open interval is unusual. Scenarios with 18 total ruptures are twice as likely as those having 24 ruptures. Corresponding whole-fault recurrence intervals are shown at right.
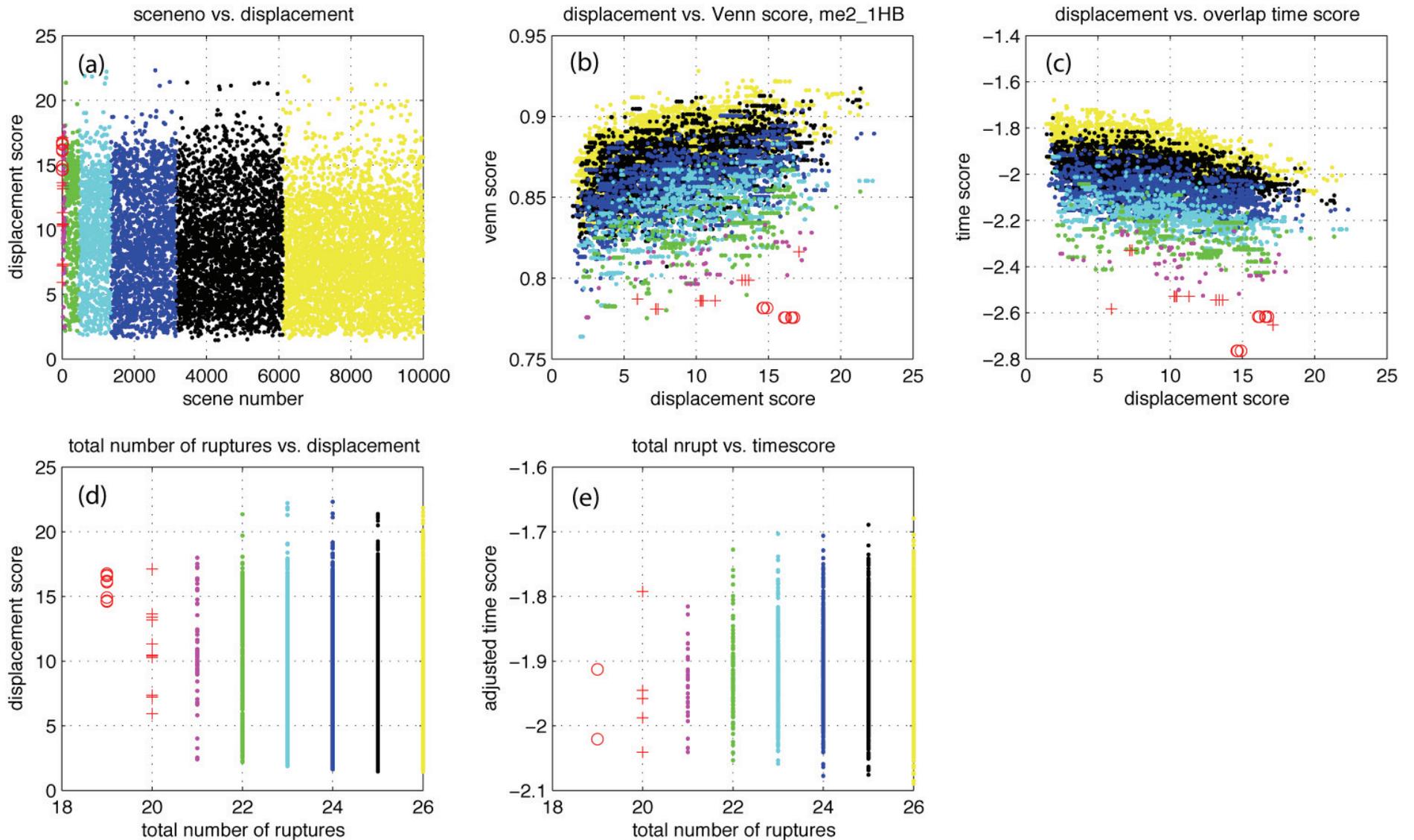
Figure 13. Scenario scoring criteria and their trade-offs, ranking all 10,000 scenarios. Colors and symbols correspond to the number of events in the scenario, with "+" and "o" being the fewest. (a) Displacement score vs. scenario number. Scenarios are numbered in order of increasing number of ruptures. Only 3-4% of scenarios have 22 or fewer ruptures. (b) The date overlap or Venn score is seen in the distribution of colors to decline with decreasing numbers of ruptures in the scenario. There is a weak trend toward improved average overlap with increasing displacement misfit. (c) Average product overlap among event dates (time score) anti-correlates in general with the number of ruptures in the scenario. A time score cut-off of -1.9 was applied to subset for Figure 14. (d) Best displacement scores appear to degrade for scenarios with fewer than about 21 ruptures, suggesting that ruptures are too long, and their displacements too large to work with the fault slip rate. (e) Adjustment of the time score for the increase in the number of events per rupture removes the linear trend in the raw time score.
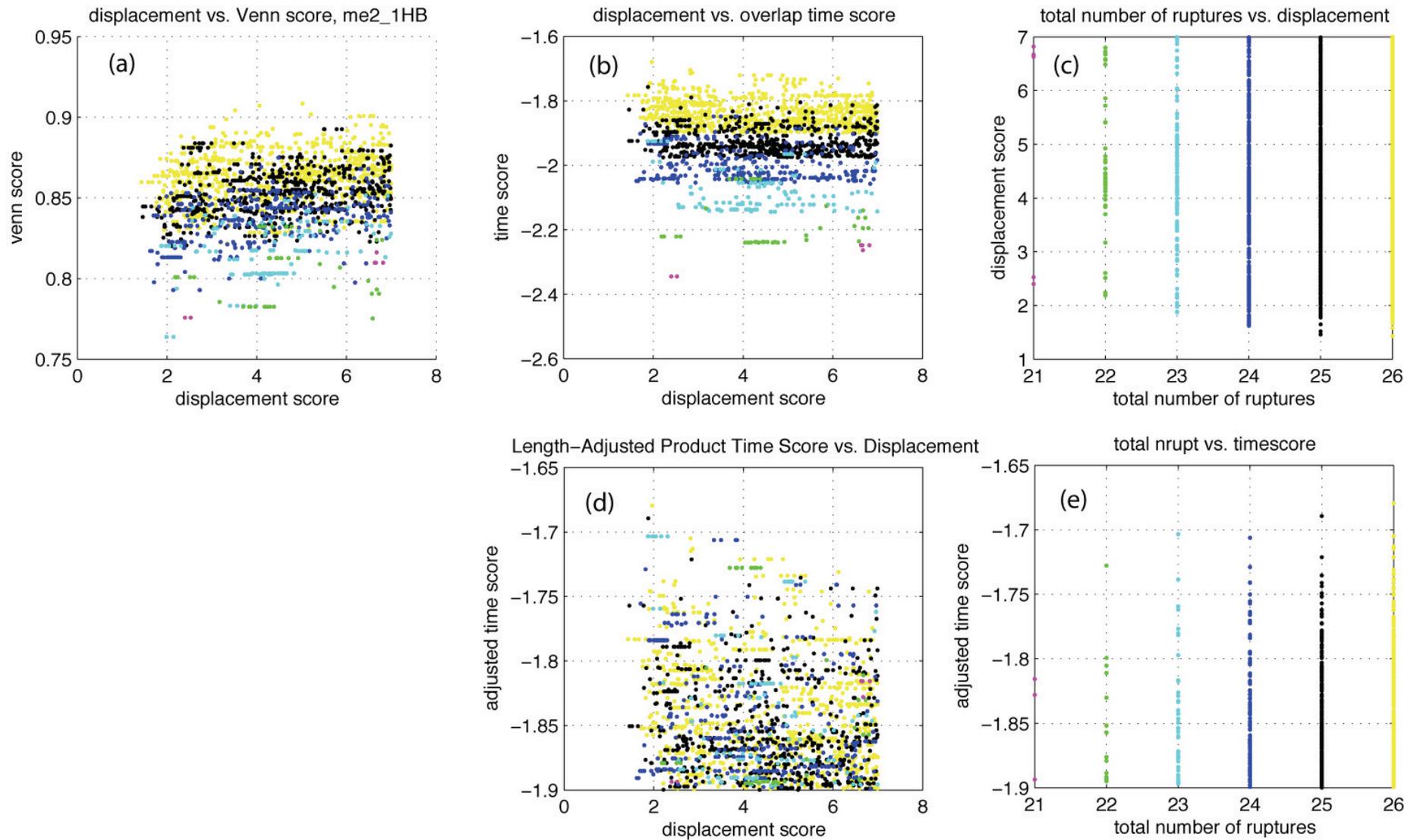
Figure 14. Detail of Figure 13 showing scenario scores for the subset with 7 m or smaller mean displacement misfit and, in (c), (d), and (e), an adjusted time product time score better than -1.9. Colors correspond to the number of ruptures in the scenario (Figure 13a). (a) Venn score versus displacement score. Higher average overlap of date pdfs is easier to achieve with a greater number of ruptures and correspondingly fewer average sites per rupture. (b) Time score vs. displacement score. An average product score of -2 would correspond to 10% of an event date overlapping with 10% in another. None of the scenarios with 19 or 20 ruptures have small enough displacement scores to be in this subset. (c) Displacement score vs. total number of ruptures. Scenarios with larger numbers of ruptures can have smaller displacement misfits because there are more ways to fit ruptures together (more degrees of freedom) for a good fit. (d) Adjusted time score vs. displacement score. For scenarios with 22 or more ruptures no strong pattern is suggested. (e) Adjusted time score vs. the total number of ruptures. Relatively few scenarios with 21 or 22 ruptures have acceptable displacement and date congruence scores. See text for further details.

Figure 15. Below are two example scenarios using WGCEP model 2.1 slip rates (Table 5). (a) A scenario with the fewest number of ruptures. (b) Best mean displacement misfit. Each example includes two panels:

(*Upper*) The horizontal axis is a "milepost" along the surface trace of the fault, referenced to the south end of the creeping section northwest of Parkfield. San Andreas fault segment boundaries (Table 5) are marked with open triangles at top. Two letter labels show the approximate milepost locations of the paleoseismic sites (Figure 1). Ruptures are shown as horizontal black lines, plotted on the vertical axis at the mean time of the combined distribution of contributing events. The red arc above is the displacement of the rupture. The vertical bar for scale in the rupture near 1500 A.D. corresponds to a maximum displacement of 15 meters. The scenario number in the title is its ordinal number in a pool of 10,000 total. *Nrupt* is the total number of ruptures in the scenario. Ruptures after A.D. 900 are included when computing the total displacement. The green lines indicate the time before which no event constraint is inferred.

(*Lower*) The total displacement for ruptures after 900 A.D is shown by the solid blue line. Blue "x" shows total predicted slip at paleoseismic sites for the particular WGCEP slip rate. Scenario displacement misfit is found from the mean of the absolute difference of the WGCEP slip rate and elapsed time (green "x") and the total from ruptures (red dots) and is computed at 20 km points. The mean misfit is 14.7 and 1.4 meters for (a) and (b), respectively. The largest individual displacement among all ruptures at each 20 km point is shown by the magenta "+" symbols. The intersection of the maximum individual displacement with the total predicted slip in (a) near milepost 460 means that a single large earthquake has equaled the total available to all ruptures there. Inspection of the upper panel shows that either one of the end-to-end events could do this
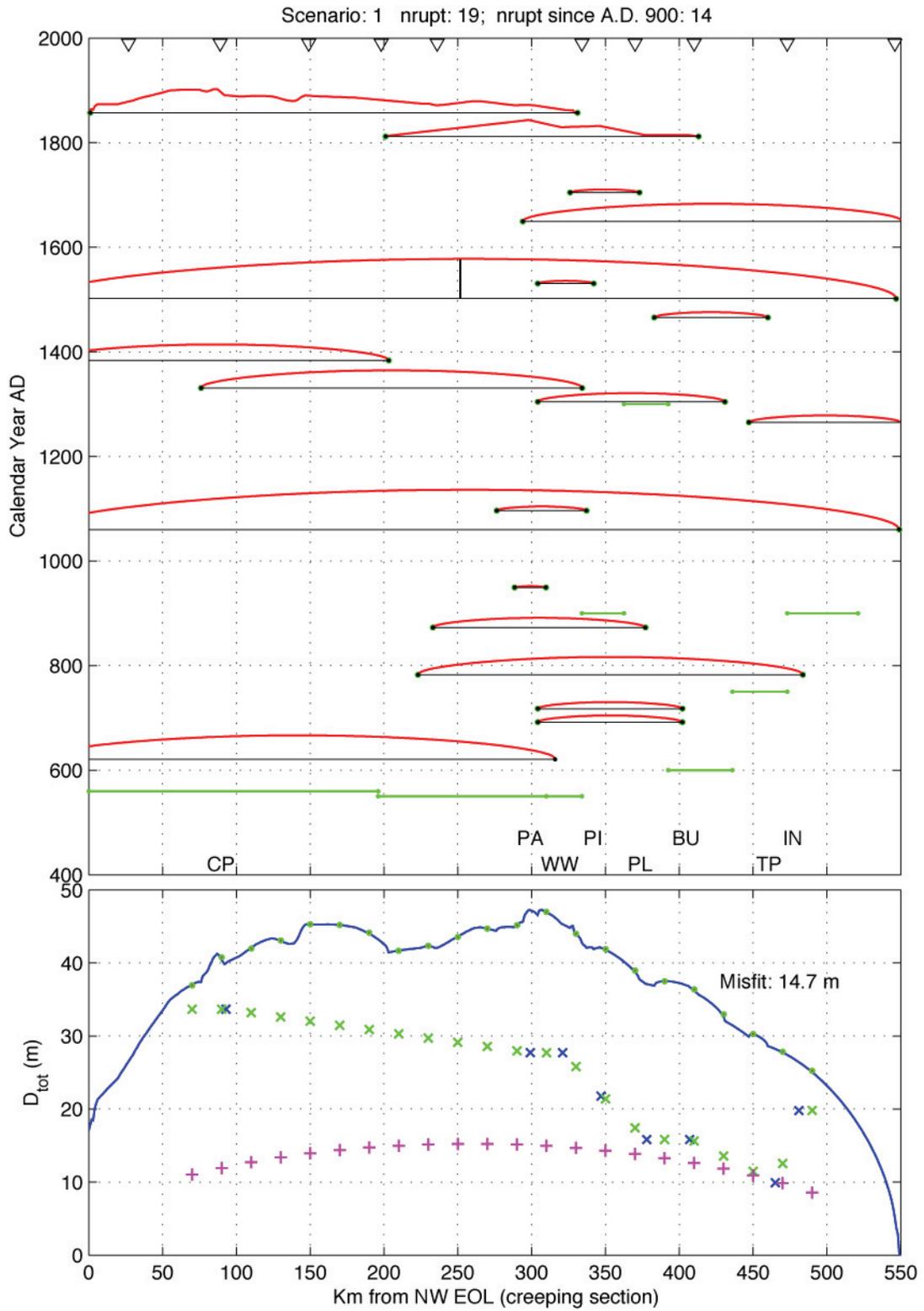
Figure 15(a)
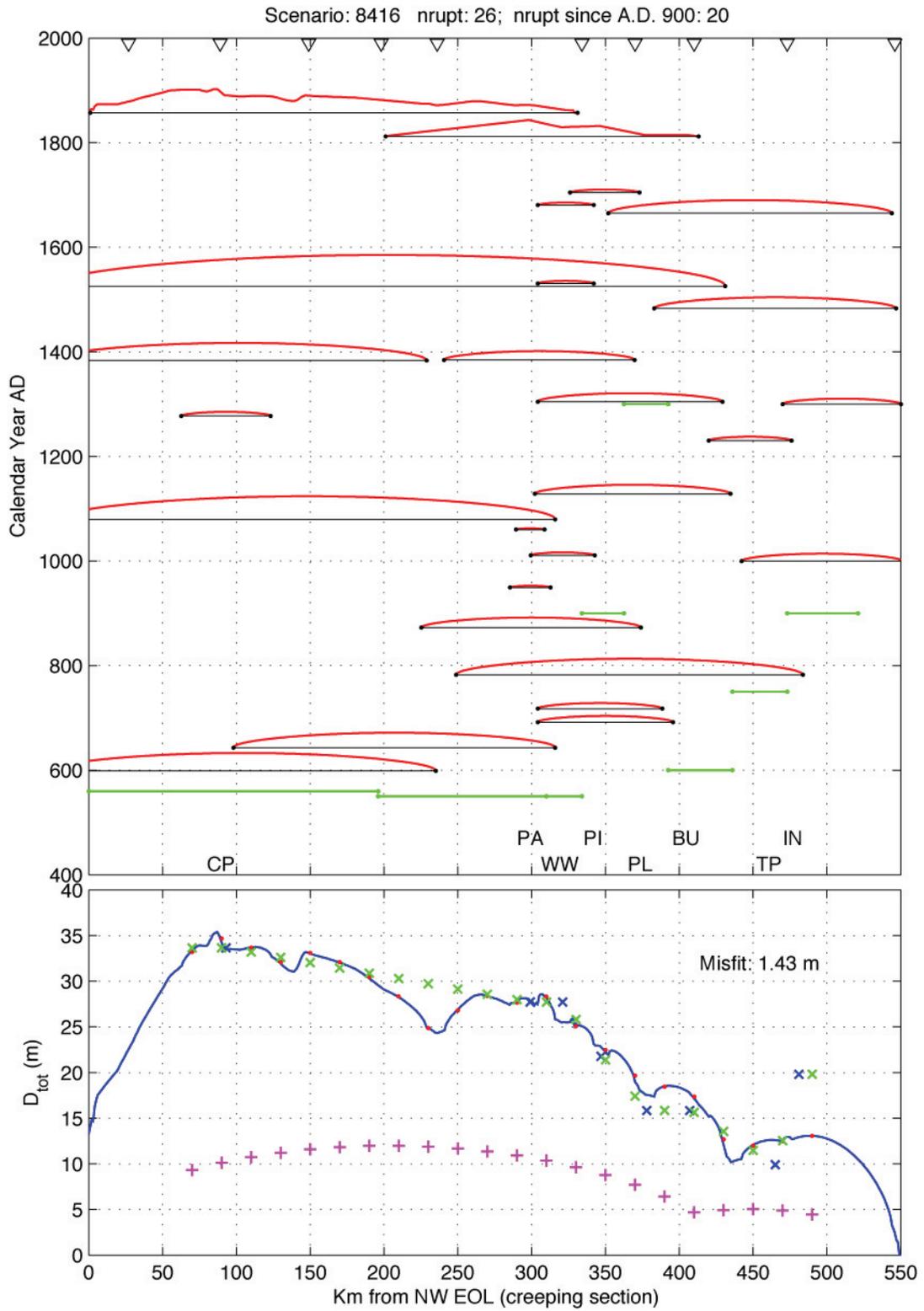
Figure 15(b)
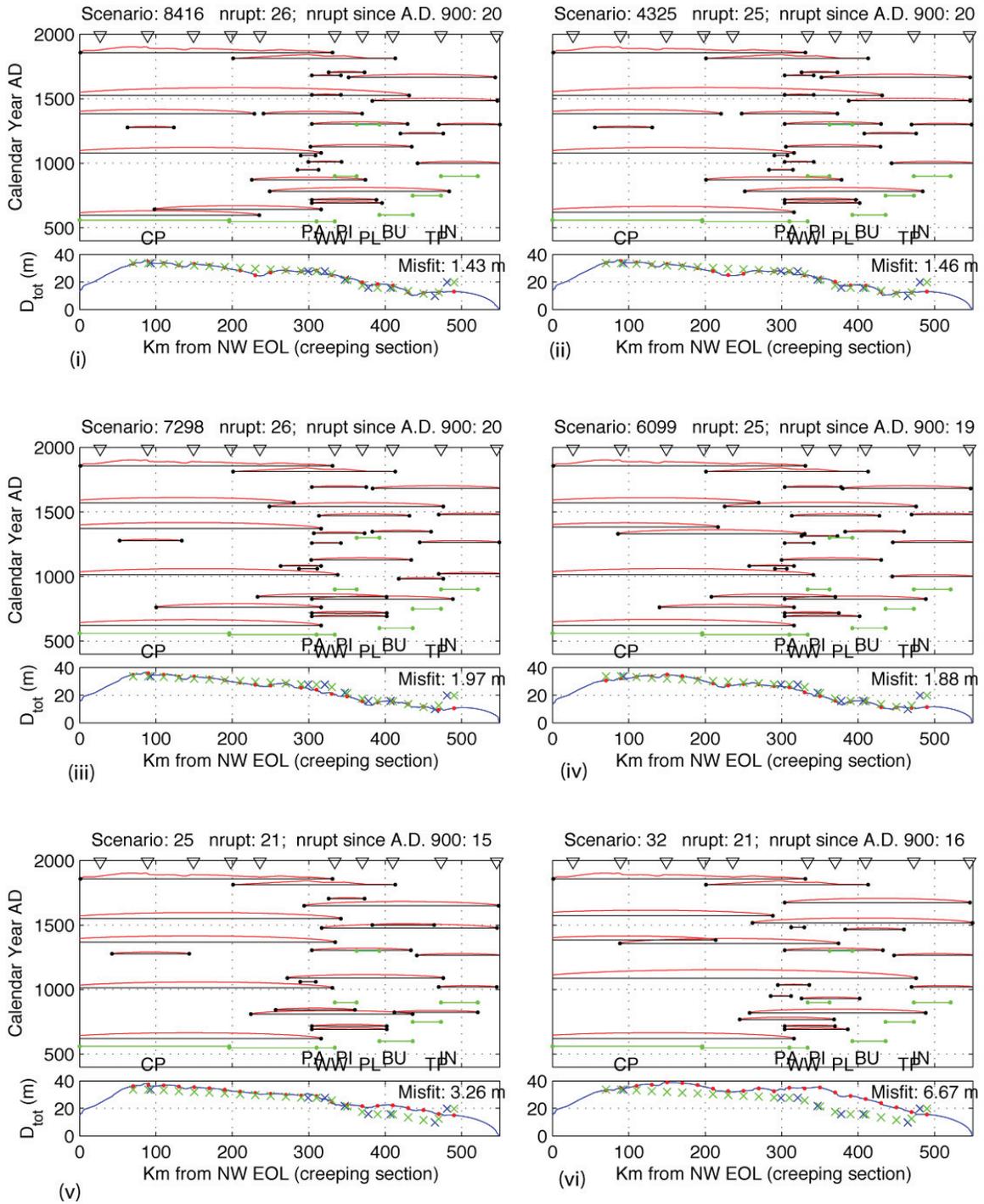
Figure 16a. Scenario for one of the three slip-rate models of Table 5 and the Hanks-Bakun length-AD regression. (i) and (ii): best fit with respect to mean displacement. (iii) and (iv): best adjusted time score. (v) and (vi): fewest number of ruptures after subsetting on a time score of -1.9 and a mean displacement misfit of 7 meters. In general total displacement fit is better for slip rate Model 2.3 with higher slip rates through the San Bernardino and San Gorgonio segments.
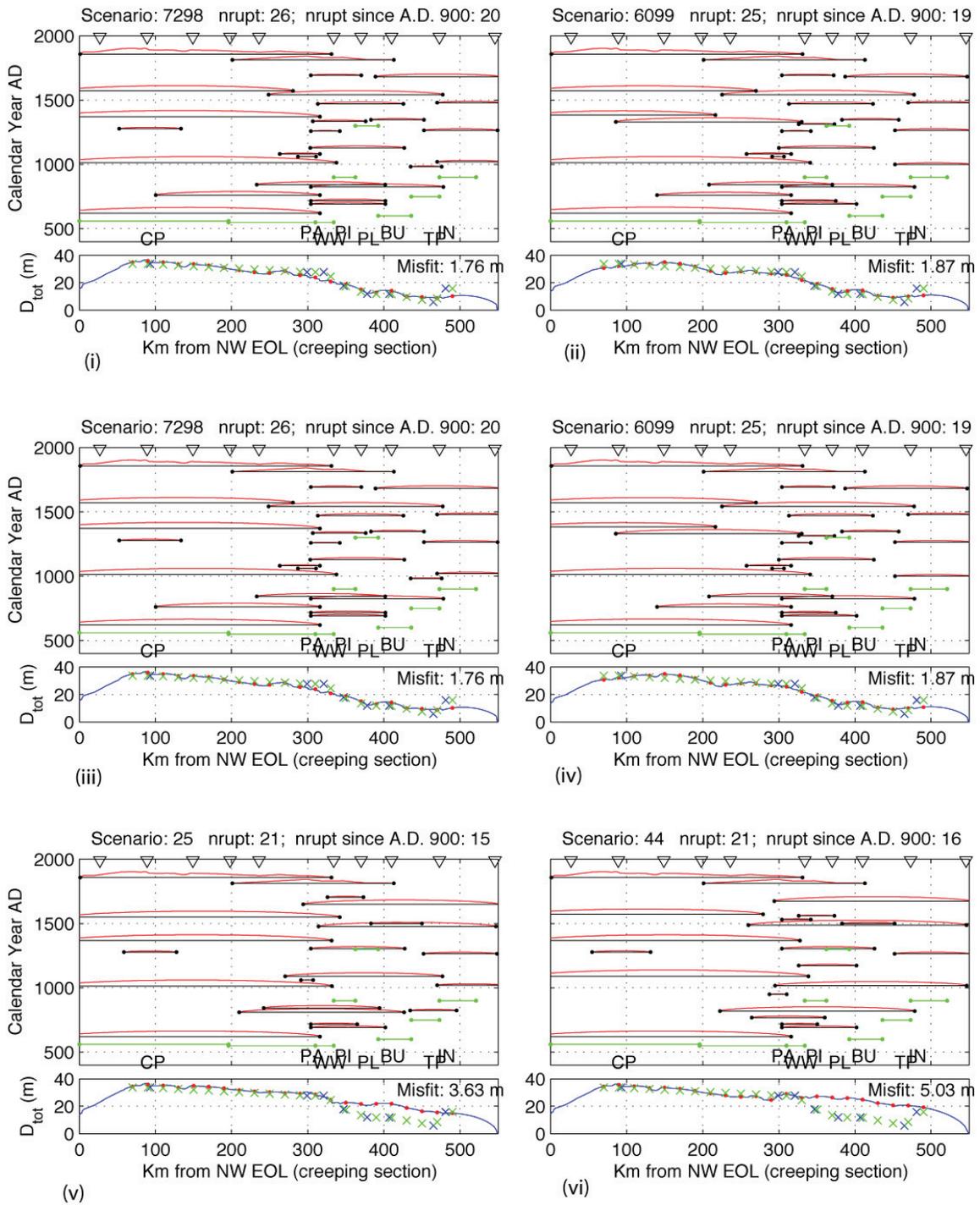
Figure 16b. Scenario for one of the three slip-rate models of Table 5 and the Hanks-Bakun length-AD regression. (i) and (ii): best fit with respect to mean displacement. (iii) and (iv): best adjusted time score. (v) and (vi): fewest number of ruptures after subsetting on a time score of -1.9 and a mean displacement misfit of 7 meters. In general total displacement fit is better for slip rate Model 2.3 with higher slip rates through the San Bernardino and San Gorgonio segments.
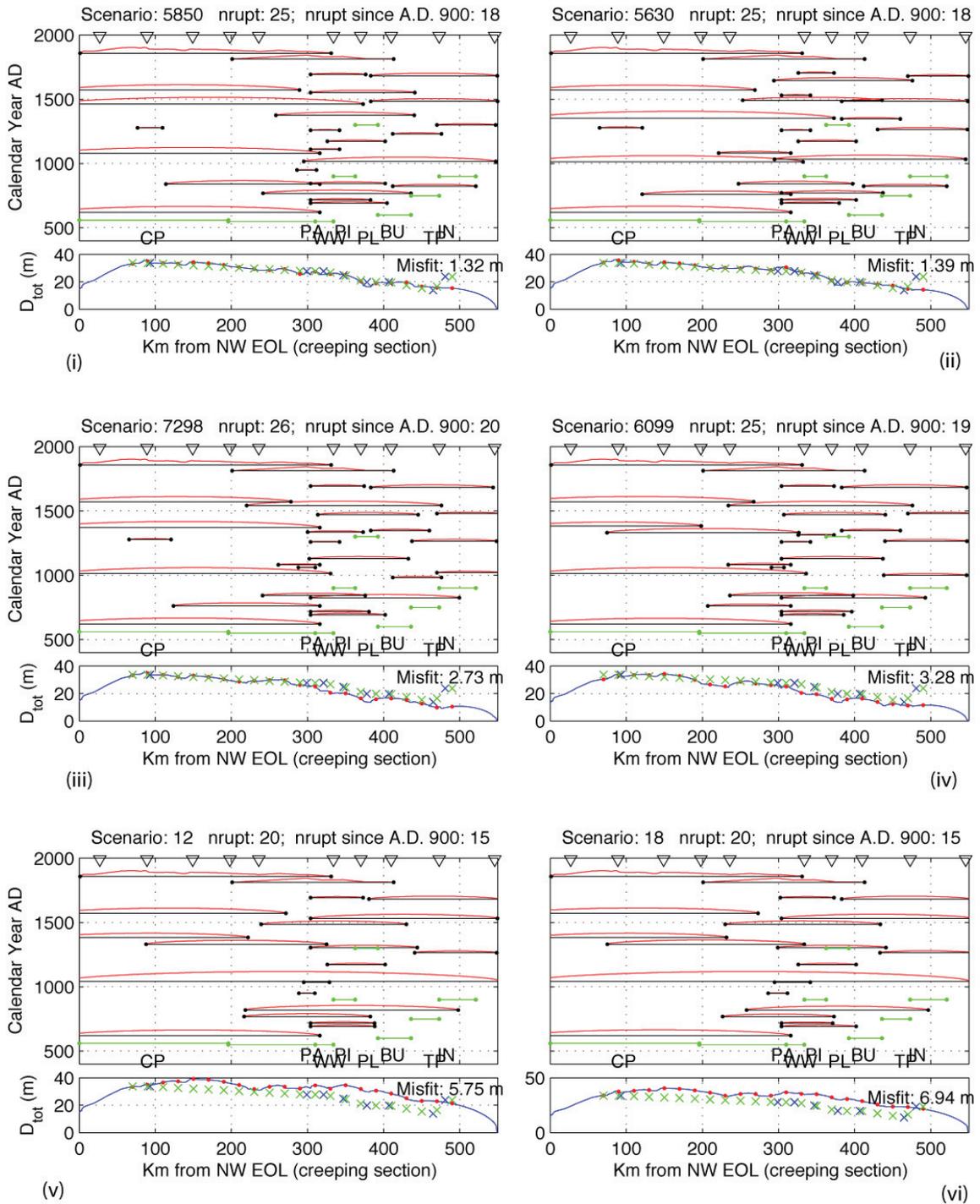
Figure 16c. Scenario for one of the three slip-rate models of Table 5 and the Hanks-Bakun length-AD regression. (i) and (ii): best fit with respect to mean displacement. (iii) and (iv): best adjusted time score. (v) and (vi): fewest number of ruptures after subsetting on a time score of -1.9 and a mean displacement misfit of 7 meters. In general total displacement fit is better for slip rate Model 2.3 with higher slip rates through the San Bernardino and San Gorgonio segments.
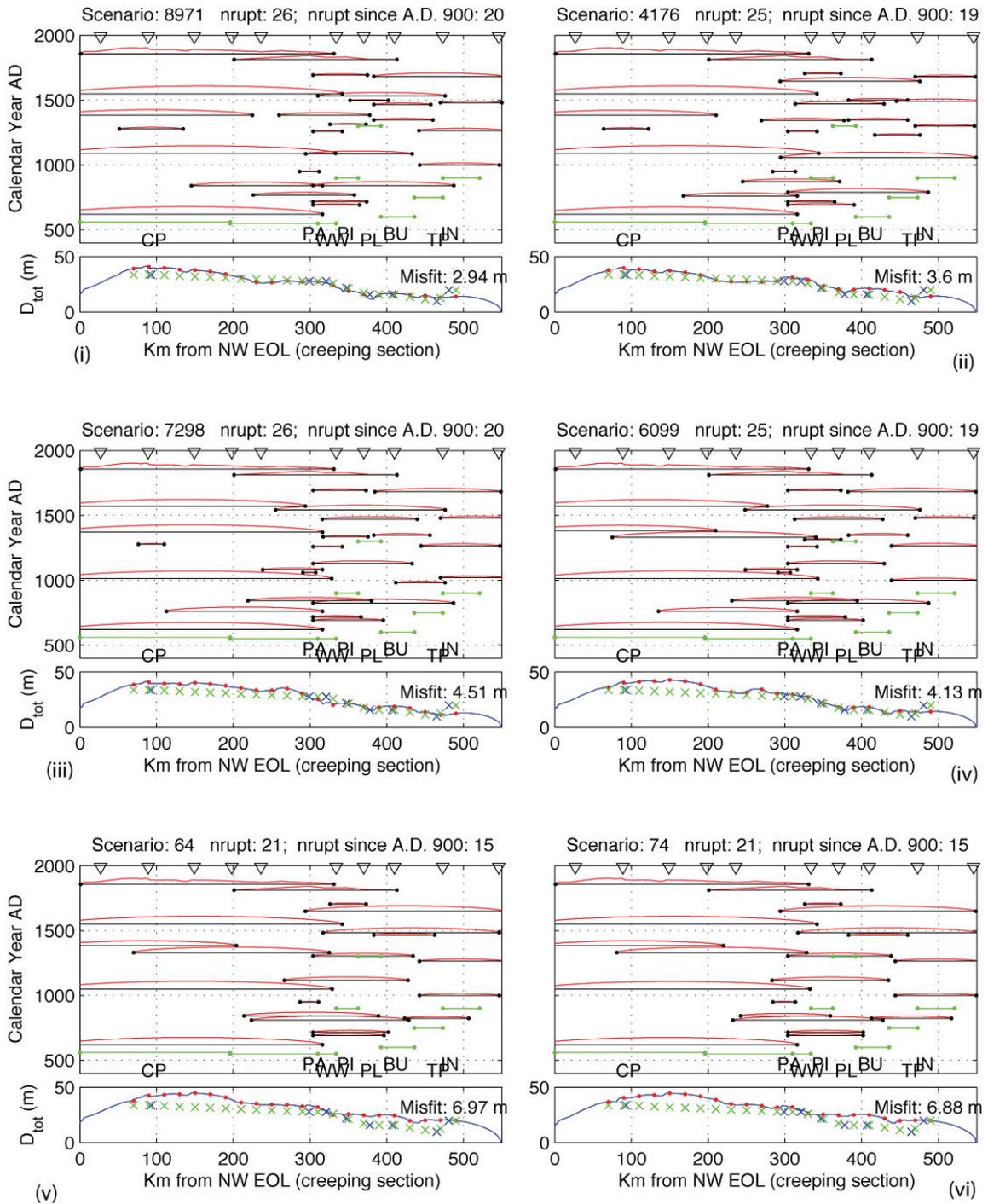
Figure 17a. Same as Figure 16, except using a modified Wells and Coppersmith (1994) regression (Equation 5). Fewer quality fits are obtained with the Wells and Coppersmith L-AD regression for all slip rate models.
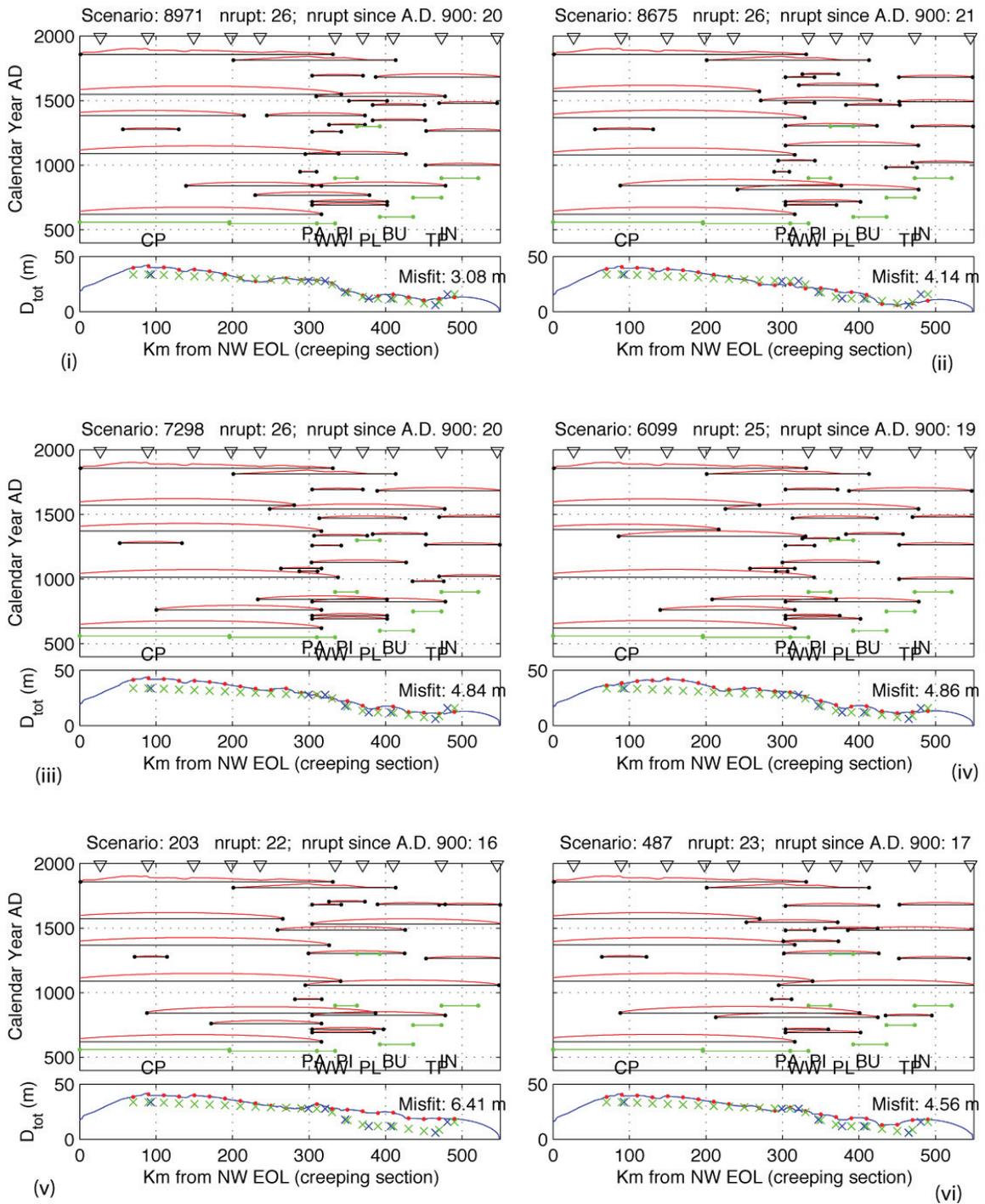
Figure 17b. Same as Figure 16, except using a modified Wells and Coppersmith (1994) regression (Equation 5). Fewer quality fits are obtained with the Wells and Coppersmith L-AD regression for all slip rate models.
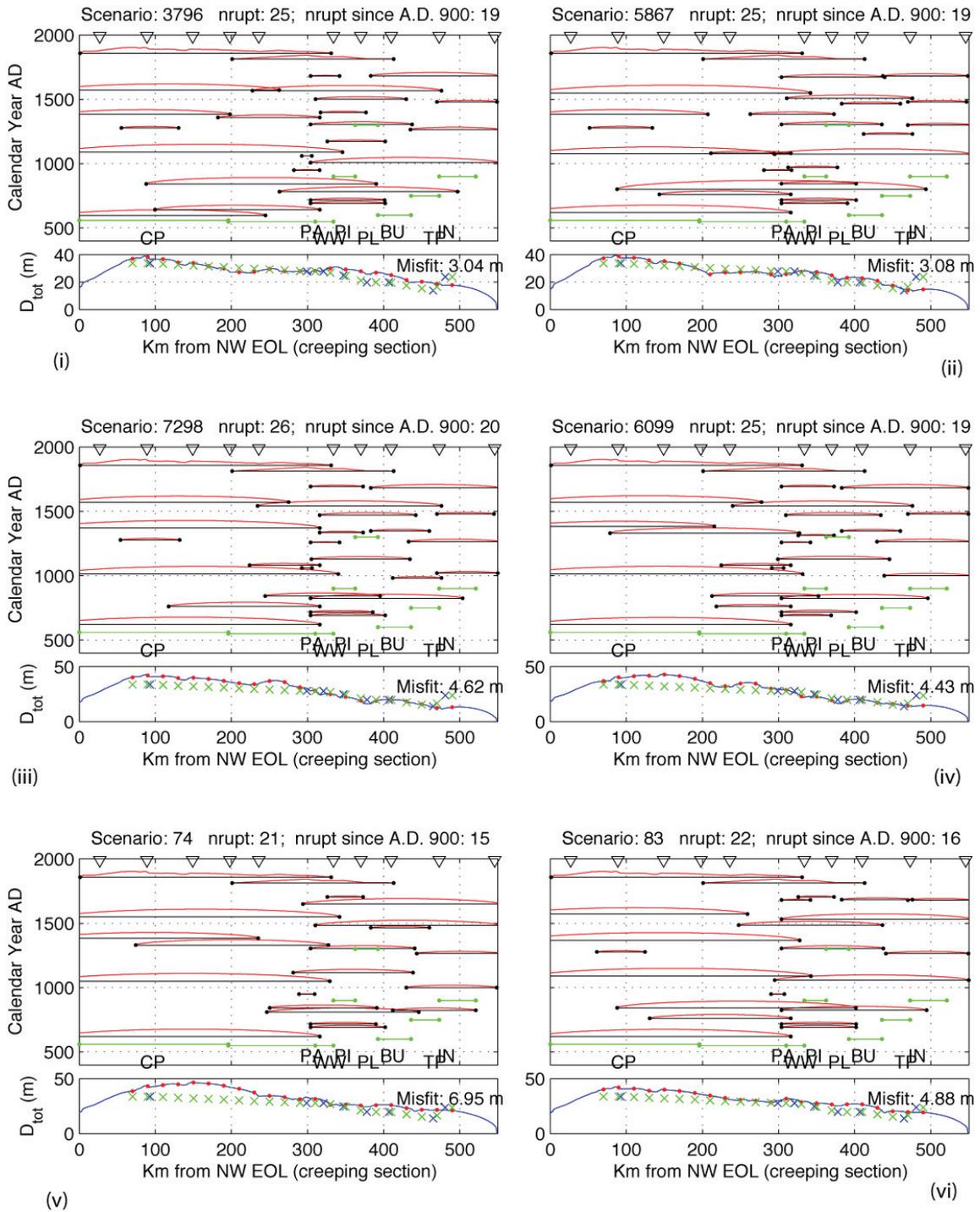
Figure 17c. Same as Figure 16, except using a modified Wells and Coppersmith (1994) regression (Equation 5). Fewer quality fits are obtained with the Wells and Coppersmith L-AD regression for all slip rate models.

Appendix: Application of Scenarios to Segmentation

The Working Group on California Earthquake Probabilities divided the southern San Andreas fault into ten segments within which slip rates and recurrence intervals were considered roughly constant. Their use of segments was motivated in part to facilitate comparison with results of previous working groups. The precise locations of segmentation boundaries, and the merits of the segmentation model itself are subjects unto themselves. Here we restrict our scope to the application of rupture scenarios to their segmentation model.

Membership of paleoseismic sites on a segment was assigned based on milepost. To assign segment membership to ruptures, first the mid-points of each segment were located in terms of their milepost number. Each end of a rupture is compared to the list of mid-points (Figure A-1). The first midpoint SE of the NW rupture end is the NW segment used below. The southeast segment end is the closest midpoint NE of the SE rupture end. This rule allows the segment ends to seem out of order if a rupture lies entirely between neighboring midpoints (example R3, below).

Ruptures involving two or fewer segments require further consideration. Two cases arise. First is when the ends of a rupture are on either end of the segment midpoint. In this case we compare the rupture length to half the segment length, and assign the rupture to that segment if the rupture length is greater. The second case is when the rupture crosses no midpoints. Ruptures centered near segment ends (e.g., Wrightwood single-site ruptures) can include some length on two segments, and have a total length up to just less than half the length of the two segments combined. Furthermore, if one of the two segments involved is shorter than the other, the rupture can be longer than the shorter segment's full length. Such ruptures counted as "sub-segment ruptures" because they take up less than half of either component segment; nonetheless they could be large earthquakes. Sub-segment ruptures are concentrated near the Wrightwood site because of the greater number of ground-rupturing earthquakes in that record.

Segment assignments are shown in Table A-1 for the 100 scenarios that best fit the displacement total from the WGCEP slip rates and elapsed time since 900 A.D. Individual entries reflect the data we have in the 1100 years of relatively complete paleoseismic data. Apparent gaps in the table may actually reflect the unlikelihood of those earthquakes, but could also reflect limitations in the paleoseismic record that would fill in with more dense coverage or longer records.

The tables include entries that at first may seem unintuitive. As a first example, most events at Carrizo have large displacements, and thus large predicted lengths. Large displacements mean the NW rupture end will be northwest of Carrizo, and few events will actually start at Carrizo. Thus to find the contribution of large Carrizo events, the Parkfield row is most relevant. As a second example, there is a concentration of events with a north end at North San Bernardino. These events are actually associated with the Wrightwood site, but they are not associated with the South Mojave segment because the mid-point of that segment is relatively distant and NW of Pallett Creek. Ruptures that do not correlate at Pallett Creek can't associate with the S. Mojave segment. Southeast of

Wrightwood there is not a similar nearby site, and the center of the N. San Bernardino segment is more easily spanned by tails of Wrightwood ruptures.

Table A-1. Segment Boundary Results

Results are given for each of the three slip models using the 100 scenarios that best fit the total displacement prediction from slip rate and elapsed time since 900 A.D. The Hanks-Bakun length-average displacement is used for all cases. The table is only completed in the upper diagonal. Row segment names refer to the starting segment; columns the ending segment. Segments are assigned if the midpoint is crossed and the rupture is half the segment or greater in length.

The exact numbers in the table refer only to the particular run that assigned lengths to ruptures. However, the results do not vary much from run to run.

Abbreviations

1:Pkfl: Parkfield	6:MojS: South Mojave
2:Cho: Cholame	7:NSBr: San Bernardino North
3:Car: Carrizo	8:SSBr: San Bernardino South
4:BBnd: Big Bend	9:SGor: San Gorgonio
5:MojN: North Mojave	10:Coac: Coachella

row=starting segment, column = ending segment
e.g., entry in 1,6 means that rupture includes Parkfield to S Mojave

Slip Model 2.1
Count one or more segments = 2012
Count including subsegment ruptures = 2304
Prob of subsegment ruptures = 0.127

	Pkfl	Chol	Carr	Bbnd	MojN	MojS	NSBr	SSBr	SGor	Coac	Total, 100 scenes
Pkfl	0	0	0	30	97	217	33	23	0	0	400
Chol	0	0	24	0	0	0	0	0	0	0	24
Carr	0	0	23	0	0	26	31	22	9	0	111
BBnd	0	0	0	0	0	22	0	0	0	0	22
MojN	0	0	0	0	0	22	11	5	3	0	41
MojS	0	0	0	0	0	33	84	61	42	13	233
NSBr	0	0	0	0	0	0	194	297	67	59	617
SSBr	0	0	0	0	0	0	0	4	127	95	226
SGor	0	0	0	0	0	0	0	0	74	48	122
Coac	0	0	0	0	0	0	0	0	0	216	216
										Total	2012

Subsegment rupture count by segment; total = 292

Pkfl	Chol	Carr	Bbnd	MojN	MojS	NSBr	SSBr	SGor	Coac	Total
0	25	0	0	0	267	0	0	0	0	292

Slip Model 2.2
Count one or more segments = 2040
Count including subsegment ruptures = 2327
Prob of subsegment ruptures = 0.123

	Pkfl	Chol	Carr	Bbnd	MojN	MojS	NSBr	SSBr	SGor	Coac	Total, 100 scenes
Pkfl	0	0	0	27	81	238	29	25	0	0	400
Chol	0	0	28	0	0	0	0	0	0	0	28
Carr	0	0	26	0	0	22	23	13	7	0	91
BBnd	0	0	0	0	0	29	0	0	0	0	29
MojN	0	0	0	0	0	23	12	5	4	0	44
MojS	0	0	0	0	0	38	88	60	44	4	234
NSBr	0	0	0	0	0	0	194	289	90	50	623
SSBr	0	0	0	0	0	0	0	7	124	73	204
SGor	0	0	0	0	0	0	0	0	114	9	123
Coac	0	0	0	0	0	0	0	0	0	264	264
										Total	2040

Subsegment rupture count by segment; total = 287

Pkfl	Chol	Carr	Bbnd	MojN	MojS	NSBr	SSBr	SGor	Coac	Total
0	25	0	0	0	262	0	0	0	0	287

Slip Model 2.3
Count one or more segments = 1957
Count including subsegment ruptures = 2278
Prob of subsegment ruptures = 0.141

	Pkfl	Chol	Carr	Bbnd	MojN	MojS	NSBr	SSBr	SGor	Coac	Total, 100 scenes
Pkfl	0	0	0	14	105	220	38	17	6	0	400
Chol	0	0	25	0	0	0	0	0	0	0	25
Carr	0	0	32	0	0	17	19	14	10	0	92
BBnd	0	0	0	0	0	35	0	0	0	0	35
MojN	0	0	0	0	0	22	10	4	5	0	41
MojS	0	0	0	0	0	26	67	47	59	19	218
NSBr	0	0	0	0	0	0	194	258	87	101	640
SSBr	0	0	0	0	0	0	0	9	129	69	207
SGor	0	0	0	0	0	0	0	0	49	126	175
Coac	0	0	0	0	0	0	0	0	0	124	124
										Total	1957

Subsegment rupture count by segment; total = 287

| Pkfl	Chol	Carr	Bbnd	MojN	MojS	NSBr	SSBr	SGor	Coac	Total
0	30	0	0	0	291	0	0	0	0	321
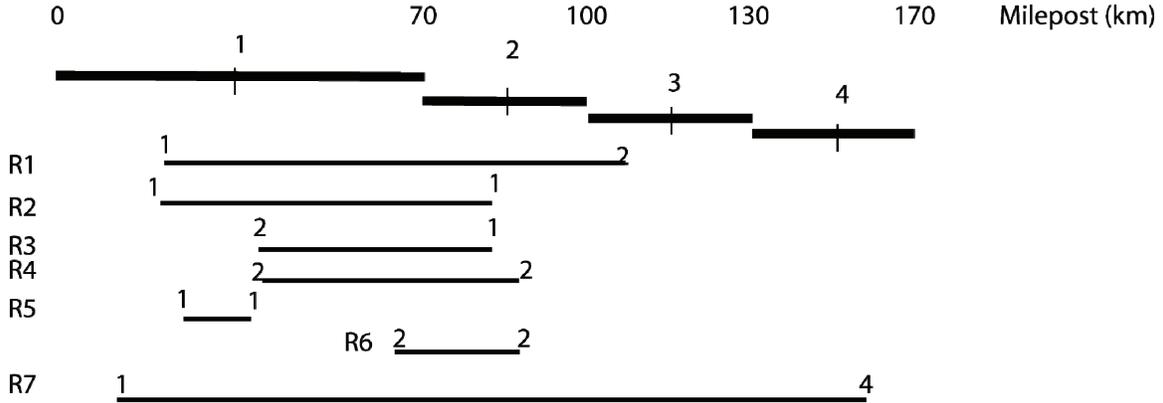
Figure A-1. Schematic illustration of how ruptures are assigned to segments, multi-segment ruptures, or are considered subsegment ruptures. Milepost numbers are approximate, and intended only to illustrate cases. R1: assigned to segments 1 and 2. R1 and R7 illustrate simple, multiple-segment ruptures. R2: Rupture over half the segment length, assigned as a single segment rupture to 1. R6 illustrates the same point, but with a rupture only slightly longer than half the length of Segment 2. R3 is considered a subsegment rupture because it is less than half on either Segment 1 or 2. Note that it is a subsegment rupture even though it is longer than Segment 2. R4: Rupture assigned to Segment 2. R5: Rupture is less than half the segment length, and thus a subsegment rupture. Note that R2, R4 and R5 are alike in that they have same segment end assignments at each end (1-1, 2-2 and 1-1, respectively).

Addenda to Appendix E: 'San Andreas Fault Rupture Scenarios From Multiple Paleoseismic Records: "Stringing Pearls"'

Glenn P. Biasi and Ray J. Weldon II

After completion of final technical reviews of WGCEP Appendix E, revised event date probability density functions were made available for four pre-1857 ground rupturing events from the Bidart Fan site. The revised dates lowered the recurrence interval for the site to 144 years. If connected with the per-event displacements of Liu et al. (2004), the shorter RI implies an excessive slip rate since ~1298, the mean date of the oldest redated event. An alternative interpretation is that some of the Liu et al. (2004) incision events actually record multiple individual earthquake slips. Slip-per-event study to resolve this question has been funded by NSF, and will be pursued over the next two years.

The shorter recurrence interval and new dates from the Bidart Fan site have consequences for scenarios developed in the man body of this report. Although the data became available too late for a complete analysis, we were able to make a suite of new scenarios that provide some insight into their importance. A new rupture pool was developed using the same "pearl-stringing" rules as in the main body of this paper. Scenarios were developed using the same sampling procedures. The new data ironically make the complete portion of the Carrizo Plain record the youngest of all major southern San Andreas fault paleoseismic sites. We considered the Carrizo Plain record to be complete only (perhaps somewhat optimistically) for the most recent 900 years, and used this period to grade scenarios.

Ruptures for which the Carrizo Plain is the NW site have NW tails extended using the same average displacement method used for all other sites except Wrightwood. Specifically, the recurrence interval from the new dates (2007-1298)/5 is multiplied times the WGCEP slip rate at the site (34 mm/yr for all three models). Ten percent of the slip is posited to occur away from the paleoseismic site, just as was done with previous models. To estimate rupture lengths, a displacement pdf is constructed and randomly sampled for the model event displacement for the rupture. The displacement is scaled to taper to the NW using rules described in the main body of the report. As a characterization, rupture lengths are more variable than previously when the large displacements of Liu et al. (2004) were associated with most events.

Figures Ad-1 and Ad-2 show six scenarios each for the WGCEP Model 2.1 slip rates. Figure Ad-1 shows best total displacement fit cases. All models fit the total displacement predicted from slip rate and total time with acceptable misfits. The pattern of displacement misfit is also similar, with models fitting the northern 450 km well and the Coachella section under-predicted. Figure Ad-2 shows six models that fit the total displacement reasonably well but do so with the fewest number of ruptures. Mean

displacement misfit must be less than 7 meters to be in this subset; most here fit closer than 4.6 m.

The shorter RI at Carrizo has little effect on the pattern of ruptures found in either case. Best displacement scenarios (Fig. Ad-1) generally include about three ruptures with 1857-class lengths. Long ruptures still tend to end within a site or two of Wrightwood. These findings are not surprising, since a fundamental premise of our models is that the known paleoseismic earthquakes must explain the total displacements we see. This results in favoring scenarios where several earthquakes correlate between Carrizo and the southern Mojave. A corollary of the model premise is that total displacements NW of Carrizo are unconstrained. If the scenarios here are similar to what the fault actually does, there is space for many frequent smaller earthquakes involving the Cholame and Parkfield sections. In all, conclusions that one would draw from scenarios with five events since ~1298 are similar to those with the previous chronology.
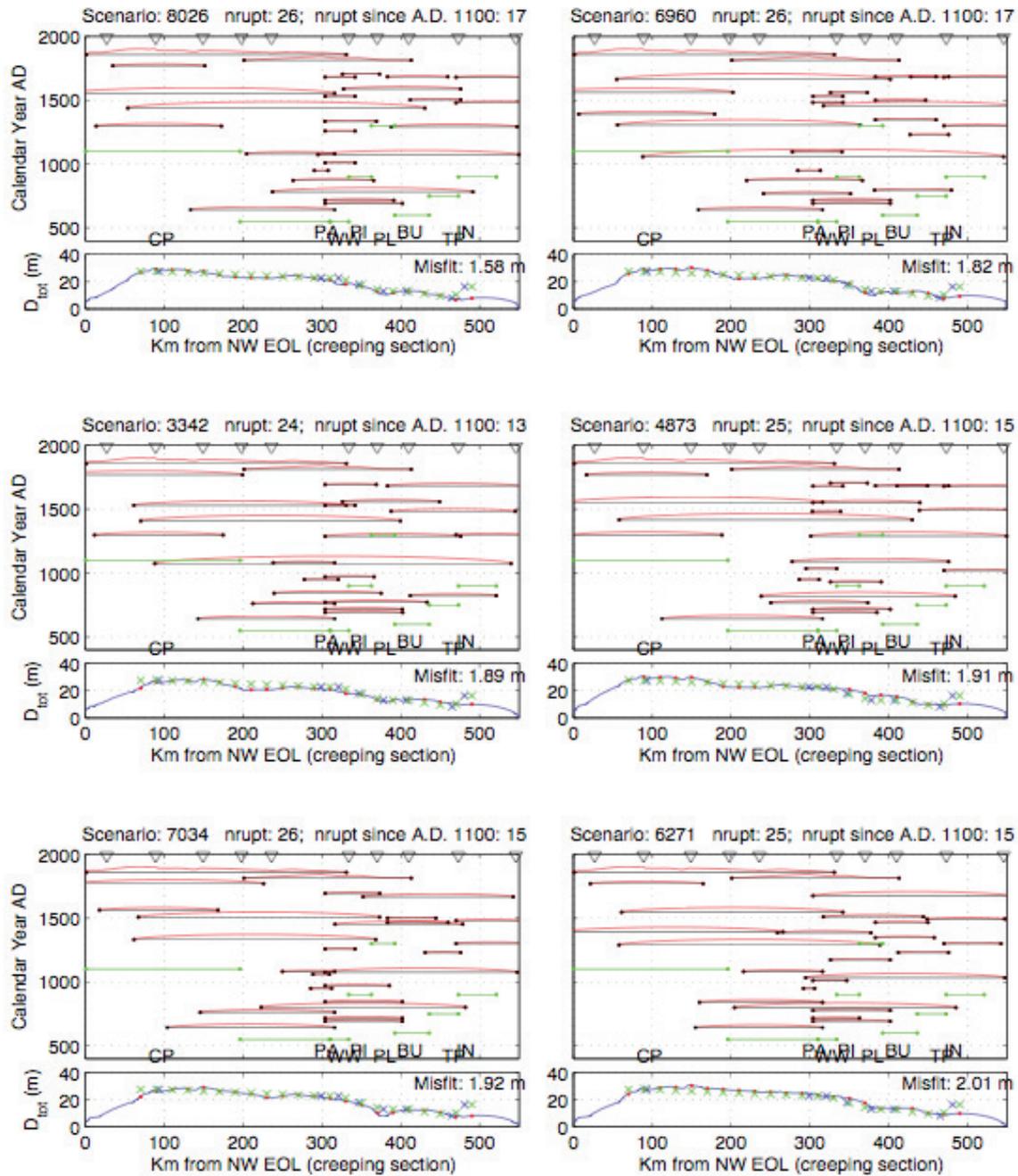
Figure Ad-1. Best-fitting scenarios using an average displacement model at Carrizo. Scenarios are graded only after AD 1100. Other details are given in the main text.
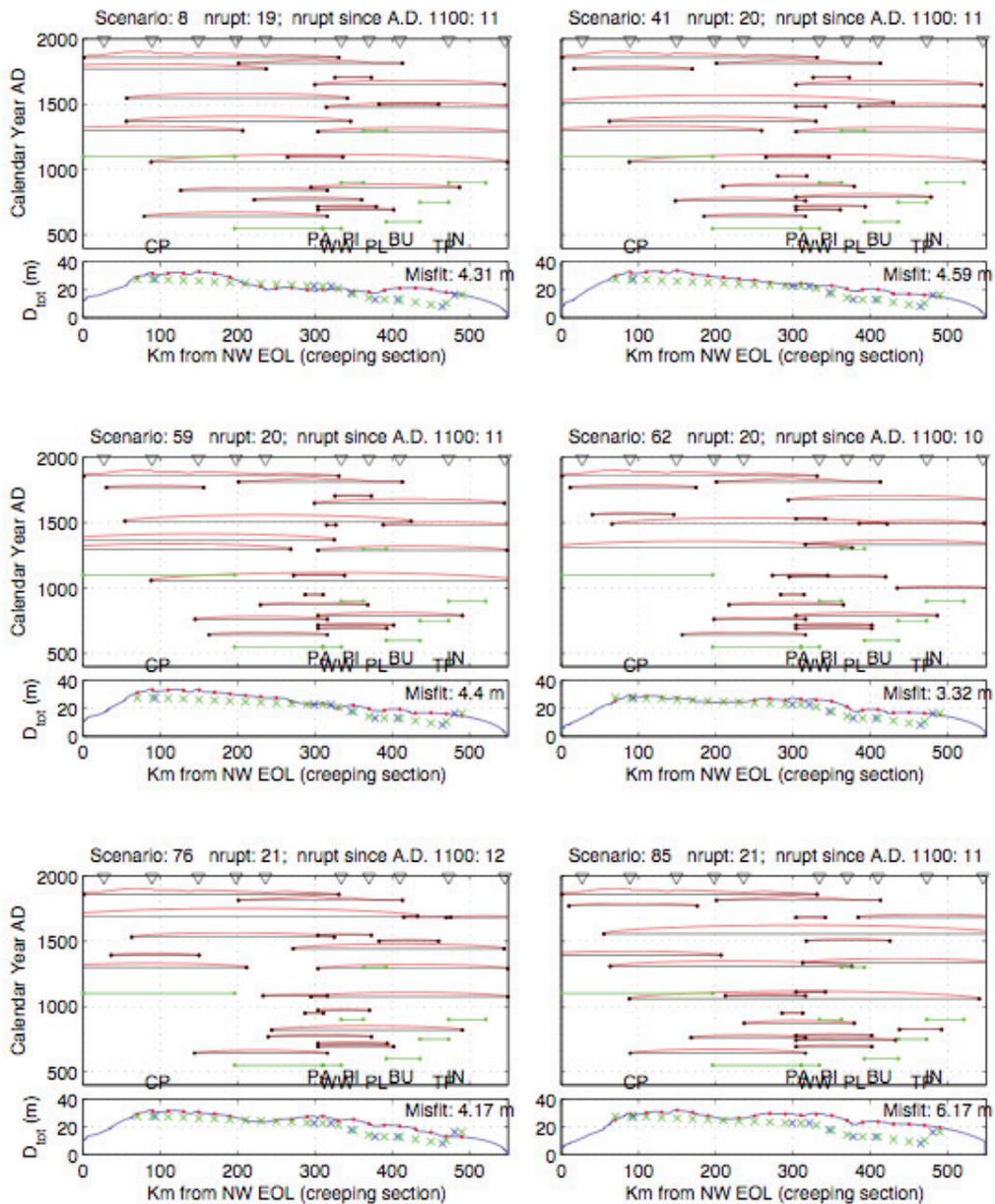
Figure Ad-2. Scenarios with the fewest ruptures meeting minimal standards for average displacement misfit. Scenarios are graded only after AD 1100. Other details are given in the main text.